


12-2020

GREAT EXPECTATIONS: PHOSPH(ON)ATE PRODRUGS IN DRUG DESIGN—OPPORTUNITIES AND LIMITATIONS

Victoria Yan

Follow this and additional works at: https://digitalcommons.library.tmc.edu/utgsbs_dissertations

 Part of the [Biochemical Phenomena, Metabolism, and Nutrition Commons](#), [Chemical and Pharmacologic Phenomena Commons](#), [Disease Modeling Commons](#), [Medical Biochemistry Commons](#), [Medical Pharmacology Commons](#), [Medicinal and Pharmaceutical Chemistry Commons](#), [Nucleic Acids, Nucleotides, and Nucleosides Commons](#), [Pharmaceutics and Drug Design Commons](#), [Translational Medical Research Commons](#), and the [Virus Diseases Commons](#)

Recommended Citation

Yan, Victoria, "GREAT EXPECTATIONS: PHOSPH(ON)ATE PRODRUGS IN DRUG DESIGN—OPPORTUNITIES AND LIMITATIONS" (2020). *The University of Texas MD Anderson Cancer Center UTHealth Graduate School of Biomedical Sciences Dissertations and Theses (Open Access)*. 1067.
https://digitalcommons.library.tmc.edu/utgsbs_dissertations/1067

This Thesis (MS) is brought to you for free and open access by the The University of Texas MD Anderson Cancer Center UTHealth Graduate School of Biomedical Sciences at DigitalCommons@TMC. It has been accepted for inclusion in The University of Texas MD Anderson Cancer Center UTHealth Graduate School of Biomedical Sciences Dissertations and Theses (Open Access) by an authorized administrator of DigitalCommons@TMC. For more information, please contact digitalcommons@library.tmc.edu.

**GREAT EXPECTATIONS: PHOSPH(ON)ATE PRODRUGS IN DRUG
DESIGN—OPPORTUNITIES AND LIMITATIONS**

by

Victoria C. Yan, A.B.

APPROVED:

Florian Muller, Ph.D.
Advisory Professor

Federica Pisaneschi, Ph.D.

Steven Millward, Ph.D.

William Plunkett, Ph.D.

Mark D. Pagel, Ph.D

APPROVED:

Dean, The University of Texas
MD Anderson Cancer Center UTHealth Graduate School of Biomedical Sciences

**GREAT EXPECTATIONS: PHOSPH(ON)ATE PRODRUGS IN DRUG
DESIGN—OPPORTUNITIES AND LIMITATIONS**

A

THESIS

Presented to the Faculty of

The University of Texas

MD Anderson Cancer Center UTHealth

Graduate School of Biomedical Sciences

in Partial Fulfillment

of the Requirements for the Degree of

MASTER OF SCIENCE

by

Victoria C. Yan, A.B.

Houston, Texas

December 2020

COPYRIGHT

Sections of this dissertation are based on previously published research. Permission has been granted for use in this thesis.

Ref. 17: Yan VC, Muller FL. 2020. Advantages of the Parent Nucleoside GS-441524 over Remdesivir for Covid-19 Treatment. *ACS Med Chem Lett* 11:1361–1366.

Ref. 29: Lin YH, Satani N, Hammoudi N, Yan VC, Barekatain Y, Khadka S, Ackroyd JJ, Georgiou DK, Pham CD, Arthur K, Maxwell D, Peng Z, Leonard PG, Czako B, Pisaneschi F, Mandal P, Sun Y, Zielinski R, Pando SC, Wang X, Tran T, Xu Q, Wu Q, Jiang Y, Kang Z, Asara JM, Priebe W, Bornmann W, Marszalek JR, DePinho RA, Muller FL. 2020. An enolase inhibitor for the targeted treatment of ENO1-deleted cancers. *Nat Metab* 2:1413–1426.

Ref. 45: Yan VC, Butterfield HE, Poral AH, Yan MJ, Yang KL, Pham C-D, Muller FL. 2020. Why Great Mitotic Inhibitors Make Poor Cancer Drugs. *Trends in Cancer* 6:924–941.

Ref. 47: Yan VC, Yang KL, Ballato ES, Khadka S, Shrestha P, Arthur K, Georgiou DK, Washington M, Tran T, Poral AH, Pham C-D, Yan MJ, Muller FL. 2020. Bio reducible Phosphonoamidate Pro-drug Inhibitor of Enolase: Proof of Concept Study. *ACS Med Chem Lett* 11:1484–1489.

Ref. 98: Yan VC, Pham CD, Arthur K, Yang KL, Muller FL. 2020. Aliphatic amines are viable pro-drug moieties in phosphonoamidate drugs. *Bioorganic Med Chem Lett* 30:127656.

Ref. 129: Yan VC, Pham C-D, Muller FL. 2020. Expedient Method for Direct Mono-amidation of Phosphonic and Phosphoric Acids. *ChemRxiv* <https://doi.org/10.26434/chemrxiv.12073131.V1>.

Ref. 182: Yan VC, Muller FL. 2020. Captisol and GS-704277, but not GS-441524, are credible mediators of remdesivir's nephrotoxicity. *Antimicrob Agents Chemother* 64:01920–1920.

To Jenny Wei, Darren Hamilton, Gary Snyder, and Florian Muller
for believing in me.

ACKNOWLEDGEMENTS

To my committee members: Florian, Marty, Steve, Federica, and Bill—thank you for your patience and constructive feedback for the past year.

To my lab: Kristine, Elliot, Cong-Dat, Kenisha, Dimitra, Jeff, Sunada, Yasaman, and Eliot—thank you for making lab fun and for being supportive for the past two years. I'll miss you all!

To my brothers: Matthew and Alexander—thanks for always having my back and being there for me.

To my dear friends who've heard the most of my journey here: Beth, Yewon, Kelly, Victoria, Anish, Yeonsoo, Amanda, Elisa, Anny—thank you for your support, kindness, and friendship. I really couldn't have done this without you.

To my parents: thank you for your support.

To my professors: Darren, Gary, Katie, and Jenny—thank you for inspiring a love of chemistry in me and for instilling in me a habit of thinking critically about pretty much everything.

GREAT EXPECTATIONS: PHOSPH(ON)ATE PRODRUGS IN DRUG DESIGN—OPPORTUNITIES AND LIMITATIONS

Victoria C. Yan, A.B.

Advisory Professor: Florian L. Muller, Ph.D.

ABSTRACT

Phosphate and phosphonates are chemical moieties with historical precedence in anticancer and antiviral nucleotide analogues. Synchronous to modern efforts identifying novel therapeutic targets in cancer, such chemical moieties are being investigated in the design of novel inhibitors with antineoplastic potential. A central challenge to the delivery of phosph(on)ate-containing drugs is their anionic character at physiological pH, which portends poor membrane permeability. This limitation has been successfully overcome through the use of prodrugs. When attached to the phosph(on)ate moiety, prodrugs mask the negative charge and easily enable cell permeability. Upon cellular entry, the promoieties are enzymatically or environmentally cleaved to unveil the active pharmacophore. A secondary and conventionally overlooked function of prodrugs is their ability to mediate cell- and tissue-specific drug localization. This arises from the intrinsically different enzymatic expression or environmental conditions specific to certain cell or tissue types. Here, I explore the challenges associated with phosph(on)ate prodrugs at the synthetic, *in vitro*, and *in vivo* levels first through the lens of a phosphonate-containing enolase inhibitor and then more broadly to other phosphate prodrugs such as cyclophosphamide, sofosbuvir, and remdesivir. The findings of this work have resulted in 1.) the development of a novel phosph(on)ate amidation reaction, 2.) the discovery of a novel promoiety, 3.) the synthesis of novel enolase inhibitor prodrugs with diverse mechanisms of bioactivation, and 4.) ongoing efforts to advance the parent nucleoside of remdesivir to the clinic for the treatment of COVID-19. Together, this work epitomizes the necessity of considering model-specific limitations at the *in vitro* and *in vivo* levels for successful implementation of prodrugs in the clinic.

TABLE OF CONTENTS

APPROVAL PAGE	I
TITLE PAGE	II
COPYRIGHT	III
DEDICATION	IV
ACKNOWLEDGEMENTS	V
ABSTRACT	VI
TABLE OF CONTENTS	VII
LIST OF FIGURES	VIII
LIST OF SCHEMES	X
LIST OF TABLES	XI
ABBREVIATIONS	XII
CHAPTER 1. INTRODUCTION	1
CHAPTER 2. DISCOVERY OF A NOVEL REACTION FOR EXPEDIENT MONO-AMIDATION OF PHOSPH(ON)ATES	21
CHAPTER 3. ALIPHATIC AMINES ARE VIABLE PROMOIETIES IN PHOSPHONOAMIDATE-CONTAINING DRUGS	48
CHAPTER 4. NITROHETEROCYCLE PRODRUGS OF AN ENOLASE INHIBITOR EXHIBIT INCREASED POTENCY UNDER HYPOXIC CONDITIONS	73
CHAPTER 5. PRODRUG IDENTITY INFLUENCES CELL- AND TISSUE- SPECIFIC LOCALIZATION	86
CHAPTER 6. GS-441524 IS THE PARENT NUCLEOSIDE OF REMDESIVIR WITH MORE FAVORABLE PHARMACOKINETIC PROPERTIES FOR COVID-19 TREATMENT	91
REFERENCES	102
VITA	125

LIST OF FIGURES

Figure 1. Collateral lethality paradigm applied to ENO1/2	1
Figure 2. Structures of HEX and previous enolase inhibitor tool compounds.	2
Figure 3. Examples of various bis-ester prodrugs.	3
Figure 4. FDA-approved McGuigan prodrugs	4
Figure 5. General bioactivation mechanism of McGuigan prodrugs.	5
Figure 6. Examples of alternative prodrugs.	5
Figure 7. Structures of POMHEX, HemiPOMHEX, and HEX with corresponding bioactivation mechanism <i>in vivo</i> .	7
Figure 8. Structure of cyclophosphamide.	9
Figure 9. Bioactivation of SOF.	10
Figure 10. <i>In vitro</i> versus <i>in vivo</i> metabolism of RDV	11
Figure 11. Structures of a phosphate (left) versus phosphonate (right).	13
Figure 12. Dimerization of BnHEX benzylamine during an Sn2 reaction	14
Figure 13. Common synthetic approaches towards phosph(on)ate prodrug synthesis	16
Figure 14. Reaction scope with phosphonic and phosphoric acids.	26
Figure 15. Mono-amidation of phosphoric acids occurs instantaneously.	27
Figure 16. Reaction between benzylamine and fludarabine monophosphate occurs exclusively with the phosphate	28
Figure 17. ^1H - ^{31}P HSQC supports that coupling between fludarabine phosphate and benzylamine occurs at phosphate.	29
Figure 18. Mono-amidates can be isolated with a single water extraction.	30
Figure 19. Proposed mechanism where phosphoric or phosphonic acids act as pro-electrophiles.	32
Figure 20. Aliphatic amines offer superior drug delivery <i>in vitro</i> .	51
Figure 21 A long-chain aliphatic phosphonoamidate efficiently delivers HEX <i>in vitro</i> .	52
Figure 22. Aliphatic amines on phosphonates are not preferential substrates for HINT1.	53
Figure 23. POMHEX is highly unstable in mouse and human plasma.	53
Figure 24. Benzylamine is a viable pro-drug group in the context of glioma.	76
Figure 25. Nitroaromatic benzylamine pro-drug exhibits greater potency under hypoxic conditions.	78

Figure 26. Nitroaromatic benzylamine pro-drugs exhibit robust stability in human plasma.	79
Figure 27. Cyclophosphamide mechanism of bioactivation.	88
Figure 28. McGuigan prodrugs on remdesivir are preferentially bioactivated in the liver.	93

LIST OF SCHEMES

Scheme 1. Strategies for mono-amidation of phosphates and phosphonates	21
<i>Scheme 2. Synthesis of structurally diverse phosphonoamidates.</i>	56
Scheme 3. Bioactivation and synthesis of bio reducible phosphonoamidate pro-drugs.	74

LIST OF TABLES

Table 1. Test reactions between BnHEX and 2-picolyamine.	24
Table 2. Test reactions between 1-naphthyl phosphate and benzylamine.	25
Table 3. Oral bioavailability of GS-441524 and acyclovir across species.	99
Table 4. Oral bioavailability acyclovir across species.	100

ABBREVIATIONS

AAV	Adenovirus associated virus
ACE2	Angiotensin converting enzyme 2
ADK	Adenosine kinase
ADV	Adefovir dipivoxil (GS-0840)
ALDH	Aldehyde dehydrogenase
ALT	Alanine transaminase
AST	Asparagine transaminase
AT2	Alveolar type 2 (cells)
AUC	Area under the curve
BAL	Bronchial alveolar lavage
BBB	Blood-brain-barrier
BID	<i>Bis in die</i> (twice per day)
CES1	Carboxylesterase 1
C _{max}	Concentration maximum
COVID-19	Coronavirus disease 2019
CRISPR	Clustered regularly interspaced short palindromic repeats
CRO	Contract Research Organization
CSF	Cerebrospinal fluid
CTSA	Cathepsin A
DBU	1,8-diazabicyclo[5.4.0]undec-7-ene
DCC	N, N'-Dicyclohexylcarbodiimide
DCM	Dichloromethane
d.e.	Diastereomeric excess
DIAD	Diisopropyl azodicarboxylate
DLT	Dose-limiting toxicity
DMF	Dimethyl formamide
dpi	Days post infection
EBOV	Ebola virus

EDC	1-ethyl-3-(3-dimethylaminopropyl)carbodiimide
ENO1/2	Enolase 1/2
ESRD	End-stage renal disease
F%	Percent oral bioavailability
FCoV	Feline coronavirus
FDA	Food and Drug Administration
FIP	Feline infectious peritonitis
GBM	Glioblastoma multiforme
HBV	Hepatitis B Virus
HCl	Hydrochloric acid
HCV	Hepatitis C Virus
HINT1	Histidine triad nucleotide-binding protein 1
HIV	Human Immunodeficiency Virus
IC ₅₀	Half maximal inhibitory concentration
IHC	Immunohistochemistry
KO	Knockout
MeCN	Acetonitrile
MeOH	Methanol
MW	Molecular weight
NCATS	National Center for Advancing Translational Sciences
NHP	Non-human primate
NIAID	National Institutes of Allergy and Infectious Diseases
NIH	National Institutes of Health
NMP	N-methyl-2-pyrrolidine
NMR	Nuclear magnetic resonance
NRTI	Nucleotide reverse transcriptase inhibitor
NS5B	Nonstructural protein 5B
NTP	Nucleoside triphosphate
PAPSS	3'-phosphoadenosine-5'-phosphosulfate synthase
PEP	Phosphoenolpyruvate
PhAH	Phosphonoacetohydroxamate

PK	Pharmacokinetic(s)
PPh ₃	Triphenyl phosphine
POC	Isopropylloxycarbonyloxymethyl
POCl ₃	Phosphorous oxychloride
POM	Pivaloyloxymethyl
QD	<i>Quaque die</i> (once per day)
RBC	Red blood cell
RCT	Randomized control trial
RdRp	RNA-dependent RNA polymerase
RT	Room temperature
RDV	Remdesivir (GS-5734)
SAR	Structure-activity-relationship
SATE	S-acyl-2-thioethyl
shRNA	Small hairpin RNA
S _n 2	Second order nucleophilic substitution
SOC	Standard-of-care
SOF	Sofosbuvir (GS-7977)
TAF	Tenofovir alafenamide (GS-7340)
TDF	Tenofovir disoproxil (GS-4331)
TFA	Trifluoroacetic acid
THF	Tetrahydrofuran
T _{max}	Time of maximum concentration
TLC	Thin Layer Chromatography
TPPO	Triphenylphosphine oxide
T _{1/2}	Half-life
WHO	World Health Organization
WT	Wild type
2-PG	2-phosphoglycerate

CHAPTER 1. INTRODUCTION

Part of this chapter has been published in (permission granted)

Lin YH, Satani N, Hammoudi N, Yan VC, Barekatin Y, Khadka S, Ackroyd JJ, Georgiou DK, Pham CD, Arthur K, Maxwell D, Peng Z, Leonard PG, Czako B, Pisaneschi F, Mandal P, Sun Y, Zielinski R, Pando SC, Wang X, Tran T, Xu Q, Wu Q, Jiang Y, Kang Z, Asara JM, Priebe W, Bornmann W, Marszalek JR, DePinho RA, Muller FL. 2020. An enolase inhibitor for the targeted treatment of *ENO1*-deleted cancers. *Nat Metab* 2:1413–1426

1.1 Overview of Collateral Lethality and the *ENO1/2* Paradigm

The phosphate moiety is prevalent in biology, serving structural, functional, and regulatory roles (1). Nucleotides are an example of phosphate-containing biomolecules that have historically been of interest for the development of chemotherapeutic and antiviral agents (2). In ongoing precision oncology therapeutic development, one class of phosphate-containing biomolecules that have garnered attention includes metabolic intermediates that are implicated in cancer-specific metabolic aberrations (3). *Collateral lethality* is an example of an emerging therapeutic strategy that

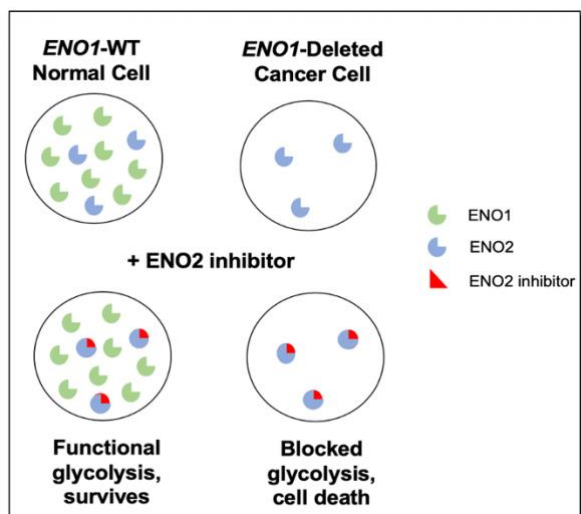


Figure 1. Collateral lethality paradigm applied to *ENO1/2*. Small molecule targeting of *ENO2* is selective for *ENO1*-deleted cancers.

capitalizes on cancer-specific metabolic vulnerabilities conferred by passenger deletion of metabolic enzymes neighboring tumor suppressor genes (4, 5). A pioneering example of this paradigm encompasses homozygous deletion of the 1p36 tumor suppressor locus, which accounts for the collateral deletion of the glycolytic enzyme enolase 1 (*ENO1*) in cancers such as glioblastoma multiforme (GBM). Enolase is a cell-essential enzyme that catalyzes the conversion of 2-phosphoglycerate (2-PG) to phosphoenolpyruvate (PEP) in the penultimate step of glycolysis. Cancers harboring homozygous deletion of *ENO1* are exceptionally sensitive to inhibition of its redundant paralogue, enolase 2 (*ENO2*) (4, 6). In contrast, normal, *ENO1*-wildtype (WT) tissue remain unperturbed, which enables selective toxicity against *ENO1*-deleted cancer cells with a sufficient therapeutic window (**Figure 1**). Independent validation by shRNA (4) and public domain

CRISPR data evidenced the therapeutic viability of ENO2 inhibition under this paradigm. Though a non-specific, pan-enolase inhibitor was initially found to demonstrate 50-fold selectivity against *ENO1*-deleted glioma cells compared to *ENO1*-WT cells *in vitro* (6), non-specific enolase inhibition is therapeutically prohibited due to on-target inhibition of ENO1 in red blood cells (RBCs) (7, 8). As ENO1 is the sole isoform expressed in RBCs, pan-enolase inhibition results in anemia, which is consistent with human Mendelian data. By conducting structure-activity-relationship (SAR) studies, our lab conceived of a phosphonate-containing enolase inhibitor, termed HEX, that demonstrates 4-fold specificity for ENO2 over ENO1 (**Figure 2**). As a substrate-competitive enolase inhibitor bearing structural resemblance to 2-PG, HEX is anionic at physiological pH, which hinders its cell and tissue permeability.

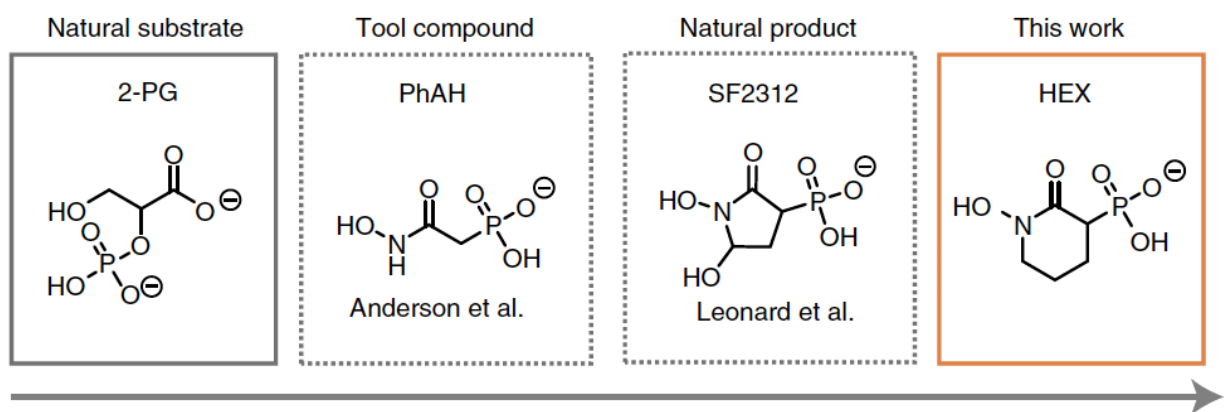


Figure 2. Structures of HEX and previous enolase inhibitor tool compounds.

1.2 Overview of Phosph(on)ate Prodrugs

Prodrugs attached to the phosph(on)ate moiety of drugs primarily serve to enhance membrane permeability by masking their negative charge and increasing lipophilicity. Due to the polyprotic nature of phosph(on)ates, two prodrug moieties must be attached to render the molecule net neutral (9). Historically, there have been two broad classes of phosph(on)ate prodrugs: 1.) bis-esters (10) and 2.) McGuigan (ProTide) prodrugs (11, 12). Common to these two classes of prodrugs is their reliance on esterases for bioactivation. Both classes have been successfully applied to FDA-approved antiviral nucleotide analogues such as anti-HIV agent tenofovir disoproxil (Viread[®]) (13) and the anti-HCV agent sofosbuvir (Sovaldi[®]) (14), respectively. A third class of prodrugs that has been the subject of more recent development efforts can be broadly characterized by the avoidance

of esterase-mediated bioactivation (15, 16); as a result, a considerable amount of structural diversity exists within this class. Ongoing development of novel phosph(on)ate prodrugs housed within this class has made the field privy to the relationship between cell- and tissue-specific expression of enzymes (in a given pathology) and prodrug structure. In other words, the field is becoming increasingly aware of the ability for prodrug identity to influence tissue localization of the active drug (15, 17, 18). A more detailed description of each class of prodrug follows in the sections below.

1.2.1 Class 1: Bis-ester prodrugs

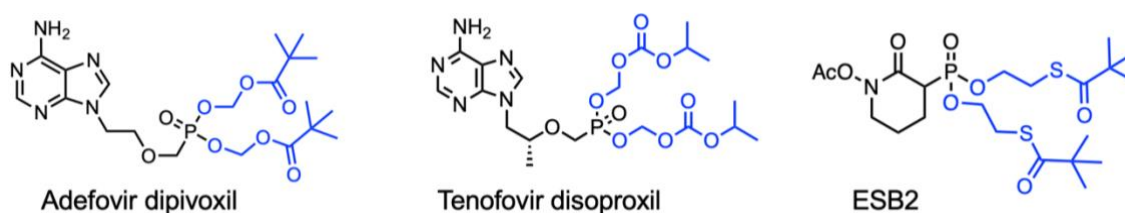


Figure 3. Examples of various bis-ester prodrugs. Left: adefovir dipivoxil is an example of a bis-POM prodrug. Middle: tenofovir disoproxil is an example of a bis-POC prodrug. Right: ESB2 is an example of a bis-SATE prodrug of HEX.

Bis-ester phosph(on)ate prodrugs are characterized by the addition of two identical ester groups onto the phosph(on)ate moiety of the drug. Three common bis-esters commonly employed include the pivaloyloxymethyl (POM; Farquhar prodrugs), isopropoxycarbonyloxymethyl (POC), and the S-acyl-2-thioethyl (SATE) prodrugs (**Figure 3**) (10, 16, 19). Notably, the synthesis and utility of the POM ester as a phosph(on)ate prodrug moiety was first reported by David Farquhar, a former professor at MD Anderson (10, 20). Bis-ester prodrugs are cleaved or bioactivated via esterases (21). Where the first POM or POC ester is initially cleaved by a class of enzymes known as carboxylesterases (20), the first SATE ester is initially cleaved by a class of enzymes known as thioesterases; the first SATE ester can also be cleaved by carboxylesterases (22). The second POM, POC, or SATE ester, is cleaved by phosphodiesterases (22). Examples of successful, FDA-approved bis-ester prodrugs include the anti-HIV drug tenofovir disoproxil (Viread[®]) (13) and the anti-HBV drug adefovir dipivoxil (Hepsera[®]) (23), which use POC and POM prodrugs, respectively. In the case of HEX, our lab initially attempted to immediately resolve the issue of poor membrane permeability and provide initial *in vivo* proof-of-concept of the collateral lethality paradigm by attaching POM esters onto the phosphonate moiety of HEX (**Figure 2**).

Bis-ester phosph(on)ate prodrugs were designed for intracellular, bioreversible delivery of monophosphate nucleotide analogues, which are anionic and poorly cell permeable (10). A major, well-documented issue with bis-ester prodrugs *in vivo* is the tendency for one ester moiety to be prematurely cleaved in the bloodstream prior to crossing the cell membrane due to the presence of serum esterases (24) capable of removing ester groups on net neutral, but not anionic substrates. If the subsequently released molecule is a phosphate monoester, it can then be subject to dephosphorylation by phosphatases or nucleosidase (if the substrate is a nucleotide analogue) (25, 26). However, if the subsequently released molecule is a phosphonate monoester, dephosphorylation is prohibited due to the inability for hydrolases to cleave C-P bonds. For bis-ester phosphonate prodrugs, the poorly permeable free phosphonate is often predominant species that circulates *in vivo* (27–29). Differential expression of serum esterases across model species greatly influences the half-life ($T_{1/2}$) and pharmacokinetic properties of bis-ester phosph(on)ate prodrugs, which is a persistent challenge for developing this class of prodrugs (29, 30).

1.2.2 Class 2: McGuigan prodrugs

McGuigan (ProTide) prodrugs are characterized by the presence of phenol and L-amino acid ester groups attached to the phosph(on)ate and were first described by Christopher McGuigan while he was at the University of Southampton (**Figure 4**) (31). McGuigan prodrugs are bioactivated through the following sequence of enzymes: 1.) carboxylesterase 1 (CES1)/cathepsin A (CTSA) and 2.) histidine triad nucleotide-binding protein 1 (HINT1; **Figure 5**) (32, 33). In contrast to bis-ester prodrugs, attachment of McGuigan prodrugs turns the phosphorous atom into a stereocenter due to the presence of four unique substituents. Bioactivation of McGuigan prodrugs occurs in a

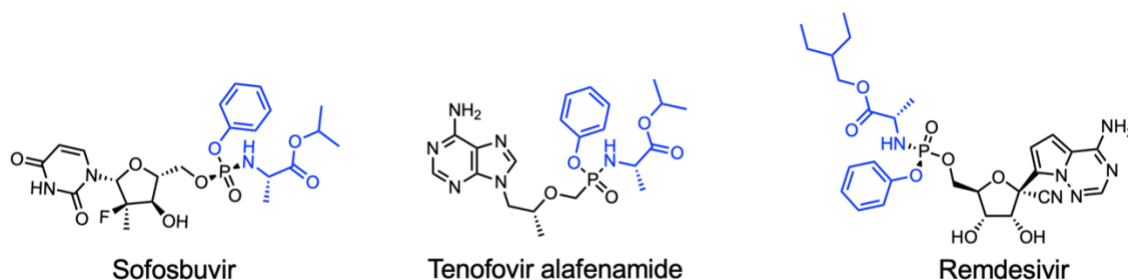


Figure 4. FDA-approved McGuigan prodrugs. Promoieties are indicated in blue. Interestingly, they are all Gilead compounds.

stereospecific manner, with the *Sp* having greater potency than the *Rp* isomer ((32–36). There are currently 3 FDA-approved drugs that employ McGuigan prodrugs: the anti-HCV drug sofosbuvir (Sovaldi®) (14) the second-generation anti-HIV agent, tenofovir alafenamide (Vemlidy®) (37), and the anti-SARS-CoV-2 drug remdesivir (Veklury®) (38). Similar to the *in vivo* outcome of bis-ester prodrugs, however, the inclusion of an esterase-labile moiety in the McGuigan prodrug results in premature hydrolysis and formation of the intermediate L-alanyl metabolite (**Figure 5**) (39–41) in plasma. Similar to formation of the phosphate mono-ester intermediate for bis-ester prodrugs, formation of the L-Ala *phosphoramidate* intermediate in plasma can also result in dephosphorylation by phosphatases or nucleosidases (if the substrate is a nucleotide analogue; **Figure 5**) (40–42). However, formation of the L-Ala *phosphonoamidate* intermediate in plasma mainly results in de-amidation rather than dephosphorylation due to the inability for enzymes to cleave P-C bonds (43, 44). Evidently, the resulting free phosphonate has poor cell permeability.

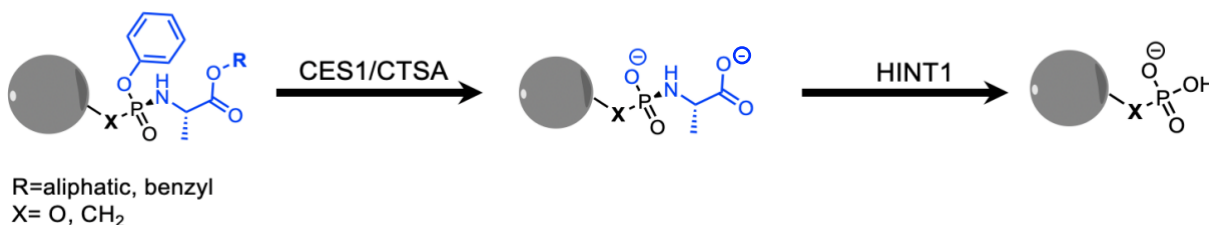


Figure 5. General bioactivation mechanism of McGuigan prodrugs. Promoiety is indicated in blue. Grey circle indicates a generic pharmacophore.

1.2.3 Class 3: Alternate prodrugs

A broad, emerging class of phosph(on)ate prodrugs attempts to forgo esterase bioactivation and harness enzymatic or environmental features unique to a given pathology. Due to the polyprotic nature of phosph(on)ates, two prodrug moieties are required to render the molecule neutral (9). Of the two promoiety, only one is required to be “directing group” that enables selective bioactivation of the drug at the site of pathology. Inevitably, this class of prodrugs is structurally diverse because the identity of the “directing group” can be tailored to

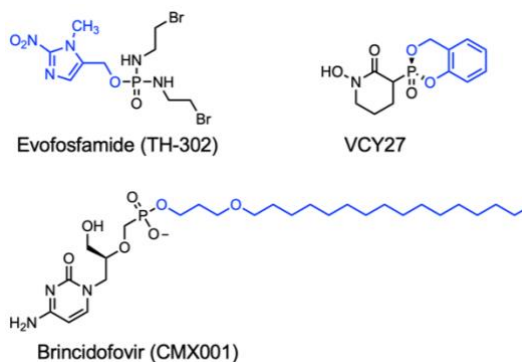


Figure 6. Examples of alternative prodrugs. Promoiety is indicated in blue. Evofosfamide is an example of a nitroheterocyclic prodrug. VCY27 is an example of a cycloSal prodrug. Brincidofovir is an example of a lipid prodrug

enzymatic or environmental distinctions of the pathology (45). One example of a Class 3 prodrug strategy capitalizes on the tendency for many solid tumors to exhibit hypoxia (46) by attaching a nitroheterocyclic promoiety to a phosphoramidate nitrogen mustard (**Figure 6**) (15). It has been proposed that, in hypoxic environments, a class of enzymes known as nitroreductases are expressed and capable of facilitating 2-electron reduction of the nitroheterocycle for removal (47). Another example of a Class 3 prodrug strategy forgoes enzymatic activation altogether and instead relies on local alkalinity or more broadly, the presence of nucleophiles, for bioactivation. The most advanced form of these nucleophilicity-activated promoieties uses salicylic alcohol derivatives to protect the phosph(on)ate and are generally known as cycloSal prodrugs (**Figure 6**) (48). In general, Class 3 prodrugs largely remain in preclinical development.

1.3 Overview of Case Study 1: HEX and POMHEX

To realize the potential of the *collateral lethality* paradigm (4, 5), our laboratory has focused on developing a small molecule inhibitor of ENO2 for selective targeting of cancers harboring homozygous deletion of ENO1. There are 3 isoforms of enolase: ENO1, ENO2, and ENO3. ENO3 is found exclusively in striated muscle tissue (49, 50). In all cell types except for muscle, ENO1 is the predominant isoform of enolase; ENO2 is expressed at about 1-10% the level of ENO1 in most cell types (Human Protein Atlas: ENO1, ENO2, ENO3). Even though ENO2 is often referred to as neuronal enolase, ENO1 is still the dominant isoform in the neuroendocrine tissue (51). Therapeutic targeting of ENO2 in ENO1-deleted cancers is possible because most tissues solely express ENO1/2: cancers harboring deletions of ENO1 are entirely reliant on ENO2 to catalyze the penultimate step of glycolysis (4).

Enolase is a glycolytic enzyme that facilitates the conversion of 2-PG to PEP. Much like other glycolytic intermediates, both 2-PG and PEP are highly polar metabolites; unsurprisingly, the transition state between 2-PG and PEP are also highly polar. Initial efforts to design a small molecule inhibitor of enolase centered on the development of an active site transition state analogue. Mechanistic biochemical experiments conducted in the 1980s showed that a phosphonate-containing tool compound (phosphoacetoxyhydroxamate; PhAH, **Figure 2**) acts as a transition-state analogue that inhibits enolase with nanomolar affinity (52, 53). Because PhAH does not exhibit sufficient selectivity for ENO2 over ENO1 (6), structure activity relationship

(SAR) studies were conducted. Achieving selectivity for ENO2 over ENO1 is challenging because the two isoforms share at least 70% identity, with even greater similarity at the active site (6, 29). It was hypothesized forming a cyclic version of PhAH would increase specificity for ENO2 because its active site is slightly more spacious compared to that of ENO1. This hypothesis resulted in the discovery of SF2312, a 5-membered ring natural product, as a noncompetitive inhibitor of enolase (6). Despite exhibiting low nanomolar affinity for enolase, SF2312 lacked sufficient specificity for ENO2. Synthesis and *in vivo* testing of a cell-permeable, bis-POM ester prodrug of SF2312 resulted in hemolytic anemia in mice due to on-target inhibition of ENO1 in red blood cells (RBCs), which is the only isoform of enolase expressed in RBCs (6, 29). Pan-enolase inhibition is thus therapeutically prohibited due to induction of hemolytic anemia (7, 8), reinforcing the need to identify a core pharmacophore with sufficient specificity for ENO2.

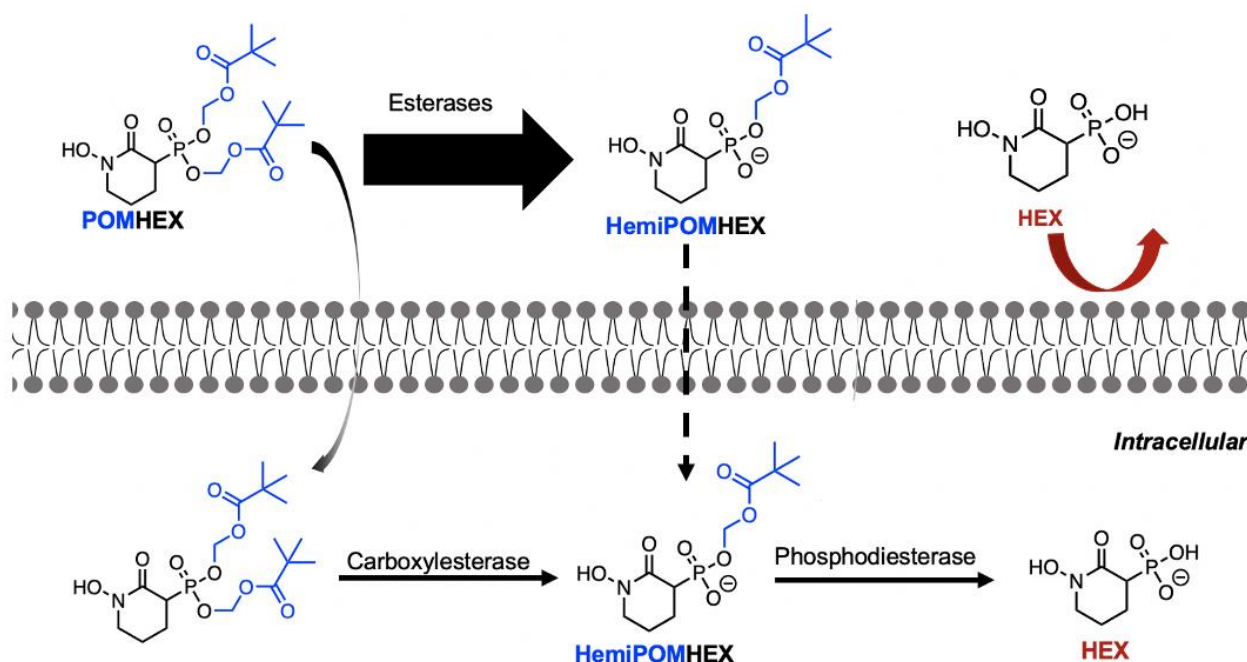


Figure 7. Structures of POMHEX, HemiPOMHEX, and HEX with corresponding bioactivation mechanism *in vivo*. HEX is a phosphonate-containing drug that is anionic at physiological pH, hampering membrane permeability. POMHEX was designed as a membrane permeable bis-ester prodrug. However, rapid extracellular hydrolysis of the first POM group reveals a negative charge (HemiPOMHEX), hindering membrane permeability.

Further expanding the backbone resulted in the generation of a cyclic, 6-membered ring version of PhAH that we termed HEX (**Figure 2**) (29). HEX is a substrate competitive inhibitor of enolase that demonstrates approximately 4-fold specificity for ENO2 over ENO1 (K_i =64 nM versus 232

nM, respectively) (29). Against cancer cells in culture, HEX showed preferential killing of *ENO1*-deleted glioma cells compared to *ENO1*-WT or isogenic-rescued cell lines at micromolar concentrations. As a phosphonate-containing inhibitor, HEX is negatively charged at physiological pH, which impedes its membrane permeability and explains its micromolar-range IC₅₀ against *ENO1*-deleted cells in culture despite possessing a nanomolar K_i for ENO2. To improve membrane permeability, a bis-POM ester prodrug of HEX, termed POMHEX, was generated (**Figure 7**). Compared to HEX, POMHEX demonstrated superior potency against *ENO1*-deleted glioma cells in culture while maintaining a wide therapeutic window against *ENO1*-WT or isogenic rescued cell lines at nanomolar concentrations. Consistent with the robust body of literature demonstrating the poor stability of bis-ester POM prodrugs in biological fluids (13, 23), POMHEX exhibited poor stability in mouse and human plasma *ex vivo* and was undetectable after administration to mice *in vivo*. Again, this is due to the presence of plasma esterases (24). As the core pharmacophore (HEX) contains a phosphonate (rather than a phosphate), premature hydrolysis of the first POM ester on POMHEX results in the formation of the HemiPOMHEX monoester in plasma without further ester hydrolysis.

While both HEX and POMHEX have their sets of shortcomings, both were still tested in xenografted orthotopic tumors harboring deletion of *ENO1* in mice to provide immediate *in vivo* proof-of-principle of the collateral lethality paradigm (29). Both compounds were capable of eradicating *ENO1*-deleted gliomas *in vivo*; HEX was dosed at 150 mg/kg IV + 100 mg/kg IP for 5 days while POMHEX was dosed at 10 mg/kg IV + 10 mg/kg IP for 5 days. Evidently, poor membrane permeability of the free phosphonate HEX was sufficiently overcome at high doses. The highly polar nature of HEX amidst its ability to cause on-target regression of tumors implanted in the brain (29) strongly suggests that it reaches the brain through the blood-CSF barrier, rather than the blood-brain-barrier (BBB). Importantly, efficacy was demonstrated even in GBM mouse xenograft models with an intact BBB; these data are particularly promising, considering that GBM is typically characterized by a breached BBB. This would concur with the latter's preference for lipophilic compounds (29) and the ability for similar, low molecular weight (MW) phosphonate compounds, such as fosfomycin, to reach the brain through the blood-CSF barrier (54, 55). The antineoplastic effects of POMHEX at much lower drug concentrations than HEX, despite its poor PK, can be rationalized by the combinatorial effects of HemiPOMHEX and HEX (released from

cells) through the blood-CSF barrier. A significant limitation with POMHEX is that rapid hydrolysis of the first POM ester results in a steep, diminishing concentration gradient of intact POMHEX and a tandem increasing concentration gradient of HemiPOMHEX away from the initial site of injection (29). As a result, a high concentration of HemiPOMHEX accumulates in the heart, which could potentially be quite detrimental. Thus, we seek to identify novel prodrugs with improved PK properties for optimal, low dose delivery of the active pharmacophore to gliomas.

1.4 Overview of Case Study 2: Cyclophosphamide

Cyclophosphamide (**Figure 8**) is a DNA-alkylating agent of the nitrogen mustard class. It is a classical chemotherapeutic agent that was initially approved by the FDA in the 1950s for use against cancers such as malignant lymphomas, among others (56). It is often used as part of various chemotherapy regimens, such as R-CHOP (rituximab, cyclophosphamide, doxorubicin, vincristine, prednisone) (57). As a DNA damaging agent, one might expect that cyclophosphamide would be far too toxic to

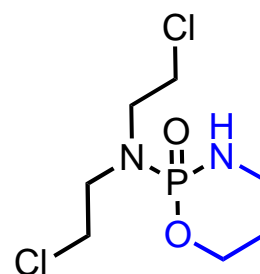


Figure 8. Structure of cyclophosphamide.
Promoiety is indicated in blue.

rapidly proliferating tissues, which oftentimes have higher proliferation indices than many cancers, to exert any meaningful therapeutic effects on cancerous tissue (45). While it is true that cyclophosphamide is toxic to many prolific tissues, it is still able to achieve a sufficient—albeit narrow—therapeutic window to impart its therapeutic effects by capitalizing on differential expression of aldehyde dehydrogenase (ALDH) between normal and cancer cells (58, 59).

1.5 Overview of Case Study 3: Sofosbuvir

Sofosbuvir (SOF) is a prodrug nucleotide analogue of the McGuigan class (**Figure 9**) designed for the treatment of HCV (42). The molecule was developed by Pharmasset, Inc. (later bought by Gilead Sciences) (34), but the parent nucleoside of SOF was initially developed by Roche (14). While the active nucleoside triphosphate (NTP) is a somewhat potent inhibitor the NS5B polymerase, with a K_i of $0.42 \pm 0.04 \mu\text{M}$ (14, 60, 61), the nucleoside of sofosbuvir (RO2433, uridine analogue) is inefficiently phosphorylated by intracellular nucleoside kinases (deoxycytidine kinase dCK, uridine kinase UCK, or thymidine kinase TK) to the corresponding

monophosphate (**Figure 6**) (61). SOF was thus designed as an orally bioavailable prodrug that would efficiently deliver the intracellular nucleoside monophosphate analogue to bypass the initial phosphorylation reaction (34, 60). Interestingly, sofosbuvir was the not the first anti-HCV nucleotide analogue to utilize the McGuigan prodrug strategy (62). However, it is one of the few anti-HCV phosphoramidate prodrugs that reached clinical trials (63, 64) and subsequently received approval by the FDA (42). As described in *Section 1.2.2*, McGuigan prodrugs such as sofosbuvir are bioactivated through CES1/CTSA and HINT1. As a result, sofosbuvir experiences hydrolysis of its L-Alanine ester promoiety in plasma (42, 65), which eventually results in release of the essentially inactive nucleoside RO2433. Inactivation of the intact prodrug to the parent nucleoside RO2433 is offset by the first-pass effect arising from oral administration of sofosbuvir, which enables high loading of sofosbuvir and its corresponding NTP in the liver. Again, this is because McGuigan prodrug activating enzymes are highly expressed in the liver (*more in Chapter 5*). For a liver-specific pathology such as hepatitis, this paradigm is ideal as any remaining release of RO2433 is essentially innocuous due to its inability to be efficiently converted to the bioactive NTP in visceral organs.

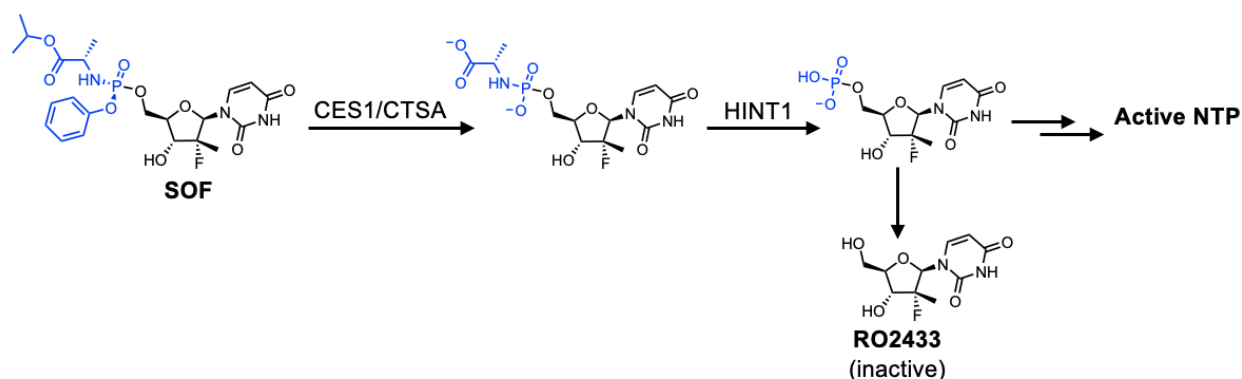


Figure 9. Bioactivation of SOF. SOF is orally administered and subject to significant hepatic extraction during first pass metabolism.

1.6 Overview of Case Study 4: GS-441524 and remdesivir

Remdesivir (RDV) is another prodrug nucleotide analogue of the McGuigan class that was initially designed for the treatment of HCV by Gilead Sciences (66), later investigated for the treatment of EBOV (67), and now FDA-approved for the treatment of COVID-19 (38, 68). In contrast to the many pyrimidine analogues that were being investigated as NS5B inhibitors (34), the nucleobase of RDV (and its corresponding nucleoside core, GS-441524) is a purine (adenine) analogue (**Figure 10**). Compared to the sofosbuvir NTP, the RDV NTP (GS-443902) had much lower

affinity for the NS5B polymerase ($K_i \sim 5 \mu\text{M}$ (35)), which could explain its failure to advance as an anti-HCV drug. The decision to attach McGuigan prodrugs onto GS-441524 was borne out of a similar rationale as that applied for sofosbuvir: because the sofosbuvir nucleoside (RO2433) was inefficiently phosphorylated by nucleoside kinases, the McGuigan prodrug approach was pursued. While no matched biochemical studies with GS-441524 supported the notion of completely inefficient phosphorylation of the nucleoside, the McGuigan prodrug strategy was nonetheless pursued to generate RDV.

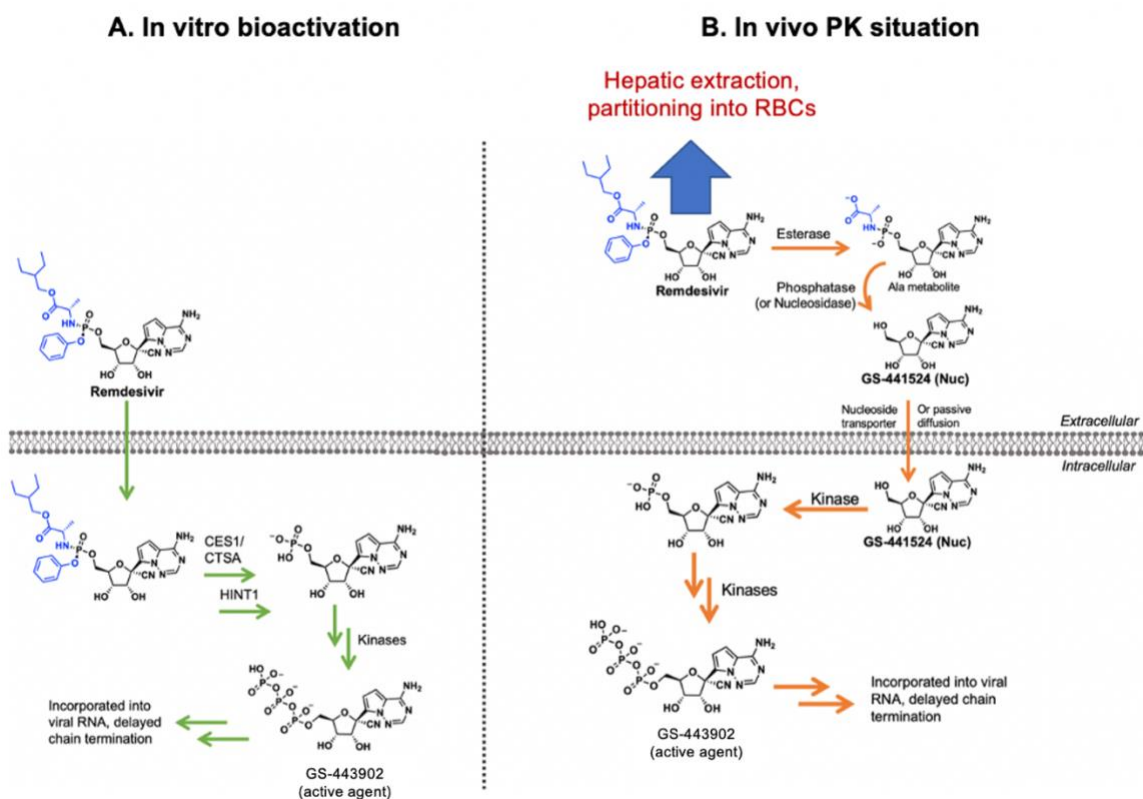


Figure 10. *In vitro* versus *in vivo* metabolism of RDV. (A) The ideal bioactivation of remdesivir predominately occurs *in vitro*. (B) The presence of serum enzymes *in vivo* predominately results in premature hydrolysis of the phosphate prodrugs, followed by dephosphorylation to the nucleoside, GS-441524. Other factors, including the influence of hepatic extraction and trapping of the L-Ala intermediate in RBCs, account for significant differences between *in vitro* and *in vivo* metabolism.

It should be noted that a 2' methylated ribose derivative of RDV, GS-6620 (32, 69), was actually the compound that Gilead Sciences elected to advance to clinical trials for HCV (63). In contrast to RDV, which has only been clinically administered IV, GS-6620 was evaluated as an oral agent in patients with chronic genotype 1 HCV (63), which is concurrent with liver-specific delivery of

McGuigan prodrugs. While GS-6620 was well-tolerated in the phase 1 trial when administered as 450 mg BID or 900 mg BID tablets or as a 450 mg solution, a central issue that Gilead encountered was high PK/PD variability (63, 69). Poor predictability of GS-6620 partly resulted in its discontinued investigation. It is speculated that a central reason for discontinued investigation of GS-6620 and similar 2' methylated ribose compounds was that a similar anti-HCV purine analogue, BMS-986094 (formerly INX198), was cardiotoxic and resulted in the death of a patient in a phase 2b trial (70–72).

Unlike GS-6620, RDV does not have a 2' methyl substituted ribose (**Figure 10**) and was synthesized as part of the family of compounds as GS-6620 that were initially developed for HCV (73). After what can essentially be considered clinical failure of GS-6620, initial clinical experience with RDV was for the treatment of the EBOV (68). Following an interim analysis in a phase 3 trial, RDV was less effective compared to competing treatments MAb114 and REGN-EB3, two monoclonal antibodies, which prompted the data safety and monitoring board to recommend that patients be re-assigned to one of the latter two treatments—ending further development of RDV for the treatment of EBOV. Having already cleared early-stage clinical trials for EBOV (NCT02818582), RDV was immediately evaluated for its anti-COVID-19 efficacy in phase 3 trials beginning in early 2020 (74).

The family of compounds that includes RDV and its parent nucleoside, GS-441524, are broad-spectrum, direct-acting antivirals with activity against several RNA viruses (66, 73, 75). Thus, while RDV and GS-441524 were not specifically designed to inhibit the RNA-dependent RNA polymerase (RdRp) of SARS-CoV-2, the active triphosphate, GS-443902, has high affinity for the SARS-CoV-2 RdRp, with a K_m of approximately 8.9 nM (76), which happens to be lower than for the HCV NS5B polymerase ($K_m \sim 5 \mu M$) (35, 66). Since its initial report in 2016 (67, 77), a vast body of literature on the biochemical and pharmacological properties of RDV have accumulated on its broad-spectrum antiviral activities *in vitro* (35, 75, 76, 78–81) and *in vivo* (39, 40, 82–84). One outstanding theme prevalent in all *in vivo* studies on RDV conducted to-date is its remarkably short $T_{1/2}$ in both preclinical species (39, 40, 67) and in patients administered RDV IV (41, 85, 86). This is similar to PK parameters of other esterase-labile phosphate prodrugs of the McGuigan class (see *Section 1.2.2*), including GS-6620 (63), GS-9148 (experimental NRTI) (87), and most

prominently, SOF (42, 88). However, unlike the multiple studies demonstrating the inactivity of the SOF parent nucleoside, RO2433 (34, 60, 61), studies with the parent nucleoside of RDV, GS-441524, showed that it was able to exert broad spectrum antiviral activity across multiple cell lines (66, 75, 81, 84, 89). These data indicate that, unlike RO2433, GS-441524 can be efficiently phosphorylated by nucleoside kinases (likely adenosine kinase, ADK). Because McGuigan prodrugs such as RDV are preferentially activated in the liver (see *Section 1.2.2*), I have proposed that GS-441524 would be superior for the treatment of non-liver-centric pathologies such as COVID-19 (17, 90, 91). Efforts to evaluate the anti-SARS-CoV-2 activity of GS-441524 *in vitro* and *in vivo* are ongoing (18, 92–94). A detailed discussion on the merits of GS-441524 over RDV in non-liver-specific pathologies is presented in *Chapter 5*.

1.7 Current approaches towards the synthesis of mixed phosph(on)ate prodrugs

Note: In this section, I introduce the terms *phosphoric acid* and *phosphonic acid*. Both terms refer to the protonated counterparts of *phosphate* and *phosphonate* (**Figure 11**), respectively. I refer to the protonated forms when discussing reactions occurring in organic solvents.

The attachment of non-identical, mixed, promoieties (e.g. Class 2 and 3) onto phosph(on)ates has traditionally been logistically challenging for three general reasons: 1.) the reactivity of phosph(on)ates is less well-characterized compared to their carboxylic acid counterparts and 2.) classical techniques readily employed in organic chemistry, such as silica-based

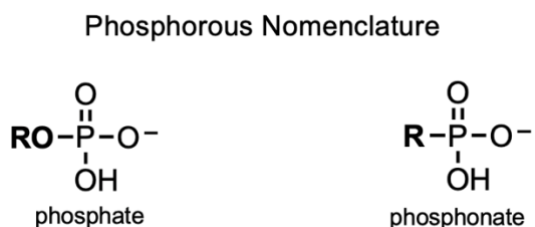


Figure 11. Structures of a phosphate (left) versus phosphonate (right).
R=aliphatic, aromatic, benzylic

chromatography, are poorly suited to oxyphosphorous compounds such as phosphate- and especially phosphonate-containing compounds. This is primarily due to the highly polar nature of the phosphorous-oxygen bond and the high affinity of silicon for oxygen. As a result, attempts to run phosph(on)ate-containing compounds on silica results in compound streaking and poor separation; the former is particularly true for phosphonate compounds. Another obstacle related to the synthesis of mixed promoieties is the need to consider chiral resolution of the phosph(on)ate product because the phosphorous atom becomes a stereocenter. While stereochemistry at

phosphorous does not appear to significantly alter bioactivity of some promoieties (95–98), isomer purification is especially important for McGuigan prodrugs, as it has been repeatedly demonstrated that hydrolysis by CES1/CTSA is more efficient for the *Sp* rather than the *Rp* configuration (14, 32, 34). Below is a brief overview of some considerations that should be kept in mind when pursuing phosph(on)ate chemistry. This is not an exhaustive account but rather a portrait of general themes intended to parse the nuances of phosphate and phosphonate chemistry. A comprehensive survey of synthetic approaches towards phosph(on)ate prodrugs was written in 2014 by Pradere *et al.* in *Chemical Reviews* (16).

The synthesis of mixed phosph(on)ate prodrugs is also technically challenging and differs from considerations made when working with their carboxylic acid counterparts (9, 16). There are 3 main challenges that must be considered when synthesizing such promoieties: 1.) hazardous reagents and highly water-sensitive intermediates, 2.) propensity for phosph(on)ates to dimerize with traditional coupling reagents, and 3.) different reactivity profile of the starting phosph(on)ate and the intermediate phosph(on)ate ester or phosphonoamidate/phosphoramidate. A key example

of how phosphonic and phosphoric acids differ from their carboxylic acid counterparts is in the formation of anhydrides. Dimerization readily occurs under typical coupling conditions (halogenation, peptide-like couplings) for all three chemical moieties. However, unlike anhydrides formed from carboxylic acids, which are susceptible to aqueous hydrolysis, phosphoanhydrides formed from phosphonic and phosphoric acids are highly stable in water provided they are anionic. This is because the negative charge repels incoming nucleophilic attack by water. If the phosphoanhydride is esterified and thus uncharged, the molecule is more susceptible to aqueous hydrolysis. This would explain Nature's use of phosphate dimers in the form of ATP (and di- and triphosphates) as energy storage molecules. While dimerization of phosphonic and phosphoric acids is seemingly not discussed in the phosph(on)ate chemistry community, it nonetheless is a

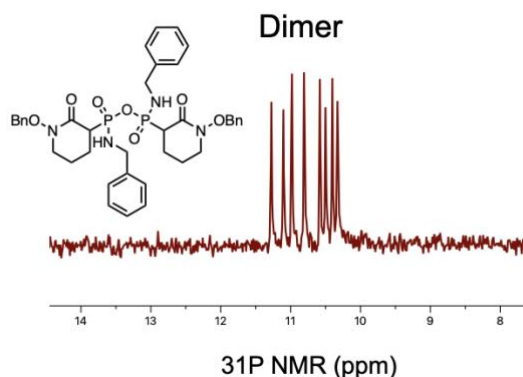


Figure 12. Dimerization of BnHEX benzylamine during an S_N2 reaction. BnHEX benzylamine is a benzyl-protected synthetic intermediate we use in prodrug synthesis.

pervasive issue that underpins most coupling reactions. In our experience, even large CROs have struggled with overcoming the issue of phosphonate dimerization.

1.7.1 Considerations for phosphate prodrug synthesis

Unlike phosphonate prodrugs, phosphate prodrugs can be (but does not necessarily have to be) assembled using standardized, convergent synthetic approaches in which the phosphate prodrug fragment and pharmacophore (usually a nucleoside) are first prepared separately and then coupled together. Common techniques to couple the prodrug fragment and parent pharmacophore include P(III)-based phosphoramidite and oxidation (99) and nucleophilic phosphoryl substitution of phosphoryl chlorides and corresponding alcohols (16). Though commonly employed in the synthesis of nucleotide prodrug analogues (16, 35, 69, 100), this fragment-based, convergent synthesis can be applied to a wide variety of structurally diverse parent pharmacophores that contain a free alcohol for attachment (101–103).

It should be noted that the approaches discussed below (*Section 1.7.2*) for the synthesis of phosphonate prodrugs can also be applied to phosphate prodrug synthesis. However, such methods are not commonly used to generate phosphate prodrugs due to the challenges associated with the subsequently described methods (16).

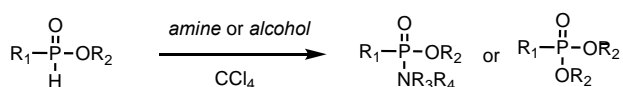
1.7.2 Considerations for phosphonate prodrug synthesis

Phosphonate prodrugs cannot be formed using a standardized approach as described for phosphate prodrugs. This is because, unlike phosphate prodrugs in which the alcohol of the parent pharmacophore is linked with the phosphate promoiety, the phosphonate promoiety is characterized by a P-C bond linkage, where the C can be alkyl, benzyl, or aryl. Fragment-based, convergent syntheses of phosphonate prodrugs are possible under specific circumstances. Two instances where the phosphonate moiety has been installed onto the parent pharmacophore is in a synthesis of the acyclic nucleotide analogues, adefovir dipivoxil (ADV) and tenofovir disoproxil (TDF) (104). Here, convergent synthesis is possible due to the presence of an oxygen atom *beta* to the phosphonate, which can be tosylated or mesylated and then linked via S_N2 with the N⁹ ethyl alcohol on the nucleobase (104–106). While this convergent synthesis unites the phosphonate component and the nucleobase portions of ADV or TDF, it is notable that the phosphonate

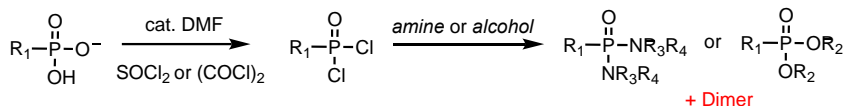
fragment is not the fully prepared, final promoiety as observed in the convergent synthesis of phosphate prodrugs. This is likely because the S_N2 reaction between the ADV or TDF nucleobase and the tosylated or mesylated phosphonate fragment proceeds under basic conditions, which contrasts the acidic or mildly alkaline conditions used for *O*-phosphorylation reactions joining the phosphate promoiety and the parent pharmacophore (35, 69). In the cases of ADV and TDF, which are phosphonate ester prodrugs (Class 1 in *Section 1.2.1*), the bis-ester moieties would likely hydrolyze under the harsh, alkoxide-catalyzed conditions of the S_N2 reaction (105, 106). Thus, for the preparation of ADV and TDF, a fragment-based approach can be used to attach the free phosphonate; however, esterification of the phosphonate is accomplished subsequently (104–106). Similar concerns of promoiety hydrolysis during the S_N2 reaction are also relevant in the synthesis of the Class 2 (see *Section 1.2.2*) relative of TDF, tenofovir alafenamide (TAF). Similar to the ester moieties on ADV and TDF, the phenol moiety on TAF is alkaline-labile and prevents assembly of the McGuigan phosphonate promoiety before S_N2 reaction with the nucleobase (106). Thus, due to the reaction condition incompatibilities—even in cases that are amenable to a fragment-based approach (ADV, TDF, TAF)—attachment of promoieties onto phosphonates typically occurs after the phosphonate is installed on the parent molecule. As a result, reactivity of functional group(s) on the parent molecule must be considered to avoid unwanted cross reactivity with the activating agent, coupling agent, or nucleophile.

Attachment of commonly used Farquhar prodrug esters can proceed via S_N2 displacement of the electrophilic alkyl halide esters and the free phosphonic acid nucleophile, as in the cases of ADV and TDF (104–106). However, attachment of non-halogenated, nucleophilic promoieties, such as those containing an alcohol or

Atherton-Todd reaction (*in situ* chlorination)



Chlorination, then nucleophilic displacement



Peptide-like couplings

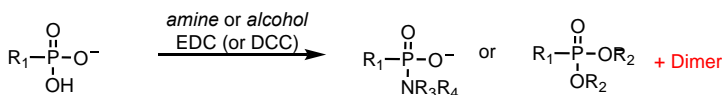


Figure 13. Common synthetic approaches towards phosph(on)ate prodrug synthesis. The Atherton-Todd reaction may also form a dimer, but I have no personal experience with this and have not encountered reports in the literature on this. R_1 , R_2 , $\text{R}_4=\text{O}$, aliphatic, benzylic, aromatic. $\text{R}_3=\text{aliphatic}$, H

amine, requires activation of the phosphonic acid to increase its electrophilicity and enable nucleophilic phosphoryl substitution reactions or variants thereof (**Figure 13**). Activation of the phosphonic acid and nucleophilic displacement can occur by either stepwise or concerted mechanisms.

Stepwise syntheses involve halogenation (typically chlorination) of the phosphonic acid. The resulting phosphoryl halide, though highly susceptible to hydrolysis in the presence of trace amounts of water, can be isolated. Commonly used reagents pairs to activate the phosphonic acid include thionyl chloride (SOCl_2)/catalytic dimethyl formamide (DMF), oxalyl chloride ($(\text{COCl})_2$)/catalytic DMF, and phosphorus oxychloride (POCl_3); such reagents are commonly used in the synthesis of acyl chlorides from carboxylic acids. However, unlike carboxylic acids, which only have one free -OH that can be halogenated, phosphonic (and phosphoric) acids have two free -OHs. While a dichlorinated phosphonic acid is amenable to reaction with nucleophilic promoieties to form the corresponding bis-ester prodrug, it is more difficult to generate mixed phosphonate prodrugs (Class 2 and Class 3 prodrugs as described in *Section 1.2.2* and *Section 1.2.3*) under such conditions. Nevertheless, mixed phosphonate prodrugs have been generated using this approach with highly variable yields (~25-60%) (107–109). In addition to experimental variability (e.g. degree of dryness of reagents and glassware), different reactivity profiles between the dichloride and mono-adduct could partly explain inconsistency in yields—especially when the mixed phosphonate prodrug contains both a P-O and P-N bond. As I will explain in greater depth in *Chapter 2*, phosphonate monoesters and phosphonoamidates exhibit different reactivity profiles. One seemingly uncommon approach to exert better control over formation of the final mixed phosphonate is by forming the monochlorinated product first and adding the first promoiety, then using a second reaction to add the next promoiety (**Figure 10**). Monochlorination of phosphonic acids can be accomplished using POCl_3 , rather than SOCl_2 or $(\text{COCl})_2$ with catalytic DMF (110); nonetheless reactions must be carefully monitored to avoid forming the dichlorinated product.

Concerted syntheses involve the use of coupling reagents in addition to the nucleophilic promoieties. In contrast to stepwise syntheses, in which the activated phosphonic acid can be isolated and the nucleophiles can be added sequentially, the activated phosphonic acid is often too unstable and transient to be isolated. Coupling reagents include those commonly used in peptide

synthesis: N, N'-dicyclohexylcarbodiimide (DCC) and 1-ethyl-3-(3-dimethylaminopropyl)carbodiimide (EDC) (16). Another less commonly used concerted addition is the coupling of nucleophiles under Mitsunobu conditions (triphenyl phosphine, PPh₃; and an azo reagent such as diisopropyl azodicarboxylate, DIAD). Reactions using DCC or Mitsunobu conditions have typically been used with alcohol nucleophiles to generate the corresponding mono- or di-ester (16) while reactions using EDC conditions have typically been used with amine nucleophiles to generate the corresponding monoamidate (111). While concerted syntheses are generally attractive for their use of less hazardous, milder conditions, a challenge associated with the aforementioned coupling conditions is the propensity for phosphonic acids to dimerize (112) more frequently than observed in stepwise syntheses (described in greater detail in *Chapter 2*), as it can act both as the nucleophile and the electrophile.

Another complicating factor for phosph(on)ate prodrugs that is exacerbated during the synthesis of phosphonate prodrugs of the McGuigan class is that chirality at phosphorous influences the efficiency of enzymatic removal by CTSA and CES1, with the *Sp* configuration often exhibiting slightly greater potency against the target cell population *in vitro* (32, 33, 35, 100). Unlike phosphate McGuigan prodrugs, in which a fragment approach can be taken to generate the McGuigan fragment with the desired stereochemistry, such an approach cannot be readily applied to phosphonate McGuigan prodrugs for reasons described earlier. Chiral resolution of the desired stereoisomer is typically achieved after the racemic phosphonate-containing parent compound is generated (**Figure 13**) (113). This is not ideal, as the undesired stereoisomer formed cannot be recycled and is essentially a dead-end product. Efforts to optimize the diastereomeric excess (d.e.) or select for the desired diastereomer include selective recrystallization, altering the salt form, altering reaction parameters (113), introducing catalysts (114), and chromatographic techniques (115, 116). There are comparatively few examples of phosphonate McGuigan prodrugs, with the best described example TAF. Currently, the *Sp* isomer of TAF is obtained via simulated moving bed chromatography followed by recrystallization (115).

Overall, there are several challenges associated with phosph(on)ate prodrug synthesis. In general, difficulties encountered during phosphate prodrug synthesis are exacerbated in phosphonate prodrug synthesis, which is largely because the latter is oftentimes not amenable to convergent

synthesis. Differences in reactivity between the starting phosphoric or phosphonic acid and the initial prodrug adduct, introducing chirality at phosphorous, the use of hazardous reagents, and the propensity for phosph(on)ates to dimerize are obstacles that differentiate phosphoric and phosphonic acids from their carboxylic acid counterparts.

1.8 Conclusions and Foreword

Currently, prodrugs comprise less than 20% of all FDA-approved drugs (9). Within this subset, six drugs are phosph(on)ate prodrugs that are specifically designed to improve cellular permeability, as opposed to simply improving the water solubility of a hydrophobic drug. Among the six FDA-approved phosph(on)ate prodrugs designed for enhanced intracellular delivery, two are Class 1 prodrugs (*Section 1.2.1*; ADV, TDF), 3 are Class 2 prodrugs (*Section 1.2.2*; SOF, TAF, RDV), and one is a Class 3 prodrug (*Section 1.2.3*; cyclophosphamide). With the exception of cyclophosphamide, all FDA-phosph(on)ate prodrugs intended for improved intracellular delivery are direct-acting antivirals. Despite comprising a small fraction of all FDA-approved drugs, phosph(on)ate prodrug development is a promising area of development for two reasons: 1.) phosph(on)ate prodrugs have historically been quite effective either alone or in combination with other drugs and 2.) with the popularity of metabolomics in cancer metabolism research, one could therapeutically actionize on cancer-specific metabolic aberrations by designing competitive inhibitors (or activators) of phosphorylated metabolites. Due to the tunability of the two promoieties phosph(on)ate prodrugs are highly amenable to cell- and tissue-specific drug delivery and could thus serve as a valuable mechanism to realize the aims of precision medicine. Thus far, only two phosph(on)ate prodrug strategies have been heavily explored: Farquhar prodrugs (Class 1, *Section 1.2.1*) and McGuigan prodrugs (Class 2, *Section 1.2.2*). The latter strategy has been applied liberally in pre-clinical research and seemingly without careful consideration of the relationship between promoiety identity and cell- and tissue-specific bioactivation and while perhaps not acknowledging some key limitations associated with *in vitro* assays and PK/PD evaluations in model species.

Here, I consider the successes, shortcomings, and opportunities of phosph(on)ate prodrug development against the backdrop of the prodrug structure-bioactivation paradigm. The breadth of this body of work was inspired by lessons that I have learned from my own work on generating

novel prodrugs of our laboratory's enolase inhibitor, HEX, and in recognition that the GS-441524/remdesivir paradigm—sprung onto the world's center stage by COVID-19—is emblematic of the core challenges associated with phosph(on)ate prodrug development. Through the 5 case studies I present herein, I attempt to answer the question “what makes a phosph(on)ate prodrug successful in the clinic?” while identifying shortcomings related to phosph(on)ate prodrug synthesis and overreliance on certain preclinical models to project clinical success. The lessons crystalized in this discussion can provide guidance for designing more precise phosph(on)ate prodrugs that have better localization to the tissue and cell type of interest of a given pathology.

CHAPTER 2. DISCOVERY OF A NOVEL REACTION FOR EXPEDIENT MONO-AMIDATION OF PHOSPH(ON)ATES

This chapter has been published in (permission granted)

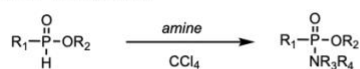
Yan VC, Pham C-D, Muller FL. 2020. Expedient Method for Direct Mono-amidation of Phosphonic and Phosphoric Acids. ChemRxiv <https://doi.org/10.26434/chemrxiv.12073131.V1>.

2.1 Abstract

Phosphoramidate or phosphonoamidate-containing prodrugs contribute to the vastly delivery of phosphate and phosphonate-containing anti-viral/cancer nucleotide analogues (16, 117, 118). However, synthetic approaches towards their formation are often harsh, unreliable, or generate water-soluble byproducts that can be difficult to separate from the anionic phosphoramidate or phosphonoamidate product (111). These technical difficulties could impede the identification of novel, more effective amine prodrugs. In this chapter, I show that direct mono-amidation of structurally complex phosphonic and phosphoric acids may be accomplished in as quickly as seconds under modified Mitsunobu conditions. Unlike traditional Mitsunobu couplings, where the triphenylphosphine oxide (TPPO) byproduct is often cited as a vulnerability (119), I use its formation as an asset. Juxtaposing the anionic nature of the generated mono-amidated product with the hydrophobicity of the oxide, the desired product may be isolated with a single water extraction. Compared to state-of-the-art strategies towards phosphoramidates and phosphonoamidates (16), this approach is mild, reliable, and enables access to a variety of aliphatic and benzylic amines for prodrug attachment.

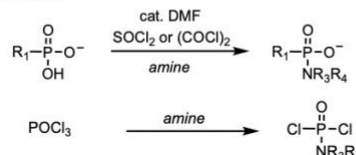
Previous work:

a.) Atherton-Todd reaction



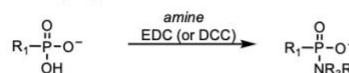
- Hazardous solvent
- Limited to H-phosphonate monoesters

b.) Chlorination



- Hazardous reagents
- Difficult to control
- Inconsistent yields

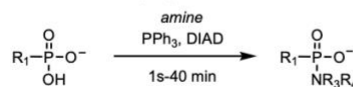
c.) Peptide coupling



- Difficult purification
- Issues with phosph(on)ate dimerization

This work:

c.) Novel Mitsunobu Coupling



$\text{R}_1, \text{R}_2 = \text{O-ester}, \text{R}_3 = \text{H, Me}, \text{R}_4 = \text{benzyl, aliphatic}$

- Mild conditions
- Short reaction times
- Reliable
- Simple purification

Scheme 1. Strategies for mono-amidation of phosphates and phosphonates

2.2 Introduction

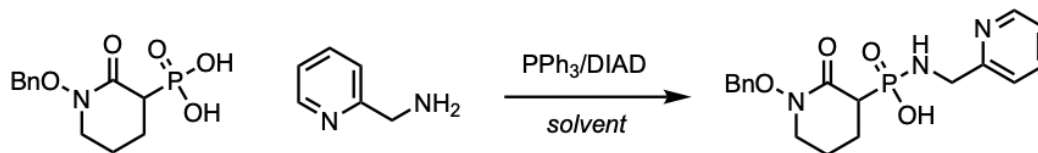
Phosphoramidates and phosphonoamidates are characterized by a single P(V)-N bond and are chemical moieties with high therapeutic relevance (120, 121). From TAF (44), to SOF (42), to RDV (38) phosphoramidates permeate the antiviral prodrug landscape. Yet for all their importance in improving the delivery of phosph(on)ate drugs, current mono-amidation strategies are subverted by their harsh reaction conditions, challenging purifications, and inconsistent yields (16) (**Scheme 1**). Two examples of common mono-amidation approaches include stepwise chlorination and concerted peptide-like couplings (*Section 1.2.7*). The former method not only requires the use of hazardous reagents, but also demands great precaution for handling the resulting phosphoryl dichloride, which is highly susceptible to hydrolysis. A similar variation on direct mono-chlorination is Atherton-Todd reaction (122), wherein reaction of dialkyl phosphite in CCl₄ produces a highly reactive mono-chlorinated intermediate that may be reacted with amines to generate the phosphoramidate. In addition to the hazardous solvent requirements, the Atherton-Todd conditions must be applied onto dialkyl phosphites (H-phosphonates) and cannot be applied directly onto phosphates or phosphonates. Finally, another set of methods include peptide couplings, which are challenged by the propensity for phosph(on)ates to dimerize, requiring vast excesses of amine and coupling reagent and/or dilute conditions to obtain the mono-amidated product (16, 123). Here, I show that direct mono-amidation of phosphonic or phosphoric acids may be accomplished using modified Mitsunobu conditions to quickly generate structurally diverse phosphonoamidates and phosphoramidates. In contrast to conventional Mitsunobu couplings, we use the resulting hydrophobicity of the TPPO byproduct as an asset, rather than a historically perceived vulnerability (124), enabling isolation of the anionic mono-amidate with a single water extraction. The mild and expedient nature of our reaction conditions enables simple attachment of various benzylic and aliphatic amines for exploration into their prodrug activity (98).

2.3 Results and Discussion

I first discovered the reaction while synthesizing mixed phosphonoamidate prodrugs of our laboratory's phosphonate-containing enolase inhibitor, HEX (29). A benzyl-protected precursor, BnHEX, was reacted with benzylamine, PPh₃, and DIAD in CH₂Cl₂ (**Figure 14a, entry 1**). After 1 hour, the desired phosphoramidate was obtained in moderate yields (~50%). While I was initially pleased that I was able to generate the desired phosphoramidates under such expedient conditions,

I found that this often resulted in a notable amount of phosphonate dimer, as noted by a doublet at ~10 ppm by ^{31}P NMR spectroscopy. Unsatisfied with this inadvertent dimerization, I decided to first form the betaine (125) by combining PPh_3 (2 equiv.) and DIAD (2 equiv.) in CH_2Cl_2 at 0°C for 30 minutes. Thereafter, we prepared a solution of BnHEX (1 equiv.), and amine (2 equiv.) in CH_2Cl_2 , which was then added dropwise to the betaine solution. After 30 minutes of reaction, we found that the desired mono-adduct was efficiently formed (~50-70% yield, **Figure 14a**) as indicated by a singlet at ~18 ppm by ^{31}P NMR spectroscopy, with minimal phosphonate dimerization (~10 ppm). These initial results show preferential reaction with benzylic amines, with the most effective reaction being with 2-picolylamine (**Table 1, Figure 14, entry 2**).

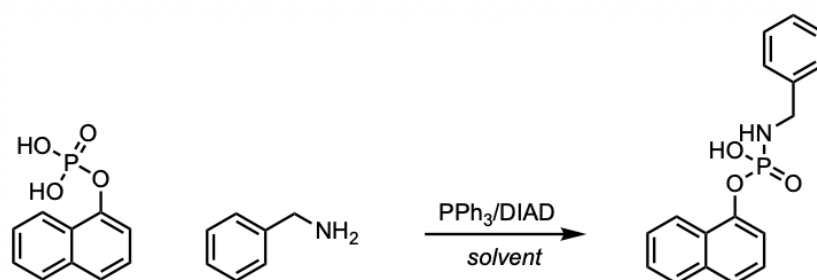
Having established the general reaction parameters for phosphonic acids, I sought to examine the reaction efficiency when using phosphoric acids. Using 1-naphtyl phosphate as a test compound, we screened a variety of aromatic and aliphatic amines (**Table 2, Figure 14b, entries 1-11**). Compared to our reactions with BnHEX, we found that pre-formation of the betaine solution was not necessary to prevent phosphate dimerization. Sequential addition of the phosphoric acid (1 equiv.), amine (1.5 equiv.), PPh_3 (1 equiv.), and DIAD (1 equiv.) in NMP at room temperature was all that was required for the desired phosphoramidate to be generated instantaneously (**Figure 12**). These optimized conditions are notably lower than that required for efficient mono-amidation of phosphonic acids (1 equiv. of acid to 2 equiv. of all other starting reagents). This can likely be attributed to the significantly faster rate of the reactions with phosphoric acids (**Figure 12**), compared to phosphonic acids. Given the expedience of the reaction with phosphoric acids, we then sought to test the limits of our reaction's exclusivity for phosphates by reacting amines



Entry	Solvent	Eq. Amine	Eq. PPh ₃	Eq. DIAD	Base	Yield (%)*
1	THF	2	2	2	none	n.d. [†]
2	DMF	2	2	2	none	n.d. [†]
3	MeCN	2	2	2	none	n.d. [†]
4	DCM	2	2	2	none	74
5	DCM	2	2	2	DBU (2 eq.)	87
6	DCM	1	1	1	TEA (2 eq.)	20
7	DCM	1	1	1	2,6-lutidine (2 eq.)	17
8	Pyridine	2	2	2	none	n.d. [†]
9	Toluene	2	2	2	none	n.d. [†]
10	NMP	2	2	2	none	n.d. [†]
11	NMP	2	2	2	DBU (2 eq.)	n.d. [†]
12	CHCl₃	2	2	2	none	74
13	CHCl₃	2	2	2	DBU (2 eq.)	86
14	CHCl ₃	1	1	1	none	n.d. [†]
15	CHCl ₃	2	1	1	none	62
16	CHCl ₃	1.5	1.5	1.5	none	64
17	CHCl ₃	1	1	1	TEA (1 eq.)	57
18	CHCl ₃	2	1	1	DBU (1 eq.)	65
19	CHCl ₃	2	1	1	DBU (2 eq.)	56

Table 1. Test reactions between BnHEX and 2-picolylamine. All reactions were performed with 5 mg BnHEX in 500 μ L solvent. Yields were calculated via ³¹P NMR spectroscopic analysis of the crude reaction mixture, using TPPO as an internal standard. [†]Products were not detected by LCMS or the reaction resulted in phosphonate dimer formation, as indicated by a ³¹P NMR chemical shift at ~10 ppm in 20% CDCl₃.

directly with fludarabine monophosphate (dihydrogen, **Figure 14b**, **entries 12-15**). Fludarabine monophosphate is a highly functionalized mononucleotide analogue of adenine with an acidic N¹-nitrogen (pK_a ~4.2) and C⁶-amine (pK_a ~9.8); its ribose sugar also contains two potentially reactive secondary alcohols. Yet even with these structural vulnerabilities, which often demand protecting groups (126), coupling with an amine solely occurred with the phosphate (**Figures 13, 14**).



Entry	Solvent	Eq. Amine	Eq. PPh ₃	Eq. DIAD	Base	Yield (%) [*]
1	NMP	2	2	2	none	74
2	NMP	2	2	2	DBU (2 eq.)	70
2	DMF	2	2	2	none	74
3	DMSO	2	2	2	none	46
4	Acetone	2	2	2	none	20
5	CHCl ₃	2	2	2	DBU (2 eq.)	100
6	CHCl ₃	2	1	1	DBU (1 eq.)	96
7	CHCl ₃	1.5	1	1	DBU (1 eq.)	100
8	CHCl₃	1.5	1	1	DBU (0.75 eq.)	100
9	CHCl ₃	1	1	1	DBU (0.75 eq.)	66
10	CHCl ₃	1.5	1	1	none	n.d. [†]

Table 2. Test reactions between 1-naphthyl phosphate and benzylamine. All reactions were performed with 5 mg 1-naphthyl phosphate in 500 μ L solvent. Yields were calculated via ³¹P NMR spectroscopic analysis of the crude reaction mixture, using triphenylphosphine oxide as an internal standard. [†] Reactants were insoluble.

Between my reactions with phosphonic acid BnHEX and phosphoric acids, I found that structurally diverse amines were much more amenable to being attached onto the latter. In an attempt to increase the efficacy of our reactions with phosphonic acids, we screened various base additives (**Table 1**). Coincidentally, I discovered that the strong, non-nucleophilic base 1,8-diazabicyclo[5.4.0]undec-7-ene (DBU) is capable of greatly improving coupling efficiencies between phosphonic acids and amines. Returning to our reaction setup for BnHEX, we added the (DBU, 2 equiv.) to our solution containing BnHEX and amine, which was then added dropwise to the betaine solution. Indeed, we found that this allowed attachment of previously inaccessible aliphatic amines to BnHEX at remarkable yields (**Figure 11a, entry 1**). It is

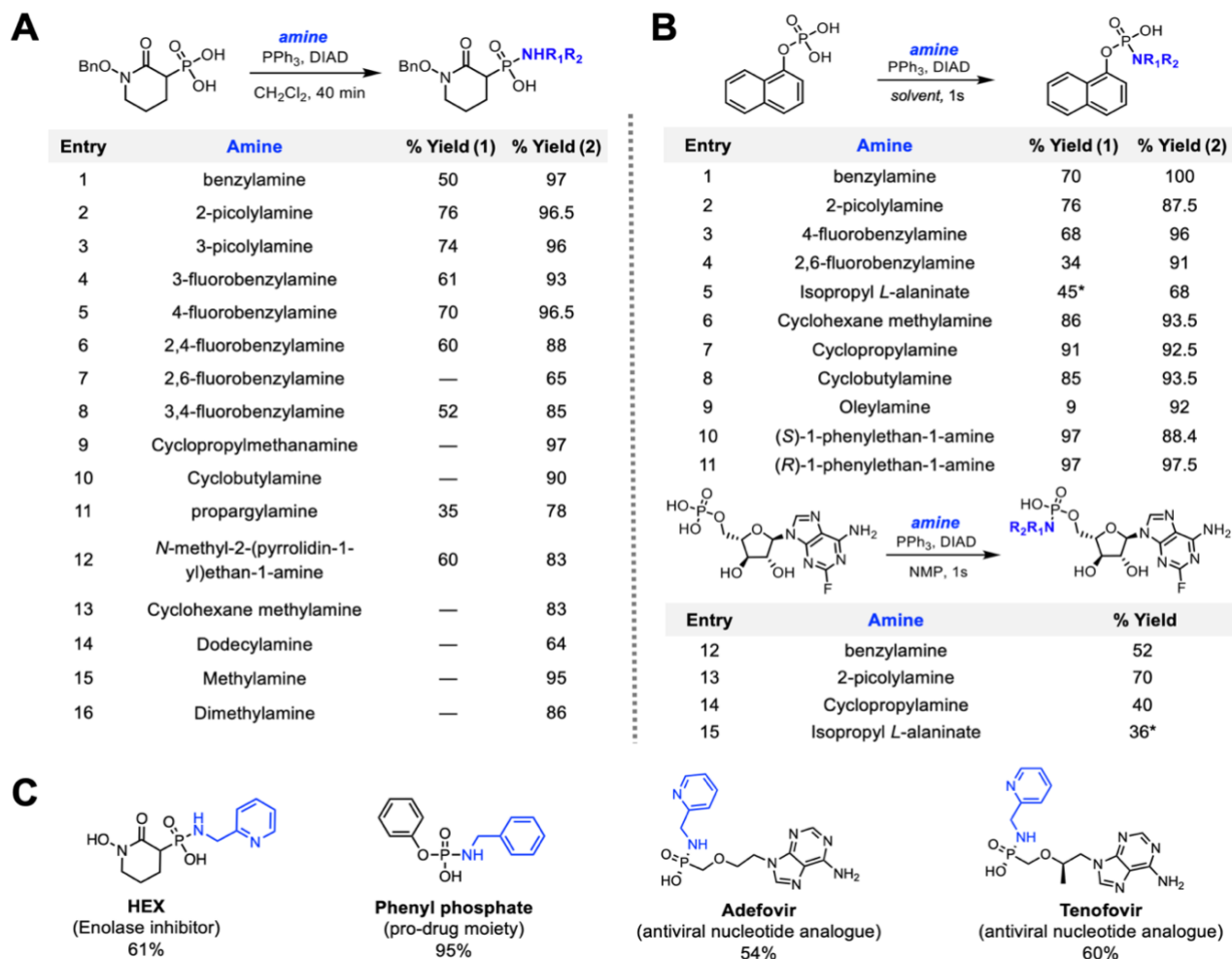


Figure 14. Reaction scope with phosphonic and phosphoric acids. Yields were calculated via ^{31}P NMR spectroscopic analysis of the crude reaction mixture, using formation of TPPO as an internal standard. **(A)** Reaction scope between a model phosphonic acid (BnHEX) and various amines. Yield (1) was obtained without the addition of DBU, while yield (2) was obtained with the addition of 2 equiv. of DBU. **(B)** Reaction scope between model phosphoric and amines Top: 1-naphtyl phosphate; yield (1) was obtained without the addition of DBU in NMP while yield (2) was obtained with the addition of 0.75 equivalents of DBU in CH_2Cl_2 . Bottom: Fludarabine monophosphate reactions in NMP. *Asterisked yields indicate the addition of 1.5 equiv. Et_3N to neutralize the HCl salt. Fludarabine monophosphate was insoluble in the CH_2Cl_2 even with the addition of 0.75-5 equiv. of DBU. **(C)** Examples of other therapeutically relevant molecules are selectively amidated at P(V).

reasonable to conclude that the addition of DBU to any of the amine couplings described will greatly improve reaction yields.

Seeking to test the limits of our reaction even further, I applied these coupling conditions to other therapeutically relevant molecules such as adefovir phosphonate and tenofovir phosphonate. From reactions with BnHEX, it had become apparent that phosphonic acids were poorly suited to coupling with amines in highly polar solvents such as NMP and DMF (**Table 1**), preferring non-polar solvent such as CH_2Cl_2 and CHCl_3 . Indeed, pilot reactions in NMP with these phosphonic acids and the most amenable amine, 2-picolyamine, proved unfruitful. However, with the discovery that DBU can facilitate the couplings between BnHEX and aliphatic amines, I proceeded to conduct with our reactions with adefovir phosphonate and tenofovir phosphonate using the same procedure as we had done for BnHEX. To our surprise, the addition of 2 equivalents of

DBU was able to dissolve these phosphonic acids in CH_2Cl_2 and CHCl_3 and the coupling product with 2-picolyamine occurred in moderate yields (**Figure 14c**). Extending this logic, we then decided to test whether HEX could be coupled using the DBU/ CH_2Cl_2 procedure. Much like adefovir phosphonate and tenofovir phosphonate, HEX was only soluble in highly polar organic solvents, precluding mono-amidation prior to discovering the effects of DBU. Indeed, we found that even HEX with its reactive hydroxamic acid could be effectively coupled with 2-picolyamine

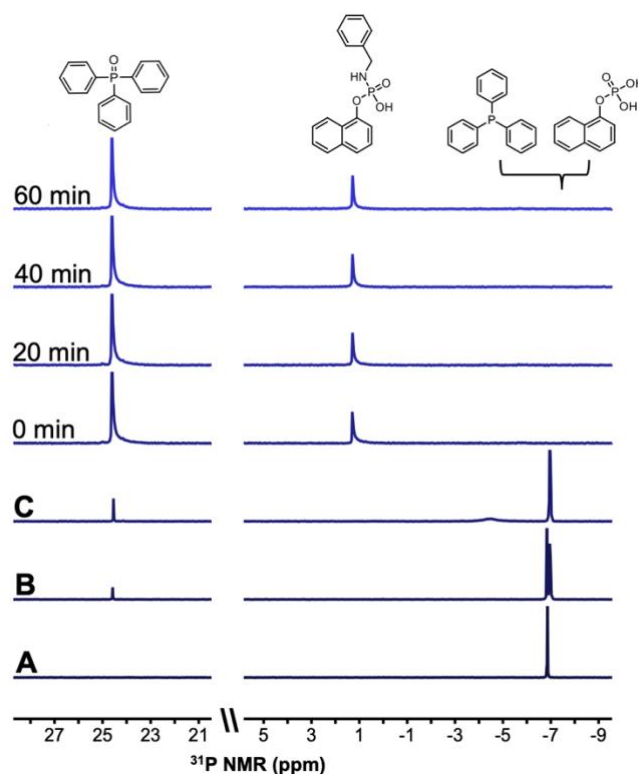


Figure 15. Mono-amidation of phosphoric acids occurs instantaneously. ^{31}P NMR spectroscopy scans were taken at 121 MHz in 80% NMP, 20% CDCl_3 . (A) 1-naphthyl phosphate, (B) 1-naphthyl phosphate + PPh_3 , (C) 1-naphthyl phosphate + PPh_3 + BnNH_2 . Mitsunobu coupling between 1-naphthyl phosphate and benzylamine was monitored over 60 minutes. Chemical shifts are as follows (left to right, ppm): TPPO, +24.6; phosphoramidate product, +1.3; PPh_3 , -6.8; 1-naphthyl phosphate, -6.9.

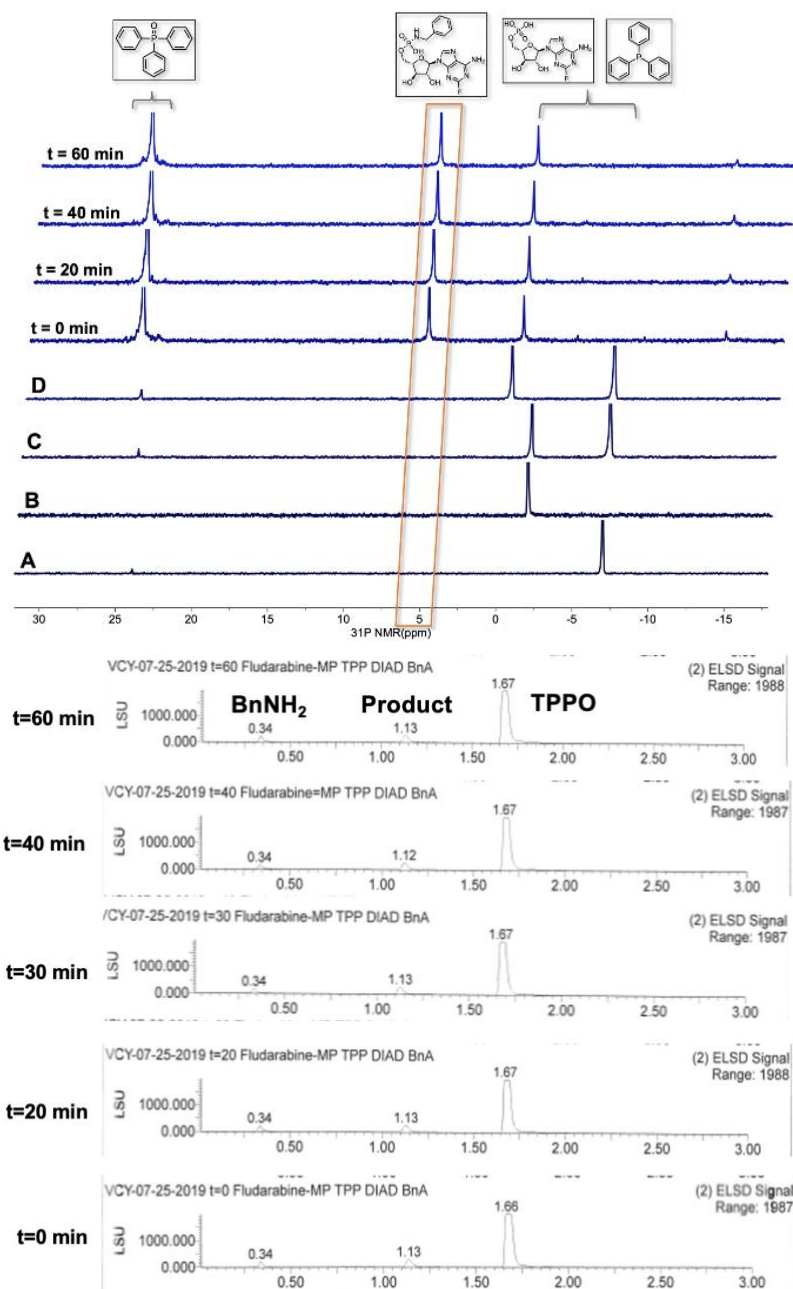


Figure 16. Reaction between benzylamine and fludarabine monophosphate occurs exclusively with the phosphate.

Top: Reaction monitoring by ^{31}P NMR. A= PPh_3 , B=fludarabine phosphate, C=fludarabine phosphate + PPh_3 , D=fludarabine phosphate + PPh_3 + BnNH_2 . Bottom: reaction monitoring by UPLC-MS; ELSD is at indicated timepoints.

solvents can be facilitated by addition of DBU, I sought to examine whether similar observations could be made for phosphonic acids. Based on conventional

with the addition of 2 equivalents of DBU (**Figure 16c**) in CH_2Cl_2 . The stark contrast in reactivity for this panel of phosphonic acids under these modified conditions supports the finding that this type of amidation with phosphonic acids must occur in non-polar solvents for optimal efficiency. To test the unlikely possibility that DBU, rather than solvent choice, was the predominant reason for the reaction's improved efficacy, we also performed the coupling between BnHEX and 2-picolylamine using 2 equivalents of DBU in NMP. After forming the betaine and reacting with the $\text{BnHEX}/2\text{-picolylamine}/\text{DBU}$ mixture for 40 minutes, the acid and amine remained unreacted. These data further highlight the necessity for phosphonic acid-amine couplings to occur in non-polar solvents.

Prompted by the finding that the dissolution of and reaction with phosphonic acids in non-polar

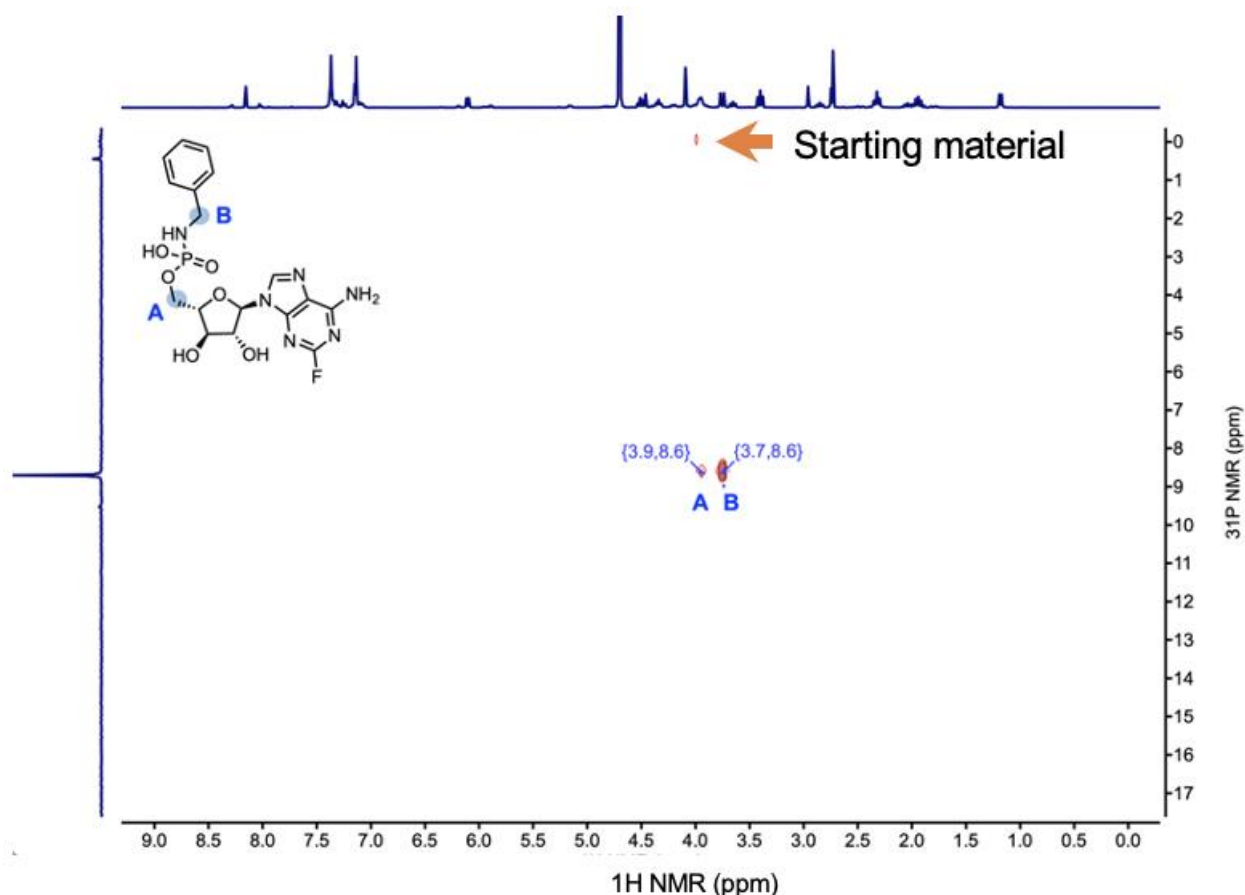


Figure 17. ^1H - ^{31}P HSQC supports that coupling between fludarabine phosphate and benzylamine occurs at phosphate. O2P=8, gpz2=32.4, cnst2=20, sw=8. Resonances correspond to protons that are, at most, J_3 to the phosphorous.

Mitsunobu couplings, we anticipated that the mono- and dibasic phosphates would not readily couple under these conditions, as an acidic proton is necessary for protonation of the betaine in the opening steps of the reaction mechanism (127). Indeed, I found that, even with the addition of DBU (0.75-2 equivalents), mono- and dibasic phosphates were essentially insoluble in CH_2Cl_2 and CHCl_3 . However, for fully protonated phosphoric acids, such as 1-naphthyl phosphate (dihydrogen, **Figure 17b**), 0.75 equivalents of DBU was the minimum amount required for dissolution in either CH_2Cl_2 or CHCl_3 after light vortexing. Overall, reaction with various benzylic and aliphatic amines proved more effective in these non-polar solvents compared to those performed in NMP without DBU (**Figure 17b**, **yield 1 versus yield 2**). This suggests that, even for phosphoric acids, monoamidation likely occurs more readily in non-polar solvents compared to highly polar ones. We note that 1-naphthyl phosphate served as a very user-friendly compound to make these observations as it was capable of dissolving in the aforementioned solvent systems. In contrast, fludarabine

monophosphate was essentially insoluble in DBU/CH₂Cl₂. Here, comparison of reaction efficiencies in different solvent systems was not possible. Thus, to ensure that these solvent-specific effects were not unique to 1-naphthyl phosphate, we also coupled phenyl dihydrogen phosphate with benzylamine in either NMP or DBU/CH₂Cl₂. Consistent with our observations with 1-naphthyl phosphate, we found that reaction efficiency was improved in the latter, non-polar solvent system (**Figure 17c**).

Irrespective of whether coupling occurred with a phosphonic or phosphoric acid, removal of the TPPO byproduct and isolation of the mono-amidate could be obtained with a single water extraction by capitalizing on the contrasting hydrophobicities of TPPO and the anionic product (**Figure 18**).

Phosphoramidates and phosphonoamidates are typically synthetic intermediates towards the synthesis of prodrug moieties (47, 98, 117) and thus require further esterification (or amidation, etc.) before becoming cell-permeable, therapeutically relevant entities. Due to the slight excess of amine added in these reactions, some amine contaminant may carry over, depending on its hydrophilicity. However, this has not problematic in subsequent reactions (98). This simple isolation approach starkly contrasts that required for conventionally used reactions (**Scheme 1**), which generate hydrophilic byproducts that can interfere with subsequent reactions. Using this workflow, various benzylic and aliphatic amines can be easily attached on to phosphate- or phosphonate-containing drugs for rapid screening of novel amine prodrug moieties (98). To emphasize the magnitude with which this workflow eases the pipeline from synthesis to cell-based screening: we are now able to generate over 20 mono-amidate prodrugs of HEX in two weeks (98)

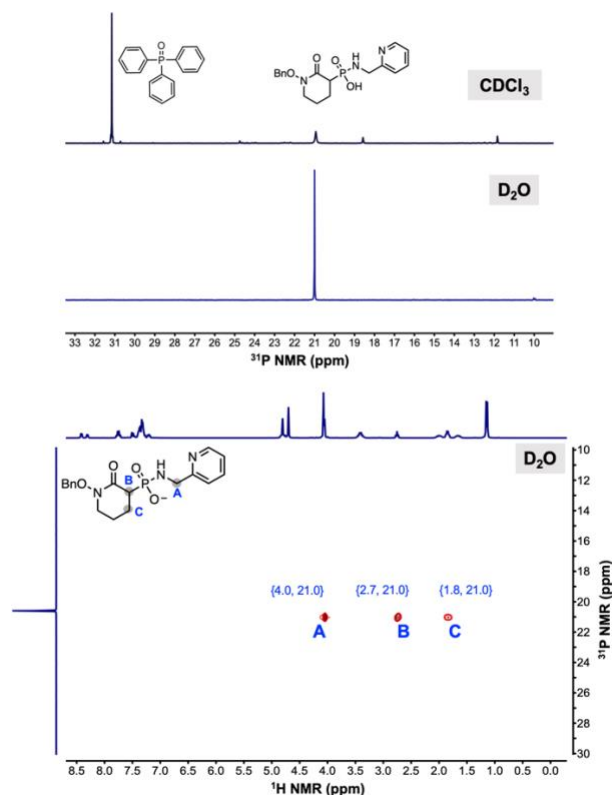


Figure 18. Mono-amidates can be isolated with a single water extraction. Top: ³¹P NMR spectrum of the crude reaction (CDCl₃) and of the isolated phosphoramidate after 1 water extraction (D₂O). Bottom: ¹H-³¹P HSQC of the extract.

rather than taking at least two weeks of reaction optimization for a single amine using other approaches (**Scheme 1a-c**), underscoring the highly consistent and versatile nature of our monoamidation method (98).

Finally, I sought to gain some mechanistic insight into our reaction. While the PPh_3/DIAD redox pair is synonymous with Mitsunobu couplings, examination of the classical Mitsunobu reaction mechanism (127) proves to be incompatible with our transformation. In canonical Mitsunobu couplings with alcohols, oxidation of PPh_3 to TPPO occurs due to formation of the alcohol- PPh_3 complex, followed by an $\text{S}_{\text{N}}2$ attack on the alcoholic carbon—resulting in the oxygen transfer from the alcohol to the phosphine to form the oxide (127). In this case, there is no such alcohol oxygen to perform this transfer to generate TPPO. We thus propose an amidation mechanism wherein the phosphonic or phosphoric acid acts as the pro-electrophile, rather than its traditional role as the pro-nucleophile (**Figure 19a**). Within our model, oxidation of the phosphine occurs through oxygen transfer from the phosphoric or phosphonic acid, as no other likely oxygen donors are present amongst the starting reagents. To gain insight into our proposed reaction mechanism, I prepared bis- ^{18}O -labeled 1-naphthyl phosphate, which was then HPLC-purified to remove any residual H_2^{18}O . The labeled phosphate was then reacted with (R)-(-)- α -methylbenzylamine (**Figure 19b**). Compared to the unlabeled control reaction, we found a significantly greater proportion of ^{18}O -labeled TPPO (**Figure 19c**, $M+1 = 281.29$ expected, 281.27 found), which coincided with the majority of the mono- ^{18}O -labeled phosphoramidate product (**Figure 19c**, $M+1 = 330.32$ expected, 330.34 found). We do note the strong 279.26 mass peak, corresponding to unlabeled TPPO. This reaction was performed with 2 equivalents of amine, PPh_3 , and DIAD; the dominant unlabeled mass peak can most likely be explained by the propensity for PPh_3 and DIAD to oxidize to the corresponding TPPO even in the absence of other starting reagents. Nonetheless, the height of the peak corresponding to the ^{18}O -labeled TPPO peak at 281.27 vastly overshadows that observed in the unlabeled reaction (**Figure 19c**). These observations strongly support our proposed mechanism of oxygen transfer to the phosphine, thereby strengthening the role of the phosphoric or phosphonic acid as the pro-electrophile in our monoamidation reactions.

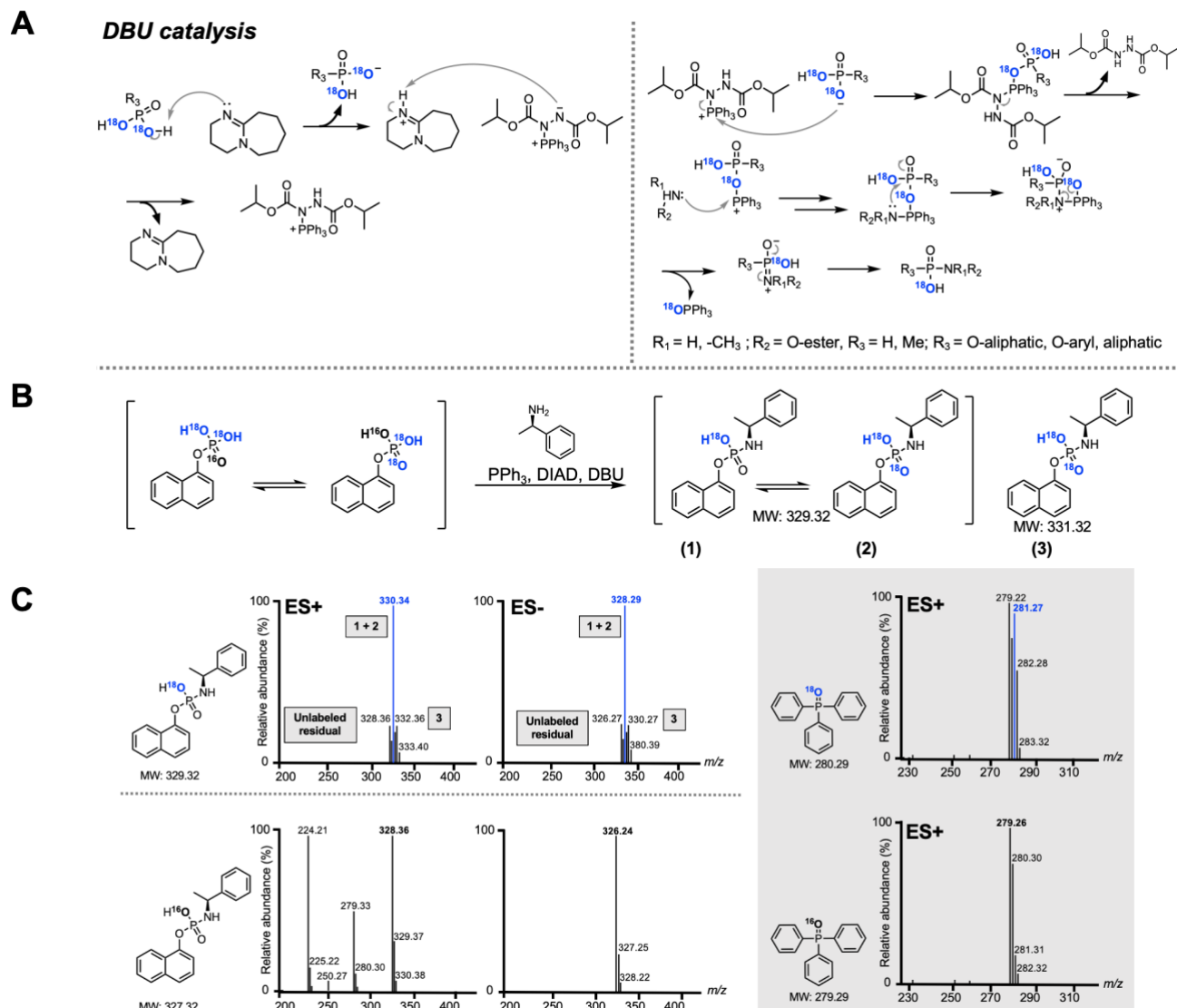


Figure 19. Proposed mechanism where phosphoric or phosphonic acids act as pro-electrophiles. (A) Proposed reaction mechanism with a generic amine and ^{18}O -labeled phosph(on)ate. (B). Labeled reaction with possible reaction product masses. (C) Mass spectrometry chromatograms of the labeled (top) and unlabeled reaction products (bottom). The peak for ^{18}O -labeled TPPO is significantly higher in the labeled compared to unlabeled reaction. The unlabeled residual is from unreacted 1-naphtyl phosphate in the initial isotope labeling experiment.

2.4 Conclusions

In sum, I have discovered a novel mono-amidation reaction that modifies traditional Mitsunobu conditions but differs in employing the acid as the pro-electrophile, rather than pro-nucleophile. This reaction enables expedient, direct mono-amidation of highly functionalized phosphate- or

phosphonate-containing species. In contrast to other coupling procedures (16), this modification on the Mitsunobu coupling is fast, reliable, and occurs under exceptionally mild conditions. Fundamentally, this reaction turns the formation of TPPO—a historically perceived inconvenience (124)—into an asset: one water extraction is all that is required for its removal and to obtain the mono-amidated product at sufficient purity to proceed with the next reaction. That our reaction is exquisitely selective for phosphates or phosphonates enables direct reaction onto highly functionalized nucleotide analogues for prodrugging efforts. Given the interest in discovering novel phosphoramidate-based prodrugs (117), this reaction is well-suited to rapidly screening a number of biologically labile amines. Taken together, our reaction not only expands the reaction scope of the traditional Mitsunobu coupling (119) but also represents a significant addition to the phosph(on)ate chemist's toolkit.

2.5 Experimental

^1H , ^{13}C , ^{31}P , and ^{19}F NMR spectra were recorded on a Bruker Avance 300 MHz spectrometer in either CDCl_3 or D_2O , unless otherwise indicated. Chemical shifts were measured in ppm relative to CDCl_3 ($\delta=7.24$ for ^1H and $\delta=77.0$ for ^{13}C) or D_2O ($\delta=4.80$ for ^1H). NMR characterizations are reported in the following order: chemical shift, multiplicity (s = singlet, bs = broad singlet, d = doublet, t = triplet, q = quartet, m = multiplet), and coupling constant (J , reported in Hertz). Where appropriate, 2-dimensional experiments (HSQC) and decoupled NMR experiments (^1H with ^{31}P decoupling) were used to support assignments. BnHEX was initially synthesized according to previously published procedures¹; subsequent syntheses were contracted to WuXi AppTec, Shanghai, China. Fludarabine Monophosphate was purchased from Selleckchem. Other starting materials were purchased at the highest commercial quality from Sigma Aldrich and were used without additional purification. Centrifugations were performed using an Eppendorf Centrifuge 5810R. Mass spectra were obtained on a Waters Acquity UPLC H-Class PLUS System (A/B: A = 30% MeCN in water, B = 0.1% formic acid in water) using an electrospray ion source.

Synthesis of phosphoramidates from BnHEX. All coupling reactions described for BnHEX (1) follow the same general procedure. Betaine formation: DIAD (2 equiv.) and triphenyl phosphine (2 equiv.) were combined in anhydrous DCM at 0°C and allowed to stir to room temperature for 30 minutes. Separately, BnHEX (1 equiv.), and the indicated amine (2 equiv.) were dissolved in

anhydrous DCM; in cases such as aliphatic amines where DBU was required, 2 equiv. of DBU were added to this solution (specified if needed below). This was then added dropwise to the betaine solution. The reaction was allowed to stir for 30 minutes. The crude reaction mixture was then transferred to a 50 mL Falcon tube, where 1 volume of water was added. The reaction was vortexed and centrifuged (4000 rpm, 4°C) for 2 minutes. The aqueous layer was then isolated and lyophilized to a white powder, unless otherwise specified.

***N*-benzyl-*P*-(1-(benzyloxy)-2-oxopiperidin-3-yl)phosphonamidic acid (A1).** Following the general procedure above, the following quantities were used: DIAD (68.17 μ L, 350.59 μ mol) and triphenylphosphine (43.87 mg, 350.59 μ mol) in anhydrous DCM (3 mL). BnHEX (**1**, 50 mg, 175.29 μ mol) and benzylamine (38.30 μ L, 350.59 μ mol) in anhydrous DCM (1 mL). Yield: 40%. Analysis by ESI+ (Expected $[M+H]^+ = 375.38$. Observed $[M+H]^+ = 375.35$). **¹H NMR** (500 MHz, D₂O) δ 7.32-7.53 (m, 10 H), 4.91-4.96 (m, 2H), 4.02-4.11 (m, 2H), 3.46-3.57 (m, 2H), 2.80-2.87 (dt, $J=21.52$ Hz, $J=21.70$ Hz, 1H), 2.07-2.13 (m, 1H), 1.92-1.98 (m, 2H), 1.72-1.79 (m, 1H). **¹³C NMR** (125.7 MHz, D₂O) δ 167.97 (d, $J=4.72$ Hz, 1C), 141.25 (d, $J=7.36$ Hz, 1C), 134.52 (s, 1C), 129.92 (s, 2C), 129.15 (s, 1C), 128.73 (s, 2C), 128.60 (s, 2C), 127.59 (s, 1C), 127.00 (s, 1C), 75.54 (s, 1C), 50.11 (s, 1C), 45.28 (s, 1C), 43.64 (d, $J=111.12$ Hz, 1C), 22.33 (d, $J=3.65$ Hz, 1C), 21.65 (d, $J=7.23$ Hz, 1C). **³¹P NMR** (202 MHz, D₂O) δ 20.91.

***P*-(1-(benzyloxy)-2-oxopiperidin-3-yl)-*N*-(pyridin-2-ylmethyl)phosphonamidic acid (A2).** Following the general procedure above, the following quantities were used: DIAD (68.17 μ L, 350.59 μ mol) and triphenylphosphine (43.87 mg, 350.59 μ mol) in anhydrous DCM (3 mL). BnHEX (**1**, 50 mg, 175.29 μ mol) and pyridin-2-ylmethanamine (37.83 μ L, 350.59 μ mol) in anhydrous DCM (1 mL). The product was lyophilized to an orange oil. Yield: 74%. Analysis by ESI+ (Expected $[M+H]^+ = 376.36$. Observed $[M+H]^+ = 376.35$). **¹H NMR** (300 MHz, D₂O) δ 8.38 (d, $J=4.73$ Hz, 1H), 7.83 (t, $J=1.77$, 1.92 Hz, 1H), 7.37-7.49 (m, 7H), 4.90 (d, $J=2.02$ Hz, 2H), 3.43-3.58 (m, 2H), 2.79-2.91 (dt, $J=21.84$ Hz, 1H), 2.06-2.14 (m, 1H), 1.91-1.99 (m, 2H), 1.70-1.81 (m, 1H). **¹³C NMR** (75 MHz, D₂O) δ 167.86 (s, 1C), 159.86 (d, $J=7.28$ Hz, 1C), 147.91 (s, 1C), 138.34 (s, 1C), 129.84 (s, 2C), 129.11 (s, 1C), 128.70 (s, 2C), 123.71 (s, 1C), 122.76 (s, 1C), 122.07, (s,1C), 71.16 (s, 1C), 50.04 (s, 1C), 46.42 (s, 1C), 43.18-44.65 (d, $J= 111.72$ Hz, 1C), 22.38 (d, $J= 3.65$ Hz, 1C), 21.54 (d, $J=7.01$ Hz, 1C). **³¹P NMR** (121 MHz, D₂O) δ 20.60.

***P*-(1-(benzyloxy)-2-oxopiperidin-3-yl)-*N*-(pyridin-3-ylmethyl)phosphonamidic acid (A3).**

Following the general procedure above, the following quantities were used: DIAD (68.17 μ L, 350.59 μ mol) and triphenylphosphine (43.87 mg, 350.59 μ mol) in anhydrous DCM (3 mL). BnHEX (**1**, 50 mg, 175.29 μ mol) and pyridin-3-ylmethanamine (37.83 μ L, 350.59 μ mol) in anhydrous DCM (1 mL). Yield: 76% Analysis by ESI+ (Expected $[M+H]^+ = 376.36$. Observed $[M+H]^+ = 376.35$). **¹H NMR** (300 MHz, D₂O) δ 8.58 (d, $J = 2.14$ Hz, 1H), 8.38-8.40 (dd, $J = 5.02$ Hz, 1H), 7.92-7.95 (dt, $J = 7.90$ Hz, 1H), 7.53-7.48 (m, 5H), 4.92 (s, 2H), 4.07-4.10 (d, $J = 9.13$ Hz, 2H), 3.47-3.55 (m, 2H), 2.76-2.88 (dt, $J = 21.88$ Hz, 1H), 2.05-2.16 (m, 1H), 1.90-2.00 (m, 2H), 1.70-1.82 (m, 1H). **¹³C NMR** (75 MHz, D₂O) 167.84 (d, $J = 4.44$ Hz, 1C), 149.20 (s, 1C), 148.82 (s, 1C), 147.65 (s, 1C), 146.93 (s, 1C), 129.88 (s, 2C), 129.62 (s, 1C), 129.13 (s, 1C), 128.71 (s, 2C), 124.09 (s, 1C), 75.47 (s, 1C), 43.15-44.63 (d, $J = 110.71$ Hz, 1C), 42.67 (s, 1C), 22.41 (d, $J = 4.10$ Hz, 1C), 2.53-2.63 (d, $J = 7.02$ Hz, 1C), 21.14-21.17 (d, $J = 2.48$ Hz, 1C). **³¹P NMR** (121 MHz, D₂O) δ 20.52.

***P*-(1-(benzyloxy)-2-oxopiperidin-3-yl)-*N*-(3-fluorobenzyl)phosphonamidic acid (A4).**

Following the general procedure above, the following quantities were used: DIAD (86.98 μ L, 441.74 μ mol) and triphenylphosphine (115.86 mg, 441.74 μ mol) in anhydrous DCM (3 mL). BnHEX (**1**, 63 mg, 220.87 μ mol) and 3-fluorophenyl methanamine (50.39 μ L, 441.74 μ mol) in anhydrous DCM (1 mL). Yield: 61%. Analysis by ESI+ (Expected $[M+H]^+ = 393.37$. Observed $[M+H]^+ = 393.42$). **¹H NMR** (300 MHz, CDCl₃) δ 7.18-7.38 (m, 9 H), 4.87 (s, 2H), 4.03 (s, 2H), 3.27-3.38 (m, 2H), 2.62-2.74 (dt, $J = 22.20$ Hz, $J = 6.9$ Hz, 1H), 2.07-2.13 (m, 1H), 1.79-1.88 (m, 2H), 1.55-1.59 (m, 1H). **¹³C NMR** (75 MHz, CDCl₃) δ 166.80 (d, $J = 4.50$ Hz, 1C), 161.13 (d, $J = 2.32$ Hz, 1C), 144.65 (d, $J = 7.36$ Hz, 1C), 135.40 (s, 1C), 129.39 (s, 2C), 129.58 (s, 1C), 128.42 (s, 2C), 124.60 (d, $J = 2.89$ Hz, 1C), 122.83 (s, 1C), 115.95 (d, $J = 21.89$ Hz, 1C), 114.24 (d, $J = 21.34$ Hz, 1C), 75.48 (s, 1C), 50.52 (s, 1C), 45.47 (s, 1C), 42.70-43.64 (d, $J = 96$ Hz, 1C), 23.12 (d, $J = 2.84$ Hz, 1C), 22.35 (d, $J = 8.16$ Hz, 1C). **³¹P NMR** (121 MHz, CDCl₃) δ 19.30. **¹⁹F NMR** (282 MHz, CDCl₃) δ -112.30.

***P*-(1-(benzyloxy)-2-oxopiperidin-3-yl)-*N*-(4-fluorobenzyl)phosphonamidic acid (A5).**

Following the general procedure above, the following quantities were used: DIAD (68.17 μ L,

350.59 μmol) and triphenylphosphine (43.87 mg, 350.59 μmol) in anhydrous DCM (3 mL). BnHEX (**1**, 50 mg, 175.29 μmol) 4-fluorophenyl methanamine (40.07 μL , 350.59 μmol) in anhydrous DCM (1 mL). Yield: 64%. Analysis by ESI+ (Expected $[\text{M}+\text{H}]^+ = 393.37$. Observed $[\text{M}+\text{H}]^+ = 393.38$). **^1H NMR** (300 MHz, D_2O) δ 7.41-7.54 (m, 5H), 7.10-7.24 (m, 4H), 4.94 (s, 2H), 4.02 (d, $J=8.76$ Hz, 2H), 3.46-3.60 (m, 2H), 2.77-2.88 (dt, $J=21.74$ Hz, 1H), 1.90-2.00 (m, 2H), 2.07-2.16 (m, 1H), 1.77-1.83 (m, 1H). **^{13}C NMR** (75 MHz, D_2O) δ 167.89 (d, $J=4.16$ Hz, 1C), 164.48 (s, 1C), 137.00-137.13 (dd, $J=7.12$ Hz, 1C), 134.52 (s, 1C), 130.95 (d, $J=8.86$ Hz, 2C), 129.90 (s, 2C), 129.15 (s, 1C), 128.73 (s, 2C), 114.89 (d, $J=21.90$ Hz, 2C), 75.51 (s, 1C), 50.09 (s, 1C), 42.95-44.41 (d, $J=110.78$ Hz, 1C), 22.31 (d, $J=4.00$ Hz, 1C), 21.59 (d, $J=8.00$ Hz, 1C), 21.34 (s, 1C). **^{31}P NMR** (121 MHz, D_2O) δ 20.78. **^{19}F NMR** (282 MHz, D_2O) δ -113.20.

***P*-(1-(benzyloxy)-2-oxopiperidin-3-yl)-*N*-(2,4-difluorobenzyl)phosphonamidic acid (A6).**

Following the general procedure above, the following quantities were used: DIAD (96.64 μL , 490.82 μmol) and triphenylphosphine (128.74 mg, 490.82 μmol) in anhydrous DCM (3 mL). BnHEX (**1**, 70 mg, 245.41 μmol) and (2,4-difluorophenyl)methanamine (58.55 μL , 490.82 μmol) in anhydrous DCM (1 mL). Yield: 61%. Analysis by ESI+ (Expected $[\text{M}+\text{H}]^+ = 411.12$. Observed $[\text{M}+\text{H}]^+ = 411.38$). **^1H NMR** (300 MHz, CDCl_3) δ 6.68-7.71 (m, 9H), 4.84 (m, 2H), 4.09 (s, 2H), 3.29 (m, 2H), 2.65 (m, 1H), 2.01 (m, 2H). 1.55 - 1.76 (2H, m); **^{13}C NMR** (75 MHz, CDCl_3) δ 176.91 (s, 1C), 158.62-164.51 (dd, $J_1=11.92$ Hz, $J_2=150.9$ Hz, 2C), 166.95 (d, $J=4.42$ Hz, 1C), 135.37 (s, 1C), 132.21 (s, 1C), 130.48 (dd, $J_1=9.60$ Hz, $J_2=150.28$ Hz, 1C), 129.31 (s, 2C), 128.59 (s, 1C), 128.41 (s, 2C), 124.55-124.88 (d, $J=3.75$ Hz, 1C), 118.25 (dq, $J_1=3.52$ Hz, $J_2=14.70$ Hz, 1C), 111.71 (dq, $J_1=3.52$ Hz, $J_2=21.00$ Hz, 1C), 103.44 (q, $J_1=25.12$ Hz, 1C), 75.41 (s, 1C), 50.49 (s, 1C), 44.78-45.56 (d, $J_1=112.50$ Hz, 1C), 39.14 (d, $J=3.50$ Hz, 1C), 36.06 (d, $J=3.50$ Hz, 1C), 23.19 (s, 1C), 22.35 (d, $J=7.57$ Hz, 1C). **^{31}P NMR** (121 MHz, CDCl_3) δ 18.98. **^{19}F NMR** (282 MHz, CDCl_3) -109.43 (d, $J=7.86$, 1F), δ -112.95 (d, $J=6.86$, 1F).

***P*-(1-(benzyloxy)-2-oxopiperidin-3-yl)-*N*-(2,6-difluorobenzyl)phosphonamidic acid (A7).**

Following the general procedure above, the following quantities were used: DIAD (96.64 μL , 490.82 μmol) and triphenylphosphine (128.74 mg, 490.82 μmol) in anhydrous DCM (3 mL). BnHEX (**1**, 70 mg, 245.41 μmol) and (2,4-difluorophenyl)methanamine (58.55 μL , 490.82 μmol) in anhydrous DCM (1 mL). Yield: 61%. Analysis by ESI+ (Expected $[\text{M}+\text{H}]^+ = 411.12$. Observed

[M+H]⁺ = 411.38). **¹H NMR** (300 MHz, CDCl₃) δ 6.68-7.71 (m, 9H), 4.84 (m, 2H), 4.09 (s, 2H), 3.29 (m, 2H), 2.65 (m, 1H), 2.01 (m, 2H). 1.55 - 1.76 (2H, m); **¹³C NMR** (75 MHz, CDCl₃) δ 176.91 (s, 1C), 158.62-164.51 (dd, J₁=11.92 Hz, J₂= 150.9 Hz, 2C), 166.95 (d, J=4.42 Hz, 1C), 135.37 (s, 1C), 132.21 (s, 1C), 130.48 (dd, J₁=9.60 Hz, J₂= 150.28 Hz, 1C), 129.31 (s, 2C), 128.59 (s, 1C), 128.41 (s, 2C), 124.55-124.88 (d, J = 3.75 Hz, 1C), 118.25 (dq, J₁ = 3.52 Hz, J₂ = 14.70 Hz, 1C), 111.71 (dq, J₁ = 3.52 Hz, J₂ = 21.00 Hz, 1C), 103.44 (q, J₁ = 25.12 Hz, 1C), 75.41 (s, 1C), 50.49 (s, 1C), 44.78-45.56 (d, J₁ = 112.50 Hz, 1C), 39.14 (d, J=3.50 Hz, 1C), 36.06 (d, J=3.50 Hz, 1C), 23.19 (s, 1C), 22.35 (d, J=7.57 Hz, 1C). **³¹P NMR** (121 MHz, CDCl₃) δ 18.98. **¹⁹F NMR** (282 MHz, CDCl₃) -109.43 (d, J=7.86, 1F), δ -112.95 (d, J=6.86, 1F).

***P*-(1-(benzyloxy)-2-oxopiperidin-3-yl)-*N*-(3,4-difluorobenzyl)phosphonamidic acid (A8).**

Following the general procedure above, the following quantities were used: DIAD (276.11 μL, 1.40 mmol) and triphenylphosphine (367.82 mg, 1.40 mmol) in anhydrous DCM (3 mL). BnHEX (**1**, 200 mg, 245.41 μmol) and (3,4-difluorophenyl)methanamine (165.89 μL, 1.40 mmol) in anhydrous DCM (1 mL). Yield: 52%. Analysis by ESI+ (Expected [M+H]⁺ = 411.36. Observed [M+H]⁺ = 411.42). **¹H NMR** (300 MHz, CDCl₃) δ 7.21-7.25 (m, 8H), 4.77 (s, 2H), 3.91 (s, 2H), 3.21-3.35 (m, 2H), 2.50-2.62 (m, 1H), 1.90-1.92 (m, 1H). 1.75-1.79 (m, 1H), 1.46-1.50 (1H, m); **¹³C NMR** (75 MHz, CDCl₃) δ 166.90 (s, 1C), 151.56-151.85 (m, 1C), 148.27-148.55 (m, 1C), 131.54-131.65 (dd, J₁ = 3.75 Hz, J₂ = 5.25 Hz, 1C), 129.28 (s, 2C), 128.69 (s, 1C), 128.46 (s, 2C), 125.51 (dd, J₁ = 3.75 Hz, J₂ = 5.25 Hz, 1C), 118.33 (d, J₁ = 17.25 Hz, 1C) 117.09 (d, J₁ = 17.25 Hz, 1C), 75.41 (s, 1C), 50.39 (s, 1C), 44.05-45.55 (d, J₁ = 112.5 Hz, 1C), 45.00 (s, 1C), 42.10 (s, 1C), 23.18 (s, 1C), 22.38 (d, J=8.25 Hz, 1C). **³¹P NMR** (121 MHz, CDCl₃) δ 18.95. **¹⁹F NMR** (282 MHz, D₂O) δ -137.06 (d, J=21.32 Hz, 1F), -138.22 (d, J=12.73, 1F).

***P*-(1-(benzyloxy)-2-oxopiperidin-3-yl)-*N*-(cyclopropylmethyl)phosphonamidic acid (A9).**

To a solution of triphenylphosphine (275.87 mg, 1.05 mmol) in DCM (15 mL), DIAD (204.50 μL, 1.05 mmol) were added with stirring at 0°C for 30 min. Separately, a solution containing BnHEX (150 mg, 525.88 μmol), cyclopropylmethanamine hydrochloride (74.80 mg, 1.05 mmol), and DBU (156.98 μL, 1.05 mmol) in DCM (2 mL) was prepared and added dropwise to the betaine solution. The reaction mixture was allowed to warm to room temperature over 30 minutes. Then, 1 volume of water was added to the crude mixture. After vigorous shaking and partitioning via

centrifugation (2 min at 4°C, 4000 rpm), the aqueous layer was isolated and lyophilized to a clear solid. Analysis by ESI+ (Expected $[M+H]^+ = 339.34$. Observed $[M+H]^+ = 339.38$). **¹³C NMR** (125 MHz, MeOD) δ 168.57 (d, $J=4.15$ Hz, 1C), 137.09 (s, 1C), 130.78 (s, 2C), 129.82 (s, 1C), 129.64 (s, 2C), 76.30 (s, 1C), 51.36 (s, 1C), 48.07 (s, 1C), 44.16-45.59 (d, $J=107.65$ Hz, 1C), 24.07 (d, $J=4.02$ Hz, 1C), 23.57 (d, $J=6.85$ Hz, 1C), 14.13 (d, $J=9.99$ Hz, 1C), 3.97 (d, $J=12.30$ Hz, 2C). **³¹P NMR** (202 MHz, MeOD) δ 19.54 ppm.

***P*-(1-(benzyloxy)-2-oxopiperidin-3-yl)-*N*-cyclobutylphosphonamidic acid (A10).**

To a solution of triphenylphosphine (919.56 mg, 3.51 mmol) in DCM (20 mL), DIAD (681.66 μ L, 3.51 mmol) were added with stirring at 0°C for 30 min. Separately, a solution containing BnHEX (500 mg, 1.75 mmol), cyclobutylamine (299.34 μ L, 3.51 mmol), and DBU (523.27 μ L, 3.51 mmol) in DCM (2 mL) was prepared and added dropwise to the betaine solution. The reaction mixture was allowed to warm to room temperature over 30 minutes. Then, 1 volume of water was added to the crude mixture. After vigorous shaking and partitioning via centrifugation (2 min at 4°C, 4000 rpm), the aqueous layer was isolated and lyophilized to a clear solid. Analysis by ESI+ (Expected $[M+H]^+ = 339.34$. Observed $[M+H]^+ = 339.41$). **¹H NMR** (300 MHz, D₂O) 7.45-7.55 (m, 5H), 4.96 (s, 1H), 3.26-3.30 (t, $J=5.55, 6.01$ Hz, 2H), 2.68-2.79 (dt, $J=21.36$ Hz, 1H), 2.19-.27 (m, 2H), 2.05-2.11 (m, 1H), 1.79-1.91 (m, 4H), 1.51-1.62 (m, 2H). **³¹P NMR** (121 MHz, D₂O) 19.47 (s, 1P).

***P*-(1-(benzyloxy)-2-oxopiperidin-3-yl)-*N*-(prop-2-yn-1-yl)phosphonamidic acid (A11).**

Following the general procedure above, the following quantities were used: DIAD (68.17 μ L, 350.59 μ mol) and triphenylphosphine (43.87 mg, 350.59 μ mol) in anhydrous DCM (3 mL). BnHEX (**1**, 50 mg, 175.29 μ mol) and propargylamine (16.84 μ L, 262.94 μ mol) in anhydrous DCM (1 mL). Yield: 35%. Analysis by ESI+ (Expected $[M+H]^+ = 323.30$. Observed $[M+H]^+ = 323.39$). **¹H NMR** (300 MHz, D₂O) δ 7.37-7.44 (m, 5H), 4.88 (s, 2H), 3.57-3.61 (dd, $J=10.85$ Hz, 2H), 3.43-3.49 (m, 2H), 2.84-2.96 (dt, $J=22.10$ Hz, 1H), 1.97-2.03 (m, 1H), 1.86-1.93 (m, 2H), 1.68-1.76 (m, 1H). **¹³C NMR** (75 MHz, D₂O) δ 167.64 (d, $J=4.50$ Hz, 1C), 134.50 (s, 1C), 129.95 (s, 2C), 129.19 (s, 1C), 128.76 (s, 2C), 76.44 (s, 1C), 50.05 (s, 1C), 43.09-44.57 (d, 111.27 Hz, 1C), 30.07 (s, 1C), 22.24-22.29 (d, $J=3.79$ Hz, 1C), 21.69-21.79 (d, $J=8.03$ Hz, 1C); some tertiary and quaternary carbons not visible under these running conditions. **³¹P NMR** (121 MHz, D₂O) δ 20.89

***P*-(1-(benzyloxy)-2-oxopiperidin-3-yl)-*N*-methyl-*N*-(2-(pyrrolidin-1-yl)ethyl**

phosphoramidic acid (A12). Following the general procedure above, the following quantities were used: DIAD (137.65 μ L, 707.17 μ mol) and triphenylphosphine (183.91 mg, 707.17 μ mol) in anhydrous DCM (5 mL). BnHEX (**1**, 100 mg, 350.59 μ mol) and *N*-methyl-2-(pyrrolidin-1-yl)ethan-1-amine (88.39 μ L, 701.17 μ mol) in anhydrous DCM (2 mL). Yield: 63%. Analysis by ESI+ (Expected $[M+H]^+ = 396.44$. Observed $[M+H]^+ = 396.51$). **¹H NMR** (300 MHz, D₂O) δ 7.47-7.54 (m, 5H), 4.99 (s, 2H), 3.59-3.63 (m, 2H), 2.99-3.04 (t, $J=6.44$, 7.03 Hz, 4H), 2.76-2.80 (dt, $J=10.9$ Hz, 1H), 2.63 (s, 3H), 2.00-2.25 (m, 7H), 1.90-1.97 (m, 4H), 1.82-1.90 (m, 1H). **¹³C NMR** (75 MHz, D₂O) δ 167.92 (d, $J=4.57$ Hz, 1C), 134.40 (s, 1C), 129.86 (s, 2C), 129.20 (s, 1C), 128.76 (s, 2C), 75.45 (s, 1C), 53.86 (s, 2C), 51.46 (s, 1C), 49.91-50.10 (d, $J=15.22$ Hz, 1C), 46.20 (s, 1C), 41.40-42.88 (d, $J=111.54$ Hz, 1C), 33.20-33.25 (d, $J=4.18$ Hz, 1C), 22.55-22.62 (d, $J=5.52$ Hz, 1C), 22.29-22.35 (d, $J=4.28$ Hz, 1C), 21.07 (s, 2C). **³¹P NMR** (121 MHz, D₂O) δ 22.00.

***P*-(1-(benzyloxy)-2-oxopiperidin-3-yl)-*N*-(cyclohexylmethyl)phosphonamidic acid (A13).** To a solution of triphenylphosphine (275.87 mg, 1.05 mmol) in DCM (6 mL), DIAD (204.50 μ L, 1.05 mmol) were added with stirring at 0°C for 30 min. Separately, a solution containing BnHEX (150 mg, 525.88 mmol), cyclohexane methylamine (136.85 μ L, 1.05 μ mol), and DBU (157.29 μ L, 1.05 mmol) in DCM (2 mL) was prepared and added dropwise to the betaine solution. The reaction mixture was allowed to warm to room temperature over 30 minutes. Then, 1 volume of water was added to the crude mixture. After vigorous shaking and partitioning via centrifugation (2 min at 4°C, 4000 rpm), the aqueous layer was isolated and lyophilized to clear oil. Analysis by ESI+ (Expected $[M+H]^+ = 381.42$. Observed $[M+H]^+ = 381.50$). **¹H NMR** (300 MHz, CDCl₃) δ 7.37-7.44 (m, 5H) 3.61-3.65 (m, 2H), (m, 1H), 2.15-2.25 (m, 1H), 1.97-2.12 (m, 2H), 1.83-1.93 (m, 1H), 1.62-1.74 (m, 6H), 1.32-1.44 (m, 1H), 0.79-0.94 (m, 3H). **³¹P NMR** (121 MHz, CDCl₃) δ 17.41 (s, 1P).

***N*-dodecyl-*P*-(1-hydroxy-2-oxopiperidin-3-yl)phosphonamidic acid (A14).** To a solution of triphenylphosphine (96 mg, 350.59 mmol) in DCM (4 mL), DIAD (68.17 μ L, 350.59 mmol) were

added with stirring at 0°C for 30 min. Separately, a solution containing BnHEX (50 mg, 175.29 mmol), dodecylamine (74.69 μ L, 350.59 μ mol), and DBU (52.33 μ L, 350.59 mmol) in DCM (1 mL) was prepared and added dropwise to the betaine solution. The reaction mixture was allowed to warm to room temperature over 30 minutes. Then, 1 volume of water was added to the crude mixture. After vigorous shaking and partitioning via centrifugation (2 min at 4°C, 4000 rpm), the aqueous layer was isolated and lyophilized to a white solid. ¹H NMR (300 MHz, CDCl₃) δ 7.37-7.44 (m, 5H), 3.55-3.63 (m, 2H), 2.85-2.93 (m, 4H), 2.12-2.17 (m, 1H), 1.96-2.03 (m, 2H), 1.76-1.81 (m, 2H), 1.56-1.66 (m, 2H), 1.41-1.51 (m, 2H), 1.18 (m, 36H), 0.79-0.83 (t, J=6.0 Hz). ³¹P NMR (121 MHz, CDCl₃) δ 31.14 (1P), 22.54 (1P).

***P*-(1-(benzyloxy)-2-oxopiperidin-3-yl)-*N*-methylphosphonamidic acid (A15).** To a solution of triphenylphosphine (183.91 mg, 701.17 mmol) in DCM (5 mL), DIAD (136.33 μ L, 701.17 mmol) were added with stirring at 0°C for 30 min. Separately, a solution containing BnHEX (100 mg, 350.59 mmol), methylamine hydrochloride (47.34 mg, 701.17 mmol), and DBU (106.75 μ L, 701.17 mmol) in DCM (1 mL) was prepared and added dropwise to the betaine solution. The reaction mixture was allowed to warm to room temperature over 30 minutes. Then, 1 volume of water was added to the crude mixture. After vigorous shaking and partitioning via centrifugation (2 min at 4°C, 4000 rpm), the aqueous layer was isolated and lyophilized to clear oil.

***P*-(1-(benzyloxy)-2-oxopiperidin-3-yl)-*N,N*-dimethylphosphonamidic acid (A16).** To a solution of triphenylphosphine (91.96 mg, 350.59 mmol) in DCM (2.5 mL), DIAD (68.17 μ L, 350.59 mmol) were added with stirring at 0°C for 30 min. Separately, a solution containing BnHEX (50 mg, 175.29 mmol), dimethylamine hydrochloride (28.59 mg, 350.59 mmol), and DBU (53.37 mg, 350.59 mmol) in DCM (1 mL) was prepared and added dropwise to the betaine solution. The reaction mixture was allowed to warm to room temperature over 30 minutes. Then, 1 volume of water was added to the crude mixture. After vigorous shaking and partitioning via centrifugation (2 min at 4°C, 4000 rpm), the aqueous layer was isolated and lyophilized to clear oil.

Synthesis of phosphoramidates from phosphates. For phosphate-containing compounds (1-naphtyl phosphate, Fludarabine monophosphate), reagents were added in the following order: 1.) phosphate starting material, 2.) DBU (0.75 equiv., for 1-naphtyl phosphate reactions only), 3.) amine (1.5 equiv.), 4.) triphenyl phosphine (1 equiv.), 5.) DIAD (1 equiv.). After 1 second, the reaction was transferred to a 5 mL Eppendorf tube and chloroform (2.5 mL), followed by water (2.5 mL) were added to the reaction. The reaction was vortexed and centrifuged (4000 rpm, 4°C) for 2 minutes. The aqueous layer was then isolated and lyophilized to a clear oil. For phosphate reactions performed in DCM or CHCl₃, DBU (0.75 equiv.) were added to the aforementioned reagents, prior to the addition of DIAD.

Naphthalen-1-yl hydrogen benzylphosphoramidate (B1). Following the general procedure above, the following quantities were used: 1-naphtyl phosphate (5 mg, 22.31 μ mol), benzylamine (3.65 μ L, 33.46 μ mol), DBU (2.50 μ L, 16.73 μ mol), triphenylphosphine (5.85 mg, 22.31 μ mol), and DIAD (4.34 μ L, 22.31 μ mol) in DCM (500 μ L). Analysis by ESI+ (Expected [M+H]⁺=314.29. Observed [M+H]⁺=314.32). **¹H NMR** (300 MHz, D₂O) δ 8.10-8.13 (d, J=7.05 Hz, 1H), 7.95 (d, J=6.77 Hz, 1H), 7.70-7.73 (d, J=8.54 Hz, 1H), 7.55-7.59 (m, 2H), 7.46-7.55 (t, J=7.79, 7.79 Hz, 1H), 7.38-7.41 (d, J=7.79 Hz, 1H), 7.22-7.28 (m, 5H), 4.05 (d, J=10.73 Hz, 2H). **¹³C NMR** (125 MHz, D₂O) δ 148.13 (d, J=7.70 Hz, 1C), 140.79 (d, J=6.73 Hz, 1C), 134.50 (s, 1C), 129.98 (s, 1C), 128.38 (s, 2C), 127.58 (s, 1C), 127.30 (s, 2C), 126.83 (s, 2C), 126.56 (s, 1C), 126.00 (d, J=3.70 Hz, 1C), 123.18 (s, 1C), 122.06 (s, 1C), 114.62 (d, J=3.68 Hz, 1C), 45.34 (s, 1C). **³¹P NMR** (121 MHz, D₂O) δ 5.11.

Naphthalen-1-yl hydrogen (pyridin-2-ylmethyl)phosphoramidate (B2). Following the general procedure above, the following quantities were used: 1-naphtyl phosphate (5 mg, 22.31 μ mol), pyridin-2-ylmethanamine (3.45 μ L, 33.46 μ mol), DBU (2.50 μ L, 16.73 μ mol), triphenylphosphine (5.85 mg, 22.31 μ mol), and DIAD (4.34 μ L, 22.31 μ mol) in DCM (500 μ L). Analysis by ESI+ (Expected [M+H]⁺=315.28. Observed [M+H]⁺=315.22). **¹H NMR** (300 MHz, D₂O) δ 8.56 (d, J= 5.07 Hz, 1H), 8.10 (d, J=5.15 Hz, 1H), 7.96-8.00 (d, J=8.67 Hz, 1H), 7.87-7.92 (t, J=7.82, 7.97 Hz, 1H), 7.81-7.84 (d, J=7.76 Hz, 1H), 7.59-7.62 (d, J=7.82 Hz, 1H), 7.35-7.52 (m, 4H), 7.13-7.15 (d, J=7.87 Hz, 1H), 4.11-4.15 (d, J=12.88 Hz, 2H). **¹³C NMR** (125 MHz, D₂O) δ 158.38 (d, J=4.91 Hz, 1C), 149.18 (s, 1C), 147.88 (d, J=7.49 Hz, 1C), 138.40 (s, 1C), 134.34 (s,

1C), 127.52 (s, 1C), 126.48 (s, 2C), 125.86 (d, $J=1.37$ Hz, 1C), 124.12 (s, 1C), 123.16 (d, $J=0.89$ Hz, 1C), 122.36 (s, 1C), 121.89 (s, 1C), 114.26 (d, $J=3.48$ Hz, 1C), 45.92 (s, 1C). **^{31}P NMR** (121 MHz, D_2O) δ 4.59.

Naphthalen-1-yl hydrogen (4-fluorobenzyl)phosphoramidate (B3). Following the general procedure above, the following quantities were used: 1-naphtyl phosphate (5 mg, 22.31 μmol), 4-fluorobenzylamine (3.82 μL , 33.46 μmol), DBU (2.50 μL , 16.73 μmol), triphenylphosphine (5.85 mg, 22.31 μmol), and DIAD (4.34 μL , 22.31 μmol) in DCM (500 μL). Analysis by ESI+ (Expected $[\text{M}+\text{H}]^+=332.28$. Observed $[\text{M}+\text{H}]^+=332.29$). **^1H NMR** (300 MHz, D_2O) δ 8.06-8.09 (d, $J=7.57$ Hz, 1H), 7.91-7.94 (d, $J=8.43$ Hz, 1H), 7.68-7.70 (d, $J=8.43$ Hz, 1H), 7.44-7.58 (m, 3H), 7.12-7.25 (m, 4H), 6.87-6.90 (d, $J=8.89$ Hz, 1H), 3.99-4.03 (d, $J=11.55$ Hz, 2H). **^{13}C NMR** (125 MHz, D_2O) δ 128.86-131.03 (dd, $J=8.95$, 9.04, 265.33 Hz, 2C), 127.52 (s, 1C), 126.52 (s, 1C), 125.92-125.5 (d, $J=3.47$ Hz, 1C), 123.08 (d, $J=1.56$ Hz, 1C), 122.03 (s, 1C), 114.60-116.03 (dd, $J=162.43$ Hz, 2C), 30.72-30.84 (d, $J=15.39$ Hz, 1C); quaternary carbons and some tertiary carbons not visible under these running conditions. **^{31}P NMR** (121 MHz, D_2O) δ 5.02. **^{19}F NMR** (282 MHz, D_2O) δ -113.24

Naphthalen-1-yl hydrogen (2,6-difluorobenzyl)phosphoramidate (B4). Following the general procedure above, the following quantities were used: 1-naphtyl phosphate (5 mg, 22.31 μmol), (2,6-difluorophenyl)methanamine (4.00 μL , 33.46 μmol), DBU (2.50 μL , 16.73 μmol), triphenylphosphine (5.85 mg, 22.31 μmol), and DIAD (4.34 μL , 22.31 μmol) in DCM (500 μL). Analysis by ESI+ (Expected $[\text{M}+\text{H}]^+=350.27$. Observed $[\text{M}+\text{H}]^+=350.25$). **^1H NMR** (300 MHz, D_2O) δ 8.25-8.27 (d, $J=6.64$ Hz, 1H), 7.96-7.99 (d, $J=7.01$ Hz, 1H), 7.83-7.90 (m, 1H), 7.74-7.77 (d, $J=8.23$ Hz, 1H), 7.60-7.74 (p, $J=2.10$, 2.29, 3.84, 3.84 Hz, 2H), 7.49-7.51 (t, $J=3.21$, 3.65 Hz, 1H), 7.42-7.45 (d, $J=7.64$ Hz, 1H), 7.08-7.13 (t, $J=8.02$, 8.11 Hz, 2H), 4.13-4.18 (d, $J=13.24$ Hz, 2H). **^{13}C NMR** (125 MHz, D_2O) δ 160.09-162.12 (dd, $J=7.28$, 246.98 Hz, 2C), 147.94 (d, $J=7.15$ Hz, 1C), 134.45 (s, 1C), 127.64 (s, 2C), 126.88 (s, 2C), 126.23 (s, 1C), 126.02 (d, $J=1.52$ Hz, 1C), 123.71 (d, $J=1.32$ Hz, 1C), 122.03 (s, 1C), 115.08 (d, $J=3.20$ Hz, 1C), 111.79-111.60 (dd, $J=5.00$, 5.00, 19.23 Hz, 1C), 33.04 (t, $J=3.56$, 3.78 Hz, 1C). **^{31}P NMR** (121 MHz, D_2O) δ 3.99. **^{19}F NMR** (282 MHz, D_2O) δ -114.99.

Isopropyl (hydroxy(naphthalen-1-yloxy)phosphoryl)-L-alaninate (B5). Following the general procedure above, the following quantities were used: 1-naphtyl phosphate (5 mg, 22.31 μmol), isopropyl L-alaninate hydrochloride (4.39 mg, 33.46 μmol), DBU (2 equiv., 6.67 μL , 44.62 μmol), triphenylphosphine (5.85 mg, 22.31 μmol), and DIAD (4.34 μL , 22.31 μmol) in DCM (500 μL). Analysis by ESI+ (Expected $[\text{M}+\text{H}]^+ = 320.34$. Observed $[\text{M}+\text{H}]^+ = 320.33$). **^1H NMR** (300 MHz, D_2O) δ 8.25-8.28 (d, $J=9.76$ Hz, 1H), 7.96-7.99 (d, $J=9.39$ Hz, 1H), 7.75-7.77 (d, $J=8.82$ Hz, 1H), 7.60-7.64 (m, 2H), 7.50-7.55 (t, $J=7.39$, 7.86 Hz, 1H), 7.43-7.46 (d, $J=7.86$ Hz, 1H), 5.07-5.15 (m, 1H), 3.80-3.85 (m, 1H), 1.54-1.57 (d, $J=7.20$ Hz, 6H), 1.24-1.27 (d, $J=7.42$ Hz, 3H). **^{13}C NMR** (125 MHz, D_2O) δ 176.27-176.30 (d, $J=4.29$ Hz, 1C), 147.95-147.89 (d, $J=7.13$ Hz, 1C), 134.46 (s, 1C), 127.66 (s, 1C), 126.71 (s, 2C), 126.25 (s, 1C), 126.04 (d, $J=1.41$ Hz, 1C), 123.73 (d, $J=1.11$ Hz, 1C), 122.04 (s, 1C), 115.07-115.09 (d, $J=3.14$ Hz, 1C), 70.22 (s, 1C), 55.83 (s, 1C), 20.26 (s, 2C), 15.04 (s, 1C). **^{31}P NMR** (121 MHz, D_2O) δ 2.66

Naphthalen-1-yl hydrogen (cyclohexylmethyl)phosphoramidate (B6). Following the general procedure above, the following quantities were used: 1-naphtyl phosphate (5 mg, 22.31 μmol), cyclohexane methylamine (4.35 μL , 33.46 μmol), DBU (2.50 μL , 16.73 μmol), triphenylphosphine (5.85 mg, 22.31 μmol), and DIAD (4.34 μL , 22.31 μmol) in DCM (500 μL). Analysis by ESI+ (Expected $[\text{M}+\text{H}]^+ = 320.34$. Observed $[\text{M}+\text{H}]^+ = 320.33$). **^1H NMR** (300 MHz, D_2O) δ 8.33 (d, $J=4.52$ Hz, 1H), 7.98 (d, $J=4.96$ Hz, 1H), 7.71-7.73 (d, $J=8.16$ Hz, 1H), 7.60-7.63 (m, 2H), 7.50-7.55 (t, $J=7.81$, 7.88 Hz, 1H), 7.44-7.45 (d, $J=7.53$ Hz, 1H), 2.61-2.66 (dd, $J=10.82$ Hz, 2H), 1.62-1.76 (m, 11H). **^{13}C NMR** (125 MHz, D_2O) 148.73 (d, $J=7.40$ Hz, 1C), 134.41 (s, 1C), 127.54 (s, 1C), 126.17 (d, $J=1.15$ Hz, 1C), 126.06 (s, 1C), 125.95 (s, 2C), 122.35 (s, 1C), 114.72 (d, $J=3.11$ Hz, 1C), 51.93 (s, 1C), 37.79 (s, 1C), 25.49 (s, 1C), 24.95 (s, 2C), 21.05 (s, 2C); some quaternary carbons not visible under these running conditions. **^{31}P NMR** (121 MHz, D_2O) δ 6.27.

Naphthalen-1-yl hydrogen cyclopropylphosphoramidate (B7). Following the general procedure above, the following quantities were used: 1-naphtyl phosphate (5 mg, 22.31 μmol), cyclopropylamine (2.32 μL , 33.46 μmol), DBU (2.50 μL , 16.73 μmol), triphenylphosphine (5.85 mg, 22.31 μmol), and DIAD (4.34 μL , 22.31 μmol) in DCM (500 μL). Analysis by ESI+ (Expected $[\text{M}+\text{H}]^+ = 264.23$. Observed $[\text{M}+\text{H}]^+ = 264.21$). **^1H NMR** (300 MHz, D_2O) δ 8.31 (d, $J=6.10$ Hz, 1H), 7.97 (d, $J=6.34$ Hz, 1H), 7.73 (d, $J=7.71$ Hz, 1H), 7.61-7.64 (p, $J=1.71$, 1.76, 3.86, 3.89 Hz,

2H), 7.50-7.55 (t, $J=7.84, 8.87$ Hz, 1H), 7.44-7.47 (d, $J=7.70$ Hz, 1H), 2.3-2.45 (m, 1H), 0.85-0.88 (d, $J=5.20$ Hz, 2H), 0.51-0.54 (d, $J=6.37$ Hz, 2H). **^{13}C NMR** (125 MHz, D_2O) δ 148.90 (d, $J=7.20$ Hz, 1C), 134.44 (s, 1C), 127.63 (s, 1C), 126.66 (s, 1C), 126.12 (s, 2C), 126.06 (d, $J=1.36$ Hz, 1C), 123.77 (d, $J=1.61$ Hz, 1C), 122.15 (s, 1C), 114.62 (d, $J=3.28$ Hz, 1C), 6.10 (s, 2C), 6.02 (d, $J=5.39$ Hz, 1C). **^{31}P NMR** (121 MHz, D_2O) δ 5.0.

Naphthalen-1-yl hydrogen cyclobutylphosphoramidate (B8). Following the general procedure above, the following quantities were used: 1-naphtyl phosphate (5 mg, 22.31 μmol), cyclobutylamine (2.86 μL , 33.46 μmol), DBU (2.50 μL , 16.73 μmol), triphenylphosphine (5.85 mg, 22.31 μmol), and DIAD (4.34 μL , 22.31 μmol) in DCM (500 μL). Analysis by ESI+ (Expected $[\text{M}+\text{H}]^+=278.26$. Observed $[\text{M}+\text{H}]^+=278.87$).

Naphthalen-1-yl hydrogen (Z)-octadec-9-en-1-ylphosphoramidate (B9). Following the general procedure above, the following quantities were used: 1-naphtyl phosphate (5 mg, 22.31 μmol), oleylamine (11.01 μL , 33.46 μmol), DBU (2.50 μL , 16.73 μmol), triphenylphosphine (5.85 mg, 22.31 μmol), and DIAD (4.34 μL , 22.31 μmol) in DCM (500 μL). Analysis by ESI+ (Expected $[\text{M}+\text{H}]^+=474.63$. Observed $[\text{M}+\text{H}]^+=474.91$).

Naphthalen-1-yl hydrogen ((S)-1-phenylethyl)phosphoramidate (B10). Following the general procedure above, the following quantities were used: 1-naphtyl phosphate (5 mg, 22.31 μmol), (*R*)-1-phenylethan-1-amine (4.26 μL , 33.46 μmol), DBU (2.50 μL , 16.73 μmol), triphenylphosphine (5.85 mg, 22.31 μmol), and DIAD (4.34 μL , 22.31 μmol) in DCM (500 μL). Analysis by ESI+ (Expected $[\text{M}+\text{H}]^+=328.32$. Observed $[\text{M}+\text{H}]^+=328.36$).

Naphthalen-1-yl hydrogen ((R)-1-phenylethyl)phosphoramidate (B11). Following the general procedure above, the following quantities were used: 1-naphtyl phosphate (5 mg, 22.31 μmol), (*R*)-1-phenylethan-1-amine (4.26 μL , 33.46 μmol), DBU (2.50 μL , 16.73 μmol), triphenylphosphine (5.85 mg, 22.31 μmol), and DIAD (4.34 μL , 22.31 μmol) in DCM (500 μL). Analysis by ESI+ (Expected $[\text{M}+\text{H}]^+=328.32$. Observed $[\text{M}+\text{H}]^+=328.36$).

((2*S*,3*R*,4*R*,5*R*)-5-(6-amino-2-fluoro-9*H*-purin-9-yl)-3,4-dihydroxytetrahydrofuran-2-yl)methyl hydrogen benzylphosphoramidate (B12). Following the general procedure above, the following quantities were used: Fludarabine monophosphate (5 mg, 13.69 μ mol), benzylamine (2.24 μ L, 20.54 μ mol), triphenylphosphine (3.59 mg, 13.69 μ mol), and DIAD (2.66 μ L, 13.69 μ mol) in NMP (500 μ L). Analysis by ESI+ (Expected $[M+H]^+ = 455.36$. Observed $[M+H]^+ = 455.48$). **¹H NMR** (300 MHz, D₂O) δ 8.26 (s, 1H), 7.42-7.47 (m, 5H), 6.20-6.22 (d, $J=6.12$ Hz, 1H), 4.59-4.63 (t, $J=6.47, 6.71$ Hz, 1H), 4.42-4.46 (t, $J=6.86, 6.86$ Hz, 1H), 4.01-4.07 (m, 3H), 3.84-3.87 (d, $J=9.65$ Hz, 2H). **¹³C NMR** (125 MHz, D₂O) δ 156.5-160.22 (d, $J=255.64$ Hz, 1C), 150.09-50.34 (d, $J=18.85$ Hz, 1C), 140.64-140.74 (d, $J=7.41$ Hz, 1C), 129.17 (s, 2C), 128.60 (s, 1C), 128.28 (s, 2C), 128.08 (s, 1C), 116.31-116.36 (d, $J=4.16$ Hz, 1C), 82.84 (s, 1C), 80.95-81.07 (d, $J=8.88$ Hz, 1C), 75.39 (s, 1C), 73.26 (s, 1C), 62.86-62.93 (d, $J=5.17$ Hz, 1C), 44.93 (s, 1C). **³¹P NMR** (121 MHz, D₂O) δ 8.70.

((2*S*,3*R*,4*R*,5*R*)-5-(6-amino-2-fluoro-9*H*-purin-9-yl)-3,4 dihydroxytetrahydrofuran-2-yl)methyl hydrogen (pyridin-2-ylmethyl)phosphoramidate (B13). Following the general procedure above, the following quantities were used: Fludarabine (5 mg, 13.69 μ mol), pyridin-2-ylmethanamine (2.12 μ L, 20.54 μ mol), triphenylphosphine (3.59 mg, 13.69 μ mol), and DIAD (2.66 μ L, 13.69 μ mol) in NMP (500 μ L). Analysis by ESI+ (Expected $[M+H]^+ = 456.34$. Observed $[M+H]^+ = 456.42$). **¹H NMR** (300 MHz, D₂O) δ 8.56-8.58 (d, $J=4.88$ Hz, 1H), 8.22 (s, 1H), 7.47-7.50 (d, $J=8.38$ Hz, 1H), 7.46-7.47 (t, $J=3.70, 3.90$ Hz, 1H), 7.16-7.20 (t, $J=6.61, 6.63$ Hz, 1H), 6.16-6.18 (d, $J=6.29$ Hz, 1H), 4.58-4.63 (t, $J=6.49, 6.95$ Hz, 1H), 4.42-4.45 (t, $J=6.95, 6.95$ Hz, 1H), 4.04-4.13 (m, 3H), 3.99-4.02 (d, $J=10.18$ Hz, 2H). **¹³C NMR** (75 MHz, D₂O) δ 151.47-154.72 (d, $J=246.11$ Hz, 1C), 149.18 (s, 1C), 147.18 (s, 1C), 141.16-141.20 (d, $J=2.47$ Hz, 1C), 138.52 (s, 1C), 123.09 (s, 1C), 122.42 (s, 1C), 82.72 (s, 1C), 80.79-80.90 (d, $J=8.60$ Hz, 1C), 75.36 (s, 1C), 73.09 (s, 1C), 62.87-62.93 (d, $J=4.82$ Hz, 1C), 45.77 (s, 1C); some quaternary carbons not visible under these running conditions. **³¹P NMR** (121 MHz, D₂O) δ 8.38.

((2*S*,3*R*,4*R*,5*R*)-5-(6-amino-2-fluoro-9*H*-purin-9-yl)-3,4-dihydroxytetrahydrofuran-2-yl)methyl hydrogen cyclopropylphosphoramidate (B14). Following the general procedure above, the following quantities were used: Fludarabine monophosphate (5 mg, 13.69 μ mol), cyclopropylamine (1.34 μ L, 20.54 μ mol), triphenylphosphine (3.59 mg, 13.69 μ mol), and DIAD

(2.66 μL , 13.69 μmol) in NMP (500 μL). Analysis by ESI+ (Expected $[\text{M}+\text{H}]^+ = 405.30$. Observed $[\text{M}+\text{H}]^+ = 405.37$). **^1H NMR** (300 MHz, D_2O) δ 8.44 (s, 1H), 6.31-6.33 (d, $J=6.08$ Hz, 1H), 4.61-4.65 (t, $J=6.29$, 6.33 Hz, 1H), 4.46-4.50 (t, $J=6.90$, 6.80 Hz, 1H), 4.14-4.22 (m, 3H), 2.24-2.32 (m, 1H), 0.86-0.89 (m, 2H), 0.44-0.467 (m, 2H). **^{13}C NMR** (75 MHz, D_2O) δ 149.25-149.43 (d, $J=13.71$ Hz, 1C), 141.07-141.10 (d, $J=2.79$ Hz, 1C), 83.40 (s, 1C), 80.09-81.11 (d, $J=8.75$ Hz, 1C), 75.51 (s, 1C), 73.16 (s, 1C), 63.15-63.18 (d, $J=3.15$ Hz, 1C), 22.92-23.00 (d, $J=5.93$ Hz, 1C), 6.11 (s, 2C); some quaternary carbons not visible under these running conditions. **^{31}P NMR** (121 MHz, D_2O) δ 7.97.

Isopropyl (((((2*S*,3*R*,4*R*,5*R*)-5-(6-amino-2-fluoro-9*H*-purin-9-yl)-3,4-dihydroxytetrahydrofuran-2-yl)methoxy)(hydroxy)phosphoryl)-*D*-alaninate (B15).

Following the general procedure above, the following quantities were used: Fludarabine monophosphate (5 mg, 13.69 μmol , **22**), isopropyl *L*-alaninate hydrochloric acid salt (3.59 mg, 27.38 μmol), triethylamine (3.82 μL , 27.39 μmol), triphenylphosphine (3.59 mg, 13.69 μmol), and DIAD (2.66 μL , 13.69 μmol) in NMP (500 μL). Analysis by ESI+ (Expected $[\text{M}+\text{H}]^+ = 479.37$. Observed $[\text{M}+\text{H}]^+ = 479.50$). **^1H NMR** (300 MHz, D_2O) δ 8.14 (s, 1H), 5.99-6.00 (d, $J=6.37$ Hz, 1H), 5.09-5.17 (m, 1H), 4.61-4.65 (t, $J=6.55$, 6.67 Hz, 1H), 4.30-4.35 (t, $J=7.99$, 7.99 Hz, 1H), 4.09-4.20 (m, 3H), 3.61-3.71 (m, 1H), 1.57-1.59 (d, $J=7.34$ Hz, 3H), 1.28-1.30 (d, $J=7.78$ Hz, 6H). **^{13}C NMR** (75 MHz, D_2O) δ 176.77-176.83 (d, $J=4.58$ Hz, 1C), 156.41-156.67 (d, $J=18.94$ Hz, 1C), 140.33-140.36 (d, $J=2.61$ Hz, 1C), 85.24 (s, 1C), 83.22-83.29 (d, $J=5.37$ Hz, 1C), 75.65 (s, 1C), 73.59 (s, 1C), 48.94 (s, 1C), 72.30 (s, 1C), 63.26-63.32 (d, $J=4.66$ Hz, 1C), 20.64 (s, 2C), 15.07 (s, 1C); some quaternary carbons not visible under these running conditions. **^{31}P NMR** (121 MHz, D_2O) δ 6.37.

Preparation of ^{18}O -labeled naphthalen-1-yl hydrogen for mechanistic studies. ^{18}O -labeled naphthalen-1-yl hydrogen was prepared using a modified version of a previously published procedure (128). To neat SOCl_2 , 1-naphtyl phosphate (5 mg, 22.31 μmol) and DMF (20 μL) were added. The reaction was allowed to proceed for 24 h. Then, the crude dichlorinated product was concentrated under a stream of nitrogen and re-dissolved in anhydrous CHCl_3 and cooled to 0°C . Then, H_2^{18}O was added dropwise and the reaction was allowed to stir for 2 h. The reaction was then concentrated under reduced pressure and purified via reverse-phase HPLC (Agilent G1361A

1260 Infinity) using a stepwise gradient (1-60% Buffer B over 25 minutes, 60-100% Buffer B over 10 minutes, 100% Buffer B over 5 minutes, 100-0% Buffer B over 1 minute; Buffer A: dH₂O with 0.1% TFA, Buffer B: CH₃CN + 0.1% TFA). Product-containing fractions were combined and lyophilized to a white solid.

NMR reaction monitoring assay. ³¹P NMR scans were taken at 121 MHz in 80% NMP 20% CDCl₃ (500 μL). Reaction conditions were similar to those described for (B1). Briefly, 1-naphtyl phosphate (5 mg, 22.31 μmol), triphenylphosphine (5.85 mg, 22.31 μmol), benzylamine (3.65 μL, 33.46 μmol), and DIAD (4.34 μL, 22.31 μmol) were added sequentially. The reaction was monitored (ns = 100) for 1 h.

CHAPTER 3. ALIPHATIC AMINES ARE VIABLE PROMOETIES IN PHOSPHONOAMIDATE-CONTAINING DRUGS

A continuation of Case Study 1.

Part of this chapter has been published in (permission granted)

Yan VC, Pham CD, Arthur K, Yang KL, Muller FL. 2020. Aliphatic amines are viable pro-drug moieties in phosphonoamidate drugs. *Bioorganic Med Chem Lett* 30:127656.

3.1 Abstract

Phosphate and phosphonates containing a single P-N bond are frequently used prodrug motifs to improve cell permeability of these otherwise anionic moieties (16). Upon entry into the cell, the P-N bond is cleaved by phosphoramidases to release the active agent (32, 33). Here, we apply a novel mono-amidation strategy (129) to our laboratory's phosphonate-containing glycolysis inhibitor and show that a diverse panel of phosphonoamidates may be rapidly generated for *in vitro* screening. We show that, in contrast to the canonical L-alanine or benzylamine moieties which have previously been reported as efficacious prodrug moieties, small and long-chain aliphatic amines demonstrate greater drug release efficacy for our phosphonate inhibitor. These results expand the scope of possible amine prodrugs that can be used as second prodrug leave groups for phosphate or phosphonate-containing drugs.

3.2 Hypothesis

Small, aliphatic amines may be more effective promoieties on phosphonoamidate prodrugs compared to benzylamine due to their increased hydrophilicity.

3.3 Introduction

Phosphoramidates are structurally intriguing chemical moieties with high biological and therapeutic relevance (16). Within the realm of drug development, the inclusion of a phosphoramidate moiety has become an increasingly attractive prodrug strategy for anionic phosphate- or phosphonate-containing drugs. Upon entering the cell, the P-N bond would eventually be cleaved by a class of enzymes known as phosphoramidases (*Section 1.2.2* (32, 33)). From anti-viral drugs such as TAF (44), SOF (42), and RDV (38) to emerging prodrugs of conventional chemotherapies such as gemcitabine (NUC-103, Accelerin (130)) and 5-fluorouracil

(NUC-3373), the phosphoramidate-containing “ProTide” approach to delivering phosphate or phosphonate drugs is a central theme in prodrug development. Common to these drugs is the presence of an α -amino acid motif, especially the L-alaninate ester moiety, which is used as a substrate for phosphoramidase cleavage. In most cases, the L-amino acid-conjugated phosph(on)ate is preferentially cleaved by HINT1; rarely is the D-amino acid-conjugated phosph(on)ate preferentially cleaved (131). To the best of our knowledge, the only other amine that has been reported in the context of phosphoramidate or phosphonoamidate clinical candidates is the benzylamine moiety found in IDX-184 (132). These observations would suggest that either the L-alaninate or benzylamine moieties would be the most optimal amine substrates for release by phosphoramidases. Fundamental biochemical studies have explored the relationship between altering the amine on phosphoramidate versions of AMP rate of hydrolysis by the phosphoramidases *in vitro*. These studies suggest that amines beyond L-alaninate esters and benzylamine may also be used as second prodrug groups. Indeed, SAR studies for a couple of aliphatic amines have been conducted for the nucleoside of IDX-184 (97). These aliphatic mono-amidates (morpholine, isopropylamine) were prepared via Atherton-Todd reaction and exhibited slightly decreased antiviral activity against HCV1b-infected MT4 cells in the subgenomic luciferase replicon assay (97). Further investigation into the structural limits of optimal amine leave groups in other contexts beyond nucleoside monophosphates have yet to be reported perhaps due to the difficulty in preparing mono-amidated substrates, especially for phosphonate prodrugs (Section 1.7). Current mono-amidation strategies are hampered by harsh reaction conditions, hazardous reagents, challenging purifications, and inconsistent yields (16). We have reported the development of a facile, convenient mono-amidation method based on the Mitsunobu coupling; when applied to either phosphonic or phosphoric acids, the corresponding mono-amidate can be generated reliably in good yields (129). Here, we report the efficacy of various structurally diverse amine prodrug groups in the context of our laboratory’s phosphonate inhibitor of the glycolytic enzyme enolase, HEX. We validate the finding that benzylamine and other benzylic amines may be used as second prodrug groups and also demonstrate that, in the context of HEX, aliphatic amines are often superior delivery moieties. These results may prompt further investigation into using aliphatic amines as prodrug moieties for phosphate or phosphonate-containing drugs.

3.4 Results and Discussion

We generated a diverse panel of phosphonoamidate prodrugs of HEX using a novel monoamidation reaction that we had previously discovered (129) while screening for amine promoieties that could deliver HEX to treat cancers harboring homozygous deletions of *ENO1* under the collateral lethality paradigm (4, 5). To evaluate the relationship between our amine promoiety and efficacy of drug delivery, we first esterified the other free hydroxyl on the phosphonic acid to enable efficient cell permeability (**Figure 20a**). We chose the pivaloyloxymethyl (POM) group as the first ester group due to its known susceptibility for hydrolysis by ubiquitously expressed esterases (29). Importantly, our decision to employ the labile POM ester minimizes the confounding effects of initial prodrug cleavage. This is because it has been established that the POM ester is readily removed *in vitro* (29, 133). Thus, differences in potency for each phosphonoamidate prodrug can be attributed to efficiency of P-N bond cleavage (**Figure 20b**). Mono-amidated products generated from reactions with BnHEX were subject to POM esterification, followed by hydrogenation to liberate the hydroxamate—an essential moiety for Enolase active site inhibition (6, 134). Esterified phosphonoamidates all demonstrated selective activity against *ENO1*-deleted glioma cells (D423) compared to ENO1-rescued (D423 ENO1) and ENO1-wildtype glioma cells (LN319) (**Figure 20c**). Given the focus on aryl and benzylic amines as prodrug motifs in the literature, we were pleasantly surprised to find that aliphatic amines proved to be more productively cleaved in our *in vitro* system. Cyclopropylmethanamine-protected HEX exhibited 10-fold greater potency compared to benzylamine-protected HEX (IC_{50} , D423 = 22 nM versus 244 nM, **Figure 18c**). Direct comparison of benzylamine-protected HEX to its saturated counterpart, cyclohexane methylamine, likewise showed greater potency of the latter (**Figure 20c, entry 3 vs. 11**).

Among the panel of amines synthesized, one that was particularly intriguing was dodecylamine, a long chain alkylamine (**Figure 21**, CDP22). Owing to its lipophilicity and structural resemblance to a phospholipid (**Figure 21**), we found that esterification of the second phosphonate hydroxyl was unnecessary to achieve good potency against D423 cells (**Figure 21**). In support of the hypothesis that CDP22 may permeate cells due to the aforementioned properties, we performed a head-to-head comparison between CDP22 and VCY33, the free phosphonoamidate counterpart to VCY32 (**Figure 21**). Compared to VCY33, which required micromolar concentrations to exert

meaningful activity against D423 cells (**Figure 21**), CDP22 demonstrated good activity at approximately 24 nM.

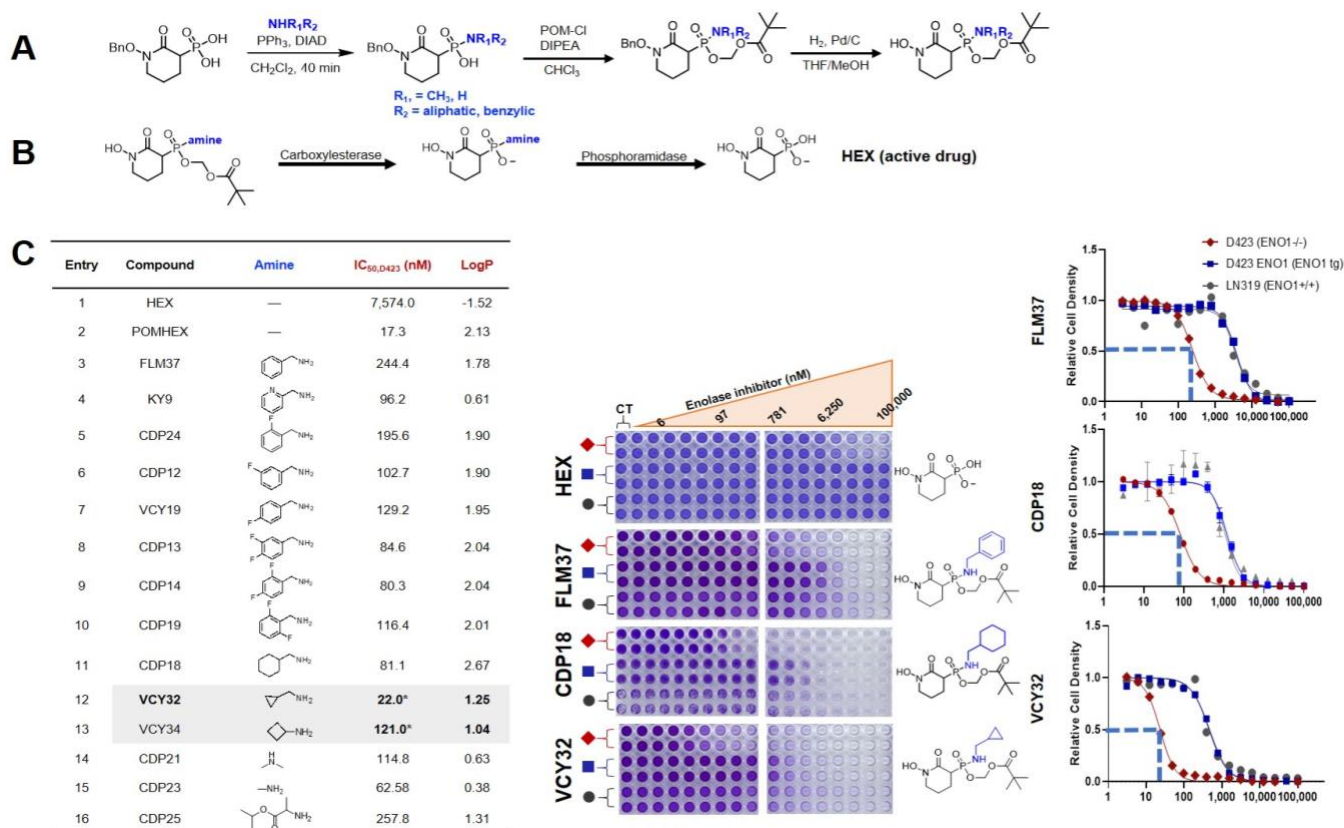


Figure 20. Aliphatic amines offer superior drug delivery *in vitro*. (A) General workflow for the synthesis and screening amidated pro-drugs. For BnHEX, POM esterification followed by de-benzylation of the hydroxamate yields the final, cell-permeable pro-drug. For specific reaction conditions, see Experimental (Section 3.6). (B) Proposed bioactivation mechanism for phosphonoamidate pro-drugs. Phosphoramidases cleave P-N bonds on anionic molecules and can thus serve as second pro-drug deprotecting enzymes. (C) The relationship between amine structure and pro-drug efficacy can be evaluated in cell-based screening. (Left) Structures of amine pro-drugs of the Enolase inhibitor with logP values (calculated from Molinspiration). (Middle) Crystal violet cell proliferation assay evidences greater cell killing against D423 cells by aliphatic amine pro-drugs compared to benzylamine. Cells were incubated with pro-drug inhibitor for 5 days. Then, cells were fixed and stained with crystal violet and quantified spectroscopically. Cell density as measured by crystal violet were plotted as a function of inhibitor. (Right) Comparison of the IC₅₀ values between model aromatic (FLM37) and aliphatic (CDP18, VCY32) pro-drugs. While all 3 pro-drugs are selective for *ENO1*-deleted cells, derivatizing from an aromatic (FLM37) to an aliphatic amidate (CDP18) increased potency by 3-fold (IC₅₀ = 81.1 nM versus 244 nM). VCY32 featuring a smaller amine exhibits 10-fold greater potency compared to FLM37 (IC₅₀ = 22 nM vs 244 nM). *IC₅₀s in reference to respective POMHEX controls (VCY32 IC₅₀ = 22 nM vs. POMHEX IC₅₀ = 41.47 nM; VCY34 IC₅₀ = 121.0 nM vs. POMHEX IC₅₀ = 217.0 nM).

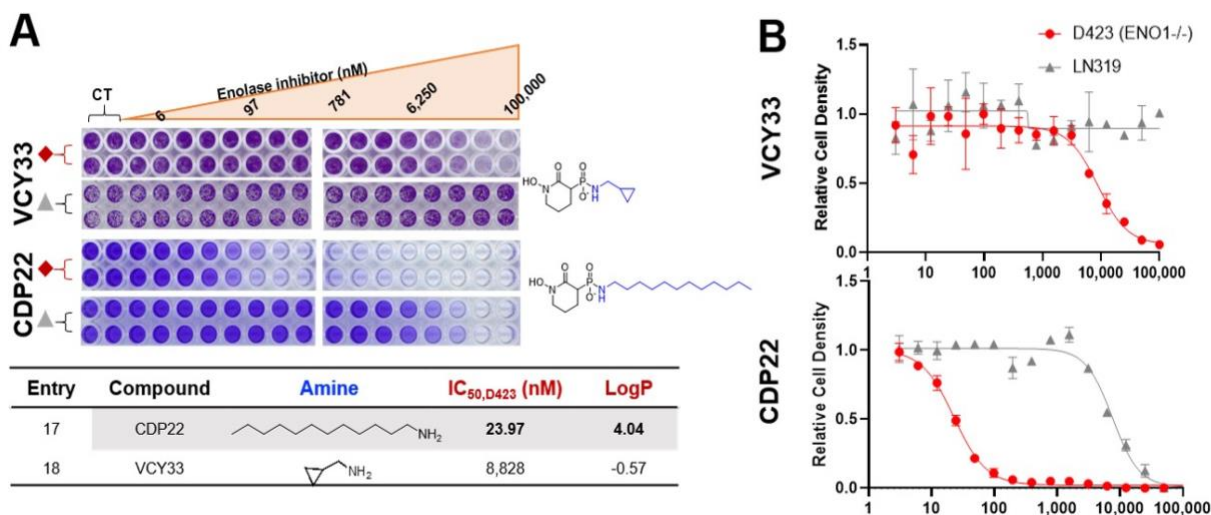


Figure 21 A long-chain aliphatic phosphonoamidate efficiently delivers HEX *in vitro*. (A) Proliferation assay evidences nanomolar cytotoxicity by the long-chain aliphatic amine prodrug against *ENO1*-deleted cells (top rows, red diamond) compared to *ENO1*-intact cells (bottom rows, grey triangle). (b) Dose-response relationship (nanomolar) between CDP22 and VCY33. While VCY33 as a small negatively charged phosphonoamidate exhibits a dramatic loss of potency (IC₅₀ = 8,828 nM) compared to its esterified counterpart, VCY32 (IC₅₀ = 22 nM), CDP22 exerts good activity despite its negative charge (IC₅₀ = 23 nM).

Preliminary investigations into the mechanism by which these aliphatic and benzylic amines are cleaved suggest a route different than that observed for L-amino acid esters in McGuigan prodrugs, which are known to be removed via HINT1 (Section 1.2.2 (32, 33)). HAP1 cells with CRISPR knockouts (KO) of either *HINT1* or *CES2* and treated with VCY32, CDP22, or POMHEX (**Figure 21**); HAP1 cells with KO of *PAPSS* (3'-phosphoadenosine-5'-phosphosulfate synthase) were used as a control. Unlike D423 cells, HAP1 cells are *ENO1* WT. Thus, while we did not anticipate low nanomolar toxicity against any of the HAP1 KO cell lines as we had observed in D423 cells, we hypothesized that, if HINT1 was the main enzyme responsible for cleaving aliphatic amines, then we would observe less cytotoxicity against *HINT1*⁻ cells. To our surprise, we found that cytotoxicity with VCY32, CDP22, and POMHEX were essentially the same across all HAP1 KO cell lines (**Figure 22**). Because there was no meaningful reduction in cytotoxicity against *HAP1*⁻ cells compared to *PAPSS*⁻ cells for VCY32 and CDP22, these data suggest that HINT1 is unlikely to be the main enzyme that cleaves aliphatic amines from phosphonates. Interestingly, we also observed no meaningful differences in cytotoxicity when VCY32 or POMHEX were tested in *CES2*⁻ cells. As discussed in Section 1.1.1, it has been extensively established that POM esters are

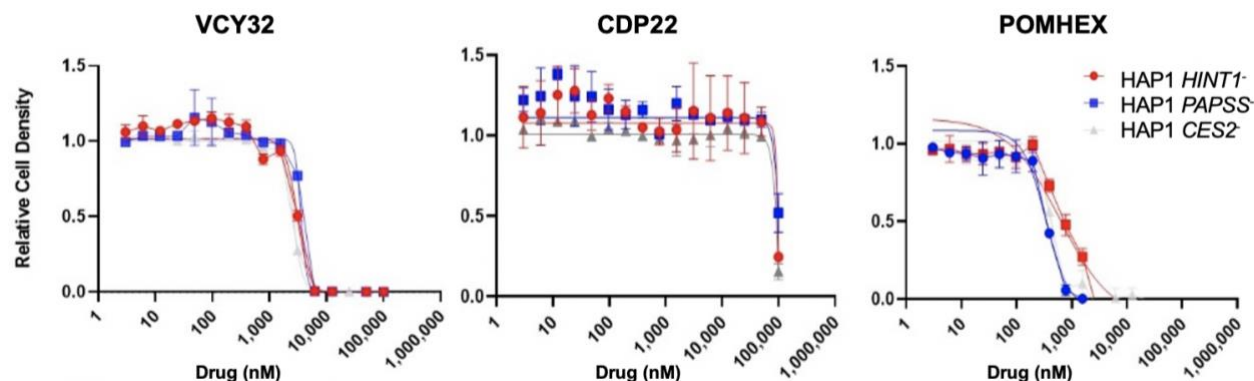


Figure 22. Aliphatic amines on phosphonates are not preferential substrates for HINT1. HAP1 cells containing CRISPR KO of either *HINT1* (red), *PAPSS* (blue, CT), or *CES2* (grey) were treated with a serial dilution of either VCY32 (left), CDP22 (middle) or POMHEX (right) for 4 days. Reduced cytotoxicity in either *HINT1*⁻ or *CES2*⁻ cells compared to CT cells (*PAPSS*⁻) was not observed for any compounds.

highly susceptible to cleavage by esterases (29). The bis-POM prodrug enolase inhibitor, POMHEX, has a transient $T_{1/2}$ in mouse plasma due to the presence of CES1 (**Figure 23**) (29); absence of CES1 in human plasma renders a slightly prolonged $T_{1/2}$ (24, 29, 39). Such observations suggest that CES1, which is highly expressed in the liver (Human Protein Atlas), is largely responsible for cleaving the first POM ester on POMHEX and related compounds such as VCY32. We conducted cytotoxicity comparisons in HAP1 *CES2*⁻ cells because CES1 is not expressed in HAP1 and because the haploid system is easily amenable to CRISPR KO. Negligible differences in cytotoxicity for POMHEX and VCY32 in HAP1 *CES2*⁻ cells seem to provide additional support that CES1, rather than CES2, is the major enzyme responsible for removing the first POM promoiety on these compounds (**Figure 23**).

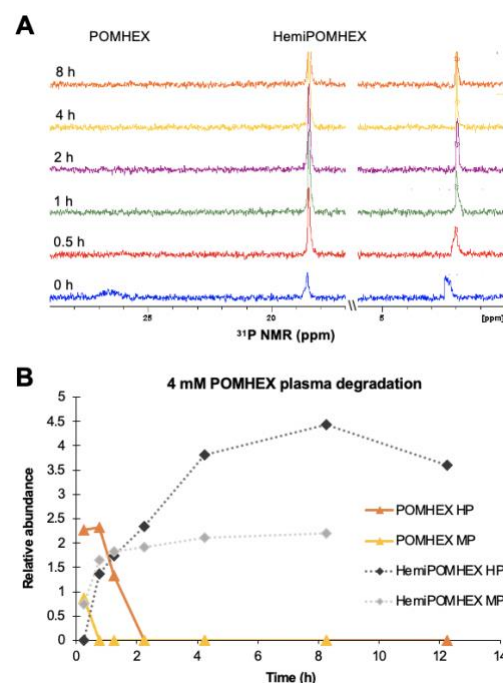


Figure 23. POMHEX is highly unstable in mouse and human plasma. 4 mM of POMHEX was dissolved in either 80% mouse (A) or human serum with 20% D₂O and assayed at the indicated time points. Chemical shifts (left to right ppm): POMHEX (27), HemiPOMHEX (15), PO₄³⁻(0). (B) Degradation of POMHEX to HemiPOMHEX in human plasma (HP) or mouse plasma (MP).

3.5 Conclusions

In sum, we have generated a panel of structurally diverse phosphonoamidate prodrugs of the Enolase inhibitor HEX that widen the scope of second leave groups possible for phosph(on)ate prodrugs. Our data show that low MW aliphatic amines are suitable promoieties that can be cleaved intracellularly at with seemingly greater efficiency than that observed for benzylamine (**Figure 20, entry 3 vs. 11**) (97). Preliminary mechanistic studies suggest that, unlike for amino acid esters on McGuigan prodrugs, these aliphatic and benzylic amines are not cleaved via HINT1. While a hydrophobic long chain alkylamine (CDP22) demonstrated good potency against *ENO1*-deleted cells *in vitro*, we found that there was no apparent correlation between potency and logP of the POM-esterified phosphonoamidate prodrugs (**Figure 20**). We have also shown that, for established second promoieties such as benzylamine, fluorine substitution is well-tolerated, pointing to the feasibility of applying ^{18}F -labeling methods to study pharmacodynamics for any phosphoramidase-labile pro-drug. Collectively, these data demonstrate the feasibility of using low MW aliphatic amines as second promoieties in phosph(on)ate-containing drugs.

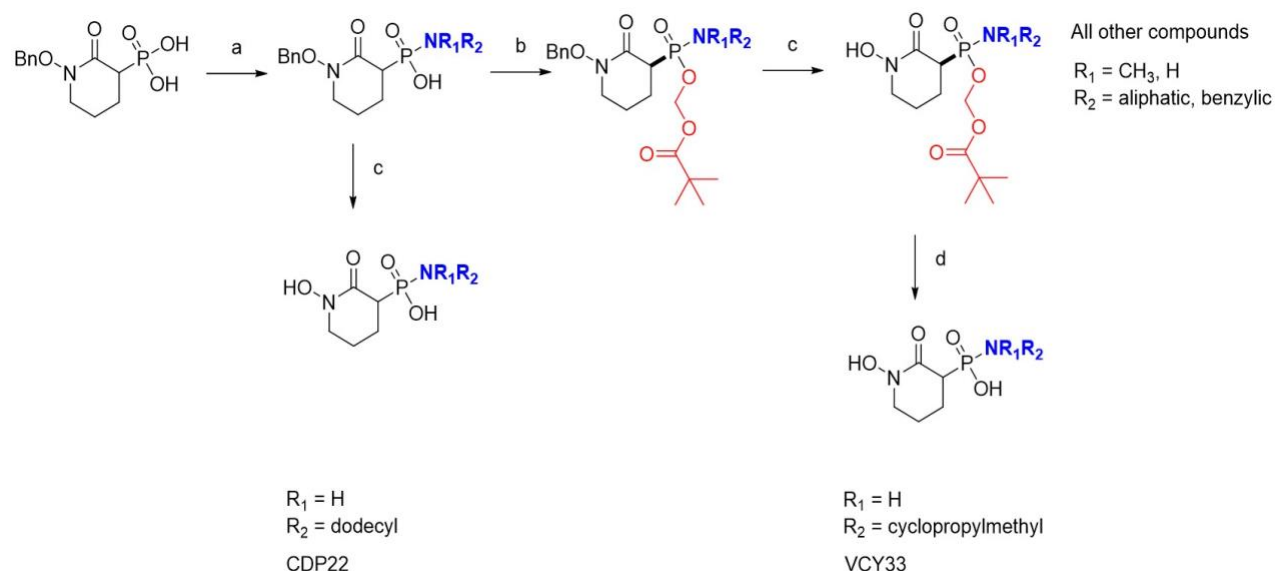
3.6 Experimental

General synthetic procedures. ^1H , ^{13}C , ^{31}P , and ^{19}F NMR spectra were recorded on a Bruker Avance 300 MHz spectrometer in either CDCl_3 or D_2O , unless otherwise indicated. Chemical shifts were measured in ppm relative to CDCl_3 ($\delta=7.24$ for ^1H and $\delta=77.0$ for ^{13}C) or D_2O ($\delta=4.80$ for ^1H). NMR characterizations are reported in the following order: chemical shift, multiplicity (s = singlet, bs = broad singlet, d = doublet, t = triplet, q = quartet, m = multiplet), and coupling constant (J, reported in Hertz). Where appropriate, 2-dimensional experiments (HSQC) and decoupled NMR experiments (^1H with ^{31}P decoupling) were used to support assignments. BnHEX was initially synthesized according to previously published procedures (29); subsequent syntheses were contracted to Wuxi AppTec, Shanghai, China. FLM37 was synthesized as described previously (47). Other starting materials were purchased at the highest commercial quality from Sigma Aldrich and were used without additional purification. Centrifugations were performed using an Eppendorf Centrifuge 5810R. Mass spectra were obtained on a Waters Acquity UPLC H-Class Plus system (A/B: a = 30% MeCN in water, b = 0.1% formic acid in water) using an electrospray ion source. HPLC purification of the final compound was performed on an Agilent Technologies 1260 infinity LC system using C18 reverse phase preparative column (Phenomenex,

Luna® 5 µm C18(2) 100 Å; LC column 250 x 21.2 mm, ax). All final compounds were determined to be at least 95% pure by LC analysis.

³¹P NMR degradation assay. 4 mM POMHEX (in DMSO) were dissolved in either 80% mouse plasma 20% D₂O or 80% human plasma, 20% D₂O in an NMR tube. Samples were run at 202 MHz, ns=500, 25°C.

***In vitro* cytotoxicity assay.** Cell culture experiments were conducted using the D423-MG cell line. 1p36 homozygous deletion in D423 includes the genes from *CAMTA1* to *SLC25A33*; this includes *ENO1*. Isogenic *ENO1* ectopically rescued lines were described previously (pCMV ENO1 5X) (4, 6, 29). An *ENO1*-intact cell line (LN319) was used as a control for sensitivity to enolase inhibitors. HAP1 CRISPR KO cells (*HINT1*⁻, *PAPSS*⁻, or *CES2*⁻) were purchased from Horizon. Cells were routinely cultured in Dulbecco's modified Eagle's medium supplemented with 10% fetal bovine serum. Cell viability was determined by crystal violet staining, as previously described (4, 6, 29). The cell lines used were D423 (*ENO1*-deleted), D423 ENO1 (overexpressing *ENO1*) and LN319 (control). Glioma cells were seeded in 96-well plates and treated with varying concentrations of the inhibitors described above for 5-7 days. Cells were then washed with PBS, fixed with 10% formalin and stained with 0.05% crystal violet. Washed and dried plates were dye-extracted using 10% acetic acid, and absorbance was measured at 595 nm using Omegastar Plate Reader (BMG Labtech). Crystal violet staining was then performed as described above.



Scheme 2. Synthesis of structurally diverse phosphonoamidates. Conditions: (a) NHR_1R_2 , PPh_3 , DIAD, CH_2Cl_2 , 30 min, 0°C -RT. (b) POM-Cl, MeCN, 50°C , 2 h. (c) H_2 , Pd/C, MeOH/THF, 2 h, RT. (d) Cs_2CO_3 , MeOH, RT, 1 h. Pro-drug moieties in blue represent a second pro-drug leave group while those in red represent a first pro-drug leave group. To screen efficacy of the amine as a second pro-drug leave group, the BnHEX phosphonoamidate was first esterified with a known, esterase-labile pivaloyloxymethyl (POM) group and then de-benzylated to liberate the crucial hydroxamate moiety. CDP22 was not esterified with a POM moiety. VCY33 was generated from VCY32 via ester cleavage with Cs_2CO_3 in MeOH.

General procedure (G1, Scheme 2a) for the synthesis of phosphonoamidates from BnHEX.

All coupling reactions described for BnHEX were performed as described in *Chapter 2*.

General procedure (G2, Scheme 2b) for the synthesis of POM esters from BnHEX phosphonoamidates.

All esterification reactions with POM-Cl follow the same general procedure. BnHEX phosphonoamidate was dissolved in CHCl_3 . To this solution DIPEA (2 eq.) was added followed by POM-Cl (2 eq.). The solution was stirred at 50°C for 2h. The crude reaction mixture was then transferred to a 50 mL Falcon tube, where 2 volumes of H_2O was added. The reaction was vortexed and centrifuged twice (4000 rpm, 4°C) each for 2 minutes. The organic layer was then isolated, washed with brine, dried over Na_2SO_4 , evaporated and lyophilized to a colorless oil, unless otherwise specified.

General procedure (G3, Scheme 2c) for the debenzylation of BnHEX phosphonoamidate POM esters. Pd (10%) on carbon (1:1 w/w) was suspended in anhydrous MeOH/THF (3:2 v/v) in an appropriate reaction vial or round bottom flask with a septum. Two balloons were filled with H₂, one of which was attached to the septum to purge for 3 min. Then the second balloon was attached and the suspension was left to stir at RT for 30 min to saturate it with H₂. BnHEX phosphonoamidate POM ester was dissolved in 200-500 μ L MeOH or THF and added to the stirring suspension which was purged for 3 min by removing 1 balloon. Then the balloon was reattached and the suspension was left to stir at RT for another 2 h. The reaction mixture was filtered with a 0.22 μ m sterile filter and filtrate was evaporated and purified via HPLC to obtain a colorless solid, unless otherwise specified.

Synthesis of KY9 (Figure 17, entry 4).

***P*-(1-(benzyloxy)-2-oxopiperidin-3-yl)-*N*-(pyridin-2-ylmethyl)phosphonamidic acid (4a).** Following the procedure G1, the following quantities were used: DIAD (68.17 μ L, 350.59 μ mol) and triphenylphosphine (43.87 mg, 350.59 μ mol) in anhydrous DCM (3 mL). BnHEX (**1**, 50 mg, 175.29 μ mol) and pyridin-2-ylmethanamine (37.83 μ L, 350.59 μ mol) in anhydrous DCM (1 mL). The product was lyophilized to an orange oil. Yield: 48.60 mg (74%). Analysis by ESI+ (Expected [M+H]⁺ = 376.36. Observed [M+H]⁺ = 376.35). ¹H NMR (300 MHz, CDCl₃) δ 8.38 (d, J=4.73 Hz, 1H), 7.83 (t, J=1.77 Hz, 1.92 Hz, 1H), 7.37-7.49 (m, 7H), 4.90 (d, J=2.02 Hz, 2H), 3.43-3.58 (m, 2H), 2.79-2.91 (dt, J=21.84 Hz, 1H), 2.06-2.14 (m, 1H), 1.91-1.99 (m, 2H), 1.70-1.81 (m, 1H). ³¹P NMR (121 MHz, CDCl₃) δ 20.60 (1P).

(((1-(benzyloxy)-2-oxopiperidin-3-yl)((pyridin-2-ylmethyl)amino)phosphoryl)oxy)-methyl pivalate (4b). Following the procedure G2, the following quantities were used: POM-Cl (37.86 μ L, 258.95 μ mol), DIPEA (45.17 μ L, 258.95 μ mol), **2a** (48.6 mg, 129.47 μ mol) in CHCl₃ (0.5 mL). Yield: 41.83 mg (66%). Analysis by ESI+ (Expected [M+H]⁺ = 490.51. Observed [M+H]⁺ = 490.41). ¹H NMR (300 MHz, CDCl₃) δ 8.81 (d, J=4.77 Hz, 1H), 8.24-8.27 (t, J=7.80 Hz, 7.87 Hz, 1H), 7.90-7.92 (d, J=7.99 Hz, 1H), 7.69-7.71 (t, J=6.44 Hz, 6.75 Hz, 1H), 7.33-7.40 (m, 5H), 5.61-5.68 (m, 2H), 4.90 (d, J=2.22 Hz, 2H), 4.64-4.80 (t, J=9.91 Hz, 9.91 Hz, 2H), 3.35-3.37 (m,

2H), 3.12-3.20 (dt, $J=23.65$ Hz, 1H), 2.09-2.15 (m, 1H), 1.94-2.05 (m, 2H), 1.69-1.75 (m, 1H), 1.18 (s, 9H). ^{31}P NMR (121 MHz, CDCl_3) δ 29.81 (1P), 29.11 (1P).

(((1-hydroxy-2-oxopiperidin-3-yl)((pyridin-2-ylmethyl)amino)phosphoryl)oxy)-methyl pivalate (KY9). Following the procedure G3, the following quantities were used: 4b (41.83 mg, 82.60 μmol), MeOH (3 ml), THF (2 ml). Analysis by ESI+ (Expected $[\text{M}+\text{H}]^+ = 400.38$. Observed $[\text{M}+\text{H}]^+ = 400.48$). Yield: 31.4 mg (92%) ^1H NMR (300 MHz, CDCl_3) δ 8.74 (d, $J=4.48$ Hz, 1H), 8.17-8.22 (t, $J=7.93$ Hz, 8.37 Hz, 1H), 7.83-7.85 (m, 1H), 7.62-7.67 (t, $J=6.53$ Hz, 6.94 Hz, 1H), 5.62-5.64 (d, $J=7.04$ Hz, 2H), 4.61-4.71 (m, 2H), 3.64 (s, 2H), 3.14-3.27 (dt, $J=25.08$ Hz, 1H), 1.99-2.19 (m, 2H), 1.78-1.91 (m, 2H), 1.18 (s, 9H). ^{13}C NMR (75 MHz, CDCl_3) δ 160.89 (d, $J=4.03$ Hz, 1C), 123.50 (d, $J=3.68$ Hz, 1C), 81.67 (d, $J=7.61$ Hz, 1C), 40.96 (s, 1C), 26.84 (s, 1C), 22.07 (d, $J=5.68$ Hz, 1C), 21.67 (d, $J=7.44$ Hz, 1C). ^{31}P NMR (121 MHz, CDCl_3) δ 26.16 (1P), 26.59 (1P).

Synthesis of CDP24 (Figure 17, entry 5)

***P*-(1-(benzyloxy)-2-oxopiperidin-3-yl)-*N*-(2-fluorobenzyl)phosphonamidic acid (5a).** Following the procedure G1, the following quantities were used: DIAD (265.50 μL , 1340 μmol) and triphenylphosphine (351.27 mg, 1340 μmol) in anhydrous DCM (3 mL). BnHEX (**1**, 191.00 mg, 669.62 μmol) and 3- fluorophenylmethane amine (152.78 μL , 1340 μmol) in anhydrous DCM (1 mL). Yield: 170.05 mg (62%). Analysis by ESI+ (Expected $[\text{M}+\text{H}]^+ = 393.37$. Observed $[\text{M}+\text{H}]^+ = 393.42$). ^1H NMR (300 MHz, CDCl_3) δ 7.15-7.34 (m, 9 H), 4.79 (s, 2H), 4.09 (s, 2H), 3.22-3.37 (m, 2H), 2.62-2.74 (dt, $J=21.5$ Hz, $J=7.5$ Hz, 1H), 2.06-2.12 (m, 1H), 1.80-1.85 (m, 2H), 1.55-1.63 (m, 1H). ^{31}P NMR (121 MHz, CDCl_3) δ 19.32 (1P).

(((1-(benzyloxy)-2-oxopiperidin-3-yl)((2-fluorobenzyl)amino)phosphoryl)oxy)-methyl pivalate. Following the procedure G2, the following quantities were used: POM-Cl (119.25 μL , 815.56 μmol), DIPEA (142.25 μL , 815.56 μmol). **5a** (160.05 mg, 407.78 μmol) in CHCl_3 (1 mL). Yield: 112 mg (70%). Analysis by ESI+ (Expected $[\text{M}+\text{H}]^+ = 507.52$ Observed $[\text{M}+\text{Na}]^+ = 529.04$). ^1H NMR (300 MHz, CDCl_3) 7.27-7.41 (m, 10H), 5.52-5.64 (m, 2H), 4.85 (s, 2H), 3.21-3.31 (m,

2H), 2.74-3.03 (m, 1H), 2.02-2.12 (m, 1H), 1.82-1.99 (m, 2H), 1.59-1.68 (m, 1H), 1.12 (s, 9H). ³¹P NMR (121 MHz, CDCl₃) δ 29.23 (1P), 29.26 (1P).

(((2-fluorobenzyl)amino)(1-hydroxy-2-oxopiperidin-3-yl)phosphoryl)oxy)methyl pivalate (CDP24). Following the procedure G3, the following quantities were used: 5b (21.17 mg, 41.79 μmol), MeOH (3 ml), THF (2 ml). Yield: 17 mg (97%). Analysis by ESI+ (Expected [M+H]⁺ = 417.16. Observed [M+H]⁺ = 417.43). ¹H NMR (300 MHz, MeOD) 7.02-7.46 (m, 1H), 5.51-5.64 (m, 2H), 4.24-4.40 (m, 2H), 3.60-3.67 (m, 2H), 2.88-3.15 (m, 1H), 2.16-2.29 (m, 1H), 1.91-2.15 (m, 2H), 1.81-1.91 (m, 1H), 1.21 (s, 9H). ¹³C NMR (75 MHz, MeOD) 176.97 (s, 1C), 162.55 (s, 1C), 160.11 (s, 1C), 129.66 (d, J=4.50 Hz, 1C), 129.33 (d, J = 8.25 Hz, 1C), 126.94 (d, J=5.25 Hz, 1C), 124.34 (d, J=3.75 Hz, 1C), 115.55 (s, 1C), 81.06 (s, 1C), 48.67 (s, 1C), 43.53 (s, 1C), 41.71-42.43 (d, J=54.00 Hz, 1C), 38.69 (s, 1C), 26.80 (s, 3C), 21.71 (m, 2C). ³¹P NMR (121 MHz, MeOD) δ 30.04 (1P), 29.13 (1P). ¹⁹F NMR (282 MHz, MeOD) δ -118.85 (s, 1F).

Synthesis of CDP12 (Figure 17, entry 6)

P-(1-(benzyloxy)-2-oxopiperidin-3-yl)-N-(3-fluorobenzyl)phosphonamidic acid (6a). Following the the procedure G1, the following quantities were used: DIAD (265.50 μL, 1340 μmol) and triphenylphosphine (351.27 mg, 1340 μmol) in anhydrous DCM (3 mL). BnHEX (**1**, 191.00 mg, 669.62 μmol) and 3- fluorophenylmethane amine (152.78 μL, 1340 μmol) in anhydrous DCM (1 mL). Yield: 160.05 mg (61%). Analysis by ESI+ (Expected [M+H]⁺ = 393.37. Observed [M+H]⁺ = 393.42). ¹H NMR (300 MHz, CDCl₃) δ 7.18-7.38 (m, 9 H), 4.87 (s, 2H), 4.03 (s, 2H), 3.27-3.38 (m, 2H), 2.62-2.74 (dt, J=22.20 Hz, J=6.9 Hz, 1H), 2.07-2.13 (m, 1H), 1.79-1.88 (m, 2H), 1.55-1.59 (m, 1H). ³¹P NMR (121 MHz, CDCl₃) δ 19.30 (1P).

(((1-(benzyloxy)-2-oxopiperidin-3-yl)((3-fluorobenzyl)amino)phosphoryl)oxy)-methyl pivalate (6b). Following the procedure G2, the following quantities were used: POM-Cl (119.25 μL, 815.56 μmol), DIPEA (142.25 μL, 815.56 μmol). **6a** (160.05 mg, 407.78 μmol) in CHCl₃ (1 mL). Yield: 112 mg (70%). Analysis by ESI+ (Expected [M+H]⁺ = 400.38. Observed [M+H]⁺ = 400.44). ¹H NMR (300 MHz, CDCl₃) 7.34-7.47 (m, 10H), 5.58-5.70 (m, 2H), 4.92-5.01 (m, 2H), 3.34-3.42 (m, 2H), 3.01-3.13 (dt, J=21.00 Hz, J=6.0 Hz, 1H), 2.17-2.28 (m, 1H), 1.89-2.15 (m, 2H), 1.68-1.77 (m, 1H), 1.25 (s, 9H). ³¹P NMR (121 MHz, CDCl₃) δ 31.18 (1P), 30.91 (1P).

(((3-fluorobenzyl)amino)(1-hydroxy-2-oxopiperidin-3-yl)phosphoryl)oxy)methyl pivalate (CDP12). Following the procedure G3, the following quantities were used: 6b (112 mg, 221.12 μ mol), MeOH (6 ml), THF (4 ml). Analysis by ESI+ (Expected $[M+H]^+ = 417.16$. Observed $[M+H]^+ = 417.43$). Yield: 90 mg (97%). **1H NMR** (300 MHz, MeOD) 7.20-7.27 (m, 1H), 7.05-7.11 (m, 2H), 6.95-6.85 (t, $J=8.29$ Hz, 8.90 Hz, 1H), 5.56 (m, 2H), 4.09-4.16 (t, $J=10.08$ Hz, 10.08 Hz, 2H), 3.49-3.53 (t, $J=5.76$, 5.78 Hz, 2H), 3.02-3.16 (dt, $J=25.13$ Hz, 1H), 1.99-2.11 (m, 2H), 1.86-1.97 (m, 1H), 1.73-1.84 (m, 1H), 1.10 (s, 9H). **^{13}C NMR** (75 MHz, MeOD) 176.89 (s, 1C), 164.66 (s, 1C), 162.23 (d, $J=1.43$ Hz, 1C), 143.39 (d, $J=3.21$ Hz, 3.21 Hz, 5.14 Hz, 1C), 129.82-129.93 (d, $J=8.16$ Hz, 2C), 113.59 (d, $J=5.25$ Hz, 2C), 81.37 (d, $J=7.5$ Hz, 1C), 50.95 (s, 1C), 43.53 (s, 1C), 41.88-43.16 (d, $J=96$ Hz, 1C), 25.84 (s, 3C), 21.51-22.03 (m, 2C). **^{31}P NMR** (121 MHz, MeOD) δ 31.18 (1P), 30.91 (1P). **^{19}F NMR** (282 MHz, MeOD) δ -114.08 (s, 1F), -114.19 (s, 1F).

Synthesis of VCY19 (Figure 17, entry 7)

***P*-(1-(benzyloxy)-2-oxopiperidin-3-yl)-*N*-(4-fluorobenzyl)phosphonamidic acid (7a).** Following the procedure G1, the following quantities were used: DIAD (68.17 μ L, 350.59 μ mol) and triphenylphosphine (43.87 mg, 350.59 μ mol) in anhydrous DCM (3 mL). BnHEX (**1**, 50 mg, 175.29 μ mol) 4-fluorophenylmethane amine (40.07 μ L, 350.59 μ mol) in anhydrous DCM (1 mL). Yield: 44 mg (64%). Analysis by ESI+ (Expected $[M+H]^+ = 393.37$. Observed $[M+H]^+ = 393.38$). **1H NMR** (300 MHz, $CDCl_3$) δ 7.41-7.54 (m, 5H), 7.10-7.24 (m, 4H), 4.94 (s, 2H), 4.02 (d, $J=8.76$ Hz, 2H), 3.46-3.60 (m, 2H), 2.77-2.88 (dt, $J=21.74$ Hz, 1H), 1.90-2.00 (m, 2H), 2.07-2.16 (m, 1H), 1.77-1.83 (m, 1H). **^{31}P NMR** (121 MHz, $CDCl_3$) δ 20.78 (1P).

(((1-(benzyloxy)-2-oxopiperidin-3-yl)((4-fluorobenzyl)amino)phosphoryl)oxy)-methyl pivalate (7b). Following the procedure G2, the following quantities were used: POM-Cl (33.11 μ L, 224.28 μ mol), DIPEA (39.12 μ L, 224.28 μ mol). 7a (44 mg, 112.14 μ mol) in $CHCl_3$ (1 mL). Yield: 40 mg (70%). Analysis by ESI+ (Expected $[M+H]^+ = 507.52$. Observed $[M+H]^+ = 507.54$). **1H NMR** (300 MHz, $CDCl_3$) 7.14-7.35 (m, 9H), 5.58-5.70 (m, 2H), 4.89-5.02 (m, 2H), 3.49-3.53 (m, 2H), 2.99-3.13 (m, 1H), 2.17-2.28 (m, 1H), 1.89-2.15 (m, 2H), 1.66-1.74 (m, 1H), 1.19 (s, 9H). **^{31}P NMR** (121 MHz, $CDCl_3$) δ 31.11 (1P), 30.81 (1P).

(((4-fluorobenzyl)amino)(1-hydroxy-2-oxopiperidin-3-yl)phosphoryl)oxy)methyl pivalate (VCY19). Following the procedure G3, the following quantities were used: 7b (40 mg, 112.14 μ mol), MeOH (3 ml), THF (2 ml). Yield: 41 mg (96%). Analysis by ESI+ (Expected $[M+H]^+ = 417.39$. Observed $[M+H]^+ = 417.44$). **1H NMR** (300 MHz, $CDCl_3$) 6.95-7.02 (m, 4H), 5.52 (s, 2H), 4.19-4.27 (m, 2H), 3.58-3.63 (m, 2H), 2.84-3.08 (m, 1H), 1.95-2.25 (m, 3H), 1.78-1.89 (m, 1H), 1.16 (s, 9H). **^{13}C NMR** (75 MHz, $CDCl_3$) 177.40 (s, 1C), 163.91 (d, $J=1.43$ Hz, 1C), 135.96 (dd, $J=3.21$ Hz, 3.21, 5.14 Hz, 1C), 129.22-129.32 (d, $J=8.16$ Hz, 2C), 115.52 (d, $J=3.14$, 2C), 81.50 (d, $J=5.96$ Hz, 1C), 49.53 (s, 1C), 43.91 (s, 1C), 41.03-42.72 (d, $J=128.22$ Hz, 1C), 27.03 (s, 3C), 21.51-22.15 (m, 2C). **^{31}P NMR** (121 MHz, $CDCl_3$) δ 27.23 (1P), 26.08 (1P). **^{19}F NMR** (282 MHz, $CDCl_3$) -116.33 (s, 1F), -116.27 (s, 1F).

Synthesis of CDP13 (Figure 17, entry 8)

***P*-(1-(benzyloxy)-2-oxopiperidin-3-yl)-*N*-(3,4-difluorobenzyl)phosphonamidic acid (8a).** Following the procedure G1, the following quantities were used: DIAD (276.11 μ L, 1.40 mmol) and triphenylphosphine (367.82 mg, 1.40 mmol) in anhydrous DCM (3 mL). BnHEX (**1**, 200 mg, 245.41 μ mol) and (3,4-difluorophenyl) methane amine (165.89 μ L, 1.40 mmol) in anhydrous DCM (1 mL). Yield: 104 mg (52%). Analysis by ESI+ (Expected $[M+H]^+ = 411.36$. Observed $[M+H]^+ = 411.42$). **1H NMR** (300 MHz, $CDCl_3$) δ 7.21-7.25 (m, 8H), 4.77 (s, 2H), 3.91 (s, 2H), 3.21-3.35 (m, 2H), 2.50-2.62 (m, 1H), 1.90-1.92 (m, 1H), 1.75-1.79 (m, 1H), 1.46-1.50 (1H, m); **^{31}P NMR** (121 MHz, $CDCl_3$) δ 18.95 (1P).

(((1-(benzyloxy)-2-oxopiperidin-3-yl)((3,4-difluorobenzyl)amino)phosphoryl)oxy)-methyl pivalate (8b). Following the procedure G2, the following quantities were used: POM-Cl (71 μ L, 487.38 μ mol), DIPEA (85.01 μ L, 487.38 μ mol), 8a (100 mg, 243.69 μ mol) in $CHCl_3$ (1 mL). Yield: 112 mg (70%). Analysis by ESI+ (Expected $[M+H]^+ = 525.20$. Observed $[M+H]^+ = 525.24$). **1H NMR** (300 MHz, $CDCl_3$) 7.26-7.34 (m, 5H), 6.95-7.04 (m, 3H), 5.58-5.70 (m, 2H), 4.92-5.01 (m, 2H), 3.29-3.37 (m, 2H), 2.75-2.88 (m, 1H), 2.05-2.13 (m, 1H), 1.81-2.00 (m, 2H), 1.59-1.73 (m, 1H), 1.14 (s, 9H). **^{31}P NMR** (121 MHz, $CDCl_3$) δ 29.53 (1P), 23.31 (1P).

(((3,4-difluorobenzyl)amino)(1-hydroxy-2-oxopiperidin-3-yl)phosphoryl)oxy)-methyl pivalate (CDP13). Following the procedure G3, the following quantities were used: 8b (85 mg,

221.12 μmol), MeOH (6 ml), THF (4 ml). Yield: 67 mg (96%). Analysis by ESI+ (Expected $[\text{M}+\text{H}]^+ = 435.15$. Observed $[\text{M}+\text{H}]^+ = 435.47$). **^1H NMR** (300 MHz, CDCl_3) 7.21 (m, 1H), 7.11 (m, 2H), 6.63 (bs, 1H), 5.60 (m, 2H), 4.28 (m, 2H), 3.61-3.64 (t, $J=3.14$ Hz, 4.17 Hz, 2H), 2.97-3.09 (dt, $J=23.84$ Hz, 1H), 2.19-2.28 (m, 1H), 1.99-2.12 (m, 2H), 1.80-1.92 (m, 1H), 1.18 (s, 9H). **^{13}C NMR** (75 MHz, CDCl_3) δ 176.98 (s, 1C), 159.87 (d, $J=1.92$ Hz, 2C), 151.46 (s, 1C), 123.15 (s, 1C), 117.47 (d, $J=17.00$ Hz, 1C), 116.20 (d, $J=18.00$ Hz, 1C), 81.06 (d, $J=7.50$ Hz, 1C), 48.56 (s, 1C), 38.76-40.54 (d, $J=134.60$ Hz, 1C), 32.15-32.25 (t, $J=3.75$ Hz, 4.04 Hz, 1C), 26.78 (s, 3C), 21.71 (d, $J=12.00$ Hz, 1C), 21.40 (d, $J=4.56$ Hz, 1C). Note: some quaternary carbons not observed. **^{31}P NMR** (121 MHz, CDCl_3) δ 29.95 (1P), 28.79 (1P). **^{19}F NMR** (282 MHz, CDCl_3) δ -137.78 (d, $J=20.79$ Hz, 1F), -137.83 (d, $J=21.62$ Hz, 1F), -140.40 (d, $J=21.17$ Hz, 1F), 140.43 (d, $J=21.33$ Hz, 1F).

Synthesis of CDP14 (Figure 17, entry 9)

***P*-(1-(benzyloxy)-2-oxopiperidin-3-yl)-*N*-(2,4-difluorobenzyl)phosphonamidic acid (9a).**

Following the procedure G1, the following quantities were used: DIAD (96.64 μL , 490.82 μmol) and triphenylphosphine (128.74 mg, 490.82 μmol) in anhydrous DCM (3 mL). BnHEX (**1**, 70 mg, 245.41 μmol) and (2,4-difluorophenyl) methane amine (58.55 μL , 490.82 μmol) in anhydrous DCM (1 mL). Yield: 54.7 mg (61%). Analysis by ESI+ (Expected $[\text{M}+\text{H}]^+ = 411.12$. Observed $[\text{M}+\text{H}]^+ = 411.38$). **^1H NMR** (300 MHz, CDCl_3) δ 6.68-7.71 (m, 8H), 4.84 (m, 2H), 4.09 (s, 2H), 3.29 (m, 2H), 2.65 (m, 1H), 2.01 (m, 2H). 1.55 - 1.76 (2H, m); **^{31}P NMR** (121 MHz, CDCl_3) δ 18.98 (1P).

(((1-(benzyloxy)-2-oxopiperidin-3-yl)((2,4-difluorobenzyl)amino)phosphoryl)oxy)-methyl pivalate (9b). Following the procedure G2, the following quantities were used: POM-Cl (30.4 μL , 208.11 μmol), DIPEA (36.30 μL , 208.11 μmol), 9a (42.7 mg, 104.06 μmol) in CHCl_3 (0.5 mL). Yield: 35 mg (66%). (Expected $[\text{M}+\text{H}]^+ = 525.20$. Observed $[\text{M}+\text{H}]^+ = 525.24$). **^1H NMR** (300 MHz, CDCl_3) 7.26-7.34 (m, 5H), 6.66-6.73 (m, 3H), 5.52-5.68 (m, 2H), 4.15-4.37 (m, 2H), 3.21-3.37 (m, 2H), 2.75-3.07 (m, 1H), 2.04-2.10 (m, 1H), 1.76-1.97 (m, 2H), 1.57-1.69 (m, 1H), 1.16 (s, 9H). **^{31}P NMR** (121 MHz, CDCl_3) δ 29.68 (1P), 29.33 (1P).

(((2,4-difluorobenzyl)amino)(1-hydroxy-2-oxopiperidin-3-yl)phosphoryl)oxy)-methyl pivalate (CDP14). Following the procedure G3, the following quantities were used: 9b (35 mg, 66.73 μmol), MeOH (3 ml), THF (2 ml). Yield: 28.2 mg (97%). Analysis by ESI+ (Expected $[\text{M}+\text{H}]^+ = 435.15$. Observed $[\text{M}+\text{H}]^+ = 435.40$). **^1H NMR** (300 MHz, CDCl_3) δ 7.42 (m, 1H), 6.86 (m, 2H), 6.12 (bs, 1H), 5.56-5.60 (dd, $J=12.77$ Hz, 2H), 4.33 (m, 2H), 3.63 (m, 2H), 2.96-3.09 (dt, $J=22.80$ Hz, 1H), 2.17-2.26 (m, 1H), 1.98-2.10 (m, 2H), 1.79-1.90 (m, 1H), 1.17 (s, 9H). **^{13}C NMR** (75 MHz, CDCl_3) δ 177.11 (s, C), 159.65 (d, $J=1.92$ Hz, 1C), 130.49 (m, 1C), 111.65 (s, 2C), 80.96 (d, $J=7.5$ Hz, 1C), 49.25 (s, 1C), 40.70-42.41 (d, $J=128.25$ Hz, 1C), 38.08 (t, $J=3.75$ Hz, 1C), 26.81 (s, 3C), 21.35-21.71 (m, 2C). Note: some quaternary carbons not observed. **^{31}P NMR** (121 MHz, CDCl_3) δ 29.94 (1P), 28.79 (1P). **^{19}F NMR** (282 MHz, CDCl_3) δ -111.55 (d, $J=7.29$ Hz, 1F), -111.66 (d, $J=7.41$ Hz, 1F), -115.2 (d, $J=7.74$ Hz, 1F), -115.18 (d, $J=7.77$ Hz, 1F).

Synthesis of CDP19 (Figure 17, entry 10)

***P*-(1-(benzyloxy)-2-oxopiperidin-3-yl)-*N*-(2,6-difluorobenzyl)phosphonamidic acid (10a).** Following the procedure G1, the following quantities were used: DIAD (96.64 μL , 490.82 μmol) and triphenylphosphine (128.74 mg, 490.82 μmol) in anhydrous DCM (3 mL). BnHEX (**1**, 70 mg, 245.41 μmol) and (2,6-difluorophenyl) methane amine (58.55 μL , 490.82 μmol) in anhydrous DCM (1 mL). Yield: 54.7 mg (61%). Analysis by ESI+ (Expected $[\text{M}+\text{H}]^+ = 411.12$. Observed $[\text{M}+\text{H}]^+ = 411.38$). **^1H NMR** (300 MHz, CDCl_3) δ 7.28-7.70 (m, 9 H), 4.90-4.94 (m, 2H), 4.00-4.03 (d, $J = 6.0$ Hz, 2H), 3.26-3.32 (m, 2H), 2.56-2.68 (dt, $J= 22.20$ Hz, $J=6.9$ Hz, 1H), 1.97-1.99 (m, 1H), 1.71-1.86 (m, 2H), 1.55-1.56 (m, 1H). **^{31}P NMR** (121 MHz, CDCl_3) δ 17.47 (1P).

(((1-(benzyloxy)-2-oxopiperidin-3-yl)((2,6-difluorobenzyl)amino)phosphoryl)oxy)-methyl pivalate (10b). Following the procedure G2, the following quantities were used: POM-Cl (30.4 μL , 208.11 μmol), DIPEA (36.30 μL , 208.11 μmol), **7a** (50 mg, 104.06 μmol) in CHCl_3 (0.5 mL). Yield: 40 mg (63%). (Expected $[\text{M}+\text{H}]^+ = 525.20$. Observed $[\text{M}+\text{Na}]^+ = 547.00$). **^1H NMR** (300 MHz, CDCl_3) δ 7.27-7.36 (m, 5H), 7.12-7.19 (m, 1H), 6.78-6.85 (m, 2H), 5.47-5.68 (m, 2H), 4.82 (s, 2H), 4.35-4.38 (m, 2H), 3.24-3.29 (m, 2H), 2.73-3.01 (m, 1H), 2.43-2.50 (m, 1H), 2.04-2.10 (m, 1H), 1.81-1.95 (m, 2H), 1.59-1.65 (m, 2H), 1.13 (s, 9H). **^{31}P NMR** (121 MHz, CDCl_3) δ 29.10 (1P), 28.88 (1P).

(((2,6-difluorobenzyl)amino)(1-hydroxy-2-oxopiperidin-3-yl)phosphoryl)oxy)-methyl pivalate (CDP19). Following the procedure G3, the following quantities were used: **10b** (35 mg, 66.73 μ mol), MeOH (6 ml), THF (4 ml). Yield: 27.1 mg (93%). Analysis by ESI+ (Expected $[M+H]^+ = 435.38$. Observed $[M+H]^+ = 435.40$). **1H NMR** (300 MHz, $CDCl_3$) δ 7.23 (m, 2H), 6.85-6.90 (t, $J = 7.51$ Hz, 8.09 Hz, 1H), 5.51-5.57 (dd, $J = 13.24$ Hz, 2H), 4.40 (m, 2H), 3.63 (m, 2H), 2.99-3.10 (dt, $J = 23.86$ Hz, 1H), 2.17-2.26 (m, 1H), 1.97-2.11 (m, 2H), 1.80-1.90 (m, 1H), 1.17 (s, 9H). **^{13}C NMR** (75 MHz, $CDCl_3$) δ 176.98 (s, 1C), 159.61 (d, $J = 1.92$ Hz, 2C), 129.58 (s, 1C), 111.65 (s, 2C), 81.03 (d, $J = 6.44$ Hz, 1C), 48.43 (s, 1C), 38.76-40.54 (d, $J = 134.60$ Hz, 1C), 32.15-32.25 (t, $J = 3.75$ Hz, 4.04 Hz, 1C), 26.78 (s, 3C), 21.71 (d, $J = 12.00$ Hz, 1C), 21.40 (d, $J = 4.56$ Hz, 1C). Note: some quaternary carbons not observed. **^{31}P NMR** (121 MHz, $CDCl_3$) δ 29.28 (1P), 28.61 (1P). **^{19}F NMR** (282 MHz, $CDCl_3$) -115.33 (s, 2F).

Synthesis of CDP18 (Figure 17, entry 11)

***P*-(1-(benzyloxy)-2-oxopiperidin-3-yl)-*N*-(cyclohexylmethyl)phosphonamidic acid (11a).** To a solution of triphenylphosphine (275.87 mg, 1.05 mmol) in DCM (6 mL), DIAD (204.50 μ L, 1.05 mmol) was added with stirring at 0°C for 30 min. Separately, a solution containing BnHEX (150 mg, 525.88 μ mol), cyclohexane methylamine (136.85 μ L, 1.05 μ mol), and DBU (157.29 μ L, 1.05 mmol) in DCM (2 mL) was prepared and added dropwise to the betaine solution. The reaction mixture was allowed to warm to room temperature over 30 minutes. Then, 1 volume of water was added to the crude mixture. After vigorous shaking and partitioning via centrifugation (2 min at 4°C, 4000 rpm), the aqueous layer was isolated and lyophilized to clear oil. Yield: 142.35 mg (83%). Analysis by ESI+ (Expected $[M+H]^+ = 381.42$. Observed $[M+H]^+ = 381.50$). **1H NMR** (300 MHz, $CDCl_3$) δ 7.37-7.44 (m, 5H) 3.61-3.65 (m, 2H), (m, 1H), 2.15-2.25 (m, 1H), 1.97-2.12 (m, 2H), 1.83-1.93 (m, 1H), 1.62-1.74 (m, 6H), 1.32-1.44 (m, 1H), 0.79-0.94 (m, 3H). **^{31}P NMR** (121 MHz, $CDCl_3$) δ 17.41 (1P).

(((1-(benzyloxy)-2-oxopiperidin-3-yl)((cyclohexylmethyl)amino)phosphoryl)oxy)-methyl pivalate (8b). Following the procedure G2, the following quantities were used: POM-Cl (108.56 μ L, 749.69 μ mol), DIPEA (115.35 μ L, 749.69 μ mol), 11a (142.35 mg, 374.84 μ mol) in $CHCl_3$ (1 mL). Yield: 113.26 mg (66%). (Expected $[M+H]^+ = 525.20$. Observed $[M+H]^+ = 525.24$). **1H NMR**

(300 MHz, CDCl₃) 7.27-7.40 (m, 5H), 5.53-5.64 (m, 2H), 4.86-4.89 (m, 2H), 3.20-3.35 (m, 2H), 2.88-2.97 (m, 1H), 2.75-2.88 (m, 2H), 2.04-2.10 (m, 1H), 1.82-1.97 (m, 2H), 1.50-1.78 (m, 8H), 1.29-1.40 (m, 1H), 1.15 (s, 9H), 0.83-0.98 (m, 4H). ³¹P NMR (121 MHz, CDCl₃) δ 29.99 (1P), 29.56 (1P).

(((Cyclohexylmethyl)amino)(1-hydroxy-2-oxopiperidin-3-yl)phosphoryl)oxy)-methyl pivalate (CDP18). Following the procedure G3, the following quantities were used: 11b (113.26 mg, 228.97 μmol), MeOH (6 ml), THF (4 ml). Yield: 88.10 mg (95%). Analysis by ESI+ (Expected [M+H]⁺ = 405.45. Observed [M+H]⁺ = 405.44). ¹H NMR (300 MHz, CDCl₃) δ 5.54-5.64 (m, 2H), 3.61-3.65 (m, 2H), 2.88-2.97 (m, 1H), 2.15-2.25 (m, 1H), 1.97-2.12 (m, 2H), 1.83-1.93 (m, 1H), 1.62-1.74 (m, 6H), 1.32-1.44 (m, 1H), 1.19 (s, 9H), 0.79-0.94 (m, 3H). ¹³C NMR (75 MHz, CDCl₃) 177.18 (s, 1C), 160.29 (d, J=1.19 Hz, 1C), 92.29 (s, 1C), 81.35-81.44 (d, J=7.52 Hz, 1C), 40.62-42.34 (d, J=130.41 Hz, 1C), 30.67 (d, J=1.28 Hz, 1C) 27.00 (s, 3C), 26.00 (s, 2C), 25.98 (s, 1C), 25.96 (s, 1C), 21.85-21.89 (d, J=2.72 Hz, 1C), 21.67-21.73 (d, J=5.09 Hz, 1C). ³¹P NMR (121 MHz, CDCl₃) δ 30.65 (1P), 29.94 (1P).

Synthesis of VCY32 (Figure 17, entry 12)

***P*-(1-(benzyloxy)-2-oxopiperidin-3-yl)-*N*-(cyclopropylmethyl)phosphonamidic acid (12a).** To a solution of triphenylphosphine (275.87 mg, 1.05 mmol) in DCM (15 mL), DIAD (204.50 μL, 1.05 mmol) was added with stirring at 0°C for 30 min. Separately, a solution containing BnHEX (150 mg, 525.88 μmol), cyclopropyl methyl amine hydrochloride (74.80 mg, 1.05 mmol), and DBU (156.98 μL, 1.05 mmol) in DCM (2 mL) was prepared and added dropwise to the betaine solution. The reaction mixture was allowed to warm to room temperature over 30 minutes. Then, 1 volume of water was added to the crude mixture. After vigorous shaking and partitioning via centrifugation (2 min at 4°C, 4000 rpm), the aqueous layer was isolated and lyophilized to a clear solid. Analysis by ESI+ (Expected [M+H]⁺ = 339.34. Observed [M+H]⁺ = 339.38). Yield: 49.50 mg (83%). ¹H NMR (300 MHz, CDCl₃) δ 7.32-7.51 (m, 5H), 4.70-4.74 (d, J=2.1 Hz, 2H), 3.10 (m, 2H), 2.67-2.75 (m, 1H), 2.44-2.50 (m, 1H), 2.02-2.06 (m, 1H), 1.89-1.94 (m, 2H), 1.69-1.75 (m, 1H), 1.08-1.12 (m, 1H), 0.76-0.86 (m, 1H), 0.23-0.27 (m, 2H), 0.01-0.02 (m, 2H). ³¹P NMR (202 MHz, CDCl₃) δ 19.54 ppm (1P).

(((1-(benzyloxy)-2-oxopiperidin-3-yl)((cyclopropylmethyl)amino)phosphoryl)oxy)-methyl pivalate (12b): Following the procedure G2, the following quantities and conditions were used: POM-Cl (43.20 μ L, 292.60 μ mol), DIPEA (51.04 μ L, 292.60 μ mol), 12a (49.50 mg, 146.30 μ mol) in CHCl_3 (1 mL). Yield: 46.20 mg (69%). $^1\text{H NMR}$ (300 MHz, CDCl_3) δ 7.32-7.51 (m, 5H), 5.51-5.61 (m, 2H), 3.59 (m, 2H), 2.79-2.90 (m, 1H), 2.77-2.83 (m, 1H), 2.08-2.18 (m, 1H), 2.08-2.13 (m, 2H), 1.79-1.82 (m, 1H), 1.15 (s, 9H), 0.41 (m, 1H), 0.12 (m, 1H). $^{31}\text{P NMR}$ (121 MHz, CDCl_3) δ 31.51 (1P), 31.12 (1P).

(((Cyclopropylmethyl)amino)(1-hydroxy-2-oxopiperidin-3-yl)phosphoryl)oxy)-methyl pivalate (VCY32). Following the procedure G3, the following quantities were used: 12b (46.20 mg, 102.10 μ mol), MeOH (3 ml), THF (2 ml). Yield: 33.3 mg (90%). Analysis by ESI+ (Expected $[\text{M}+\text{H}]^+ = 363.36$. Observed $[\text{M}+\text{H}]^+ = 363.39$). $^1\text{H NMR}$ (300 MHz, CDCl_3) δ 5.54-5.59 (m, 2H), 3.59 (m, 2H), 2.92-2.98 (dt, $J=18.06$ Hz, 1H), 2.78-2.82 (q, $J=6.81$ Hz, 7.07 Hz, 7.07 MHz, 1H), 2.14-2.20 (m, 1H), 2.07-2.13 (m, 2H), 1.77-1.85 (m, 1H), 1.16 (s, 9H), 0.44 (m, 1H), 0.17 (m, 1H). $^{13}\text{C NMR}$ (75 MHz, CDCl_3) δ 177.12 (s, 1C), 160.77 (d, $J=5.46$ Hz, 1C), 81.23 (d, $J=2.76$ Hz, 1C), 49.98 (s, 1C), 45.87 (d, $J=0.95$ Hz, 1C), 42.36-41.35 (d, $J=127.79$ Hz, 1C), 38.87 (s, 1C), 27.03 (s, 3C), 22.03 (d, $J=4.83$ Hz, 1C), 21.64 (d, $J=4.83$ Hz, 1C), 13.38 (d, $J=6.46$ Hz, 1C), 3.62 (s, 1C), 3.60 (s, 1C). $^{31}\text{P NMR}$ (121 MHz, CDCl_3) δ 30.15 (1P), 28.65 (1P).

Synthesis of VCY33

***N*-(cyclopropylmethyl)-*P*-(1-hydroxy-2-oxopiperidin-3-yl)phosphonamidic acid (VCY33).** VCY32 (35.00 mg, 96.59 μ mol) and CsCO_3 (31.9 mg, 96.59 μ mol) were dissolved in MeOH (0.5 ml). The reaction mixture was stirred at RT for 1 h, then evaporated, purified via HPLC and lyophilized to obtain a white solid. Yield: 23.3 mg (97%). Analysis by ESI+ (Expected $[\text{M}+\text{H}]^+ = 249.23$. Observed $[\text{M}+\text{Na}]^+ = 271.89$). Yield: 21.85 mg (91%) $^1\text{H NMR}$ (300 MHz, D_2O) δ 3.38-3.51 (m, 2H), 2.49-2.74 (m, 3H), 1.95-2.05 (m, 1H), 1.82-1.92 (m, 2H), 1.66-1.75 (m, 1H), 0.83-0.94 (m, 1H), 0.37-0.40 (m, 2H), 0.04-0.09 (m, 2H). $^{13}\text{C NMR}$ (75 MHz, D_2O) δ 163.18 (s, 1C), 52.38 (s, 1C), 46.47 (s, 1C), 40.94-42.40 (d, $J=34.5$ Hz, 1C), 21.06 (s, 1C), 17.01 (s, 1C), 11.99-12.11 (d, $J=10.5$ Hz, 1C), 2.71 (d, $J=2.25$ Hz, 2C). $^{31}\text{P NMR}$ (121 MHz, D_2O) δ 24.26 (1P).

Synthesis of VCY34 (Figure 17, entry 13)

***P*-(1-(benzyloxy)-2-oxopiperidin-3-yl)-*N*-cyclobutylphosphonamidic acid (13a).** To a solution of triphenylphosphine (919.56 mg, 3.51 mmol) in DCM (20 mL), DIAD (681.66 μ L, 3.51 mmol) were added with stirring at 0°C for 30 min. Separately, a solution containing BnHEX (500 mg, 1.75 mmol), cyclobutylamine (299.34 μ L, 3.51 mmol), and DBU (523.27 μ L, 3.51 mmol) in DCM (2 mL) was prepared and added dropwise to the betaine solution. The reaction mixture was allowed to warm to room temperature over 30 minutes. Then, 1 volume of water was added to the crude mixture. After vigorous shaking and partitioning via centrifugation (2 min at 4°C, 4000 rpm), the aqueous layer was isolated and lyophilized to a clear solid. 49.50 mg (83%). Analysis by ESI+ (Expected $[M+H]^+ = 339.34$. Observed $[M+H]^+ = 339.41$). **¹H NMR** (300 MHz, CDCl₃) 7.45-7.55 (m, 5H), 4.96 (s, 1H), 3.26-3.30 (t, $J=5.55$ Hz, 6.01 Hz, 2H), 2.68-2.79 (dt, $J=21.36$ Hz, 1H), 2.19-.27 (m, 2H), 2.05-2.11 (m, 1H), 1.79-1.91 (m, 4H), 1.51-1.62 (m, 2H). **³¹P NMR** (121 MHz, CDCl₃) 19.47 (1P).

(((1-(benzyloxy)-2-oxopiperidin-3-yl)((cyclobutyl)amino)phosphoryl)oxy)-methyl pivalate (10b): Following the procedure G2, the following quantities and conditions were used: POM-Cl (43.20 μ L, 292.60 μ mol), DIPEA (51.04 μ L, 292.60 μ mol), **13a** (50 mg, 144.83 μ mol) in CHCl₃ (0.5 mL). Yield: 46.1 mg (69%). Analysis by ESI+ (Expected $[M+H]^+ = 453.50$. Observed $[M+Na]^+ = 475.02$). **¹H NMR** (300 MHz, CDCl₃) δ 7.28-7.40 (m, 5H), 5.52-5.57 (m, 2H), 3.77-3.96 (m, 1H), 3.23-3.35 (m, 2H), 2.70-2.93 (m, 1H), 2.22-2.29 (m, 2H), 2.02-2.11 (m, 1H), 1.83-1.96 (m, 2H), 1.48-1.69 (m, 1H), 1.19 (s, 9H). **³¹P NMR** (121 MHz, CDCl₃) δ 27.53 (1P), 27.08 (1P).

(((Cyclobutylamino)(1-hydroxy-2-oxopiperidin-3-yl)phosphoryl)oxy)methyl pivalate (VCY34). Following the procedure G3, the following quantities were used: **13b** (46.20 mg, 102.10 μ mol), MeOH (3 mL), THF (2 mL). Yield: 33.6 mg (90%). Analysis by ESI+ (Expected $[M+H]^+ = 363.36$. Observed $[M+H]^+ = 363.98$). **¹H NMR** (300 MHz, CDCl₃) δ 5.55-5.57 (d, $J=5.32$ Hz, 2H), 3.78-3.91 (m, 1H), 3.57 (t, $J=4.76$ Hz, 6.89 Hz, 2H), 2.90-2.98 (dt, $J=14.04$ Hz, 1H), 2.26 (m, 2H), 2.10 (m, 2H), 1.99 (m, 2H), 1.89 (m, 2H), 1.60 (m, 2H), 1.15 (s, 9H). **¹³C NMR** (75 MHz, CDCl₃) δ 179.81 (s, 1C), 177.09-177.19 (d, $J=7.21$ Hz, 1C), 81.20-81.30 (d, $J=7.85$ Hz, 1C), 50.15 (s, 1C), 46.56 (d, $J=3.64$ Hz, 1C), 41.19-41.88 (d, $J=128.81$ Hz, 1C), 38.79 (s, 2C), 26.92 (s, 1C), 22.02 (s,

1C), 21.94 (d, $J=4.50$ Hz, 1C), 21.69 (d, $J=5.22$ Hz, 1C). ^{31}P NMR (121 MHz, CDCl_3) δ 28.31 (1P), 27.47 (1P).

Synthesis of CDP21 (Figure 17, entry 14)

***P*-(1-(benzyloxy)-2-oxopiperidin-3-yl)-*N,N*-dimethylphosphonamidic acid (14a).** To a solution of triphenylphosphine (91.96 mg, 350.59 μmol) in DCM (2.5 mL), DIAD (68.17 μL , 350.59 μmol) were added with stirring at 0°C for 30 min. Separately, a solution containing BnHEX (50 mg, 175.29 μmol), dimethylamine hydrochloride (28.59 mg, 350.59 μmol), and DBU (53.37 mg, 350.59 μmol) in DCM (1 mL) was prepared and added dropwise to the betaine solution. The reaction mixture was allowed to warm to room temperature over 30 minutes. Then, 1 volume of water was added to the crude mixture. After vigorous shaking and partitioning via centrifugation (2 min at 4°C , 4000 rpm), the aqueous layer was isolated and lyophilized to clear oil. Yield: 47 mg (86%). Analysis by ESI+ (Expected $[\text{M}+\text{H}]^+ = 313.13$ Observed $[\text{M}+\text{H}]^+ = 313.20$). ^1H NMR (300 MHz, CDCl_3) δ 7.28-7.46 (m, 5H), 5.50-5.60 (m, 2H), 3.23-3.50 (m, 2H), 2.98-3.02 (m, 1H), 2.68-2.73 (d, $J=9.0$ Hz, 6H), 2.20-2.23 (m, 1H), 2.02-2.06 (m, 1H), 1.89-1.92 (m, 1H), 1.55-1.64 (m, 2H). ^{31}P NMR (121 MHz, CDCl_3) δ 31.69 (1P), 29.85 (1P), 29.13 (1P).

(((1-(benzyloxy)-2-oxopiperidin-3-yl)(dimethylamino)phosphoryl)oxy)methyl pivalate (14b): Following the procedure G2, the following quantities and conditions were used: POM-Cl (43.59 μL , 300.99 μmol), DIPEA (52.50 μL , 300.99 μmol), **14a** (47 mg, 150.49 μmol) in CHCl_3 (1 mL), 40°C . Yield: 42.36 mg (66%). Analysis by ESI+ (Expected $[\text{M}+\text{H}]^+ = 427.20$ Observed $[\text{M}+\text{Na}]^+ = 449.18$) ^1H NMR (300 MHz, CDCl_3) δ 7.37-7.47 (m, 5H), 5.58-5.70 (m, 2H), 4.92-5.01 (m, 2H), 3.34-3.42 (m, 2H), 3.01-3.13 (m, 1H), 2.82 (d, $J=9.8$ Hz, 6H), 2.17-2.28 (m, 1H), 1.89-2.15 (m, 2H), 1.67-1.77 (m, 9H). ^{31}P NMR (121 MHz, CDCl_3) δ 31.96 (1P), 30.13 (1P).

(((dimethylamino)(1-hydroxy-2-oxopiperidin-3-yl)phosphoryl)oxy)methyl pivalate (CDP21). Following the procedure G3, the following quantities were used: **14b** (113.26 mg, 228.97 μmol), MeOH (3 mL), THF (2 mL). Yield: 33 mg (98%). Analysis by ESI+ (Expected $[\text{M}+\text{H}]^+ = 337.15$ Observed $[\text{M}+\text{Na}]^+ = 358.95$). ^1H NMR (300 MHz, CDCl_3) δ 5.54-5.64 (m, 2H), 3.56-3.71 (m, 2H), 2.99-3.09 (m, 1H), 2.71-2.74 (d, $J=9.8$ Hz, 6H), 1.83-2.37 (m, 2H), 2.00-2.20 (m, 2H), 1.62-1.74 (m, 9H). ^{13}C NMR (75 MHz, CDCl_3) 177.15 (s, 1C), 160.12 (d, $J=1.19$ Hz, 1C), 80.05-81.07

(d, $J=6.0$ Hz, 1C), 50.79 (s, 1C), 38.17-39.84 (d, $J=123$ Hz, 1C), 38.80 (s, 1C), 36.39-36.47 (d, $J=5.25$ Hz, 2C), 26.90 (s, 3C), 22.49 (d, $J=2.72$ Hz, 1C), 21.39 (d, $J=2.72$ Hz, 1C). ^{31}P NMR (121 MHz, CDCl_3) δ 30.99 (1P), 29.14 (1P).

Synthesis of CDP23 (Figure 17, entry 15)

***P*-(1-(benzyloxy)-2-oxopiperidin-3-yl)-*N*-methylphosphonamidic acid (15a).** To a solution of triphenylphosphine (183.91 mg, 701.17 μmol) in DCM (5 mL), DIAD (136.33 μL , 701.17 μmol) was added with stirring at 0°C for 30 min. Separately, a solution containing BnHEX (100 mg, 350.59 μmol), methylamine hydrochloride (47.34 mg, 701.17 μmol), and DBU (106.75 μL , 701.17 μmol) in DCM (1 mL) was prepared and added dropwise to the betaine solution. The reaction mixture was allowed to warm to room temperature over 30 minutes. Then, 1 volume of water was added to the crude mixture. After vigorous shaking and partitioning via centrifugation (2 min at 4°C , 4000 rpm), the aqueous layer was isolated and lyophilized to clear oil. Yield: 57.8 mg (55%) Analysis by ESI+ (Expected $[\text{M}+\text{H}]^+ = 299.12$ Observed $[\text{M}+\text{H}]^+ = 299.14$) ^1H NMR (300 MHz, CDCl_3) δ 7.16-7.40 (m, 5H), 4.63 (s, 2H), 3.39-3.44 (m, 2H), 2.77-2.83 (m, 2H), 2.44-2.55 (m, 1H), 2.34-2.38 (d, $J = 12$ Hz, 3H), 1.80-1.84 (m, 2H), 1.62-1.69 (m, 1H), 1.42-1.55 (m, 1H), 1.32-1.39 (m, 1H). ^{31}P NMR (121 MHz, CDCl_3) δ 24.49 (1P).

(((1-(benzyloxy)-2-oxopiperidin-3-yl)(methylamino)phosphoryl)oxy)methyl pivalate (15b): Following the procedure G2, the following quantities and conditions were used: POM-Cl (112.24 μL , 775.11 μmol), DIPEA (135.20 μL , 775.11 μmol), **15a** (57.8 mg, 193.78 μmol) in CHCl_3 (1 mL), 40°C . Yield: 54.57 mg (68%). Analysis by ESI+ (Expected $[\text{M}+\text{H}]^+ = 413.18$ Observed $[\text{M}+\text{Na}]^+ = 435.17$) ^1H NMR (300 MHz, CDCl_3) δ 7.37-7.54 (m, 5H), 5.63-5.75 (m, 2H), 4.88-5.01 (m, 2H), 3.29-3.43 (m, 2H), 2.94-3.12 (m, 1H), 2.83 (d, $J=12.2$ Hz, 6H), 2.12-2.24 (m, 1H), 1.88-2.11 (m, 2H), 1.63-1.81 (m, 9H). ^{31}P NMR (121 MHz, CDCl_3) δ 31.74 (1P), 31.70 (1P).

(((1-hydroxy-2-oxopiperidin-3-yl)(methylamino)phosphoryl)oxy)methyl pivalate (CDP23). Following the procedure G3, the following quantities were used: **15b** (113.26 mg, 228.97 μmol), MeOH (3 mL), THF (2 mL). Yield: 41 mg (98%). Analysis by ESI+ (Expected $[\text{M}+\text{H}]^+ = 323.14$ Observed $[\text{M}+\text{Na}]^+ = 344.91$). ^1H NMR (300 MHz, CDCl_3) δ 5.60-5.69 (m, 2H), 3.86 (brs, 1H), 3.66-3.70 (m, 2H), 2.92-3.03 (dt, $J = 6.0$ Hz, $J = 16.8$ Hz, 1H), 2.71-2.74 (dd, $J = 5.4$ Hz, $J=12.3$

Hz, 3H), 2.08-2.25 (m, 2H), 1.87-1.96 (m, 1H), 1.5 (s, 9H). ¹³C NMR (75 MHz, CDCl₃) 177.05 (s, 1C), 160.11 (d, J=5.25 Hz, 1C), 81.01-81.10 (d, J=6.75 Hz, 1C), 48.32 (s, 1C), 41.69 (s, 1C), 40.98 (s, 1C), 40.00 (s, 1C), 38.74 (s, 1C), 26.89 (s, 3C), 21.64 (s, 1C), 21.50 (s, 1C). ³¹P NMR (121 MHz, CDCl₃) δ 29.93 (1P).

Synthesis of CDP25 (Figure 17, entry 16)

***P*-(1-(benzyloxy)-2-oxopiperidin-3-yl)-*N*-(1-isopropoxy-1-oxopropan-2-yl)phosphonamidic acid (16a).** To a solution of triphenylphosphine (183.91 mg, 701.17 μmol) in DCM (5 mL), DIAD (136.33 μL, 701.17 μmol) was added with stirring at 0°C for 30 min. Separately, a solution containing BnHEX (100 mg, 350.59 μmol), L-alanine isopropylester hydrochloride (117.54 mg, 701.17 μmol), and DBU (106.75 μL, 701.17 μmol) in DCM (1 mL) was prepared and added dropwise to the betaine solution. The reaction mixture was allowed to warm to room temperature over 30 minutes. Then, 1 volume of water was added to the crude mixture. After vigorous shaking and partitioning via centrifugation (2 min at 4°C, 4000 rpm), the aqueous layer was isolated and lyophilized to clear oil. Yield: 57.8 mg (55%) Analysis by ESI+ (Expected [M+H]⁺ = 399.17 Observed [M+Na]⁺ = 399.21) ¹H NMR (300 MHz, CDCl₃) δ 5.64-5.73 (m, 2H), 5.10-5.14 (m, 2H), 4.01-4.67 (m, 1H), 3.65-3.69 (m, 2H), 2.97-3.35 (m, 1H), 2.20-2.29 (m, 1H), 1.97-2.82 (m, 2H), 1.83-1.97 (m, 2H), 1.42-1.49 (m, 1H), 1.22-1.29 (m, 1H). ³¹P NMR (121 MHz, CDCl₃) δ 23.59 (1P).

(((1-(benzyloxy)-2-oxopiperidin-3-yl)((1-isopropoxy-1-oxopropan-2-yl)amino)phosphoryl)oxy)methyl pivalate (16b): Following the procedure G2, the following quantities and conditions were used: POM-Cl (112.24 μL, 775.11 μmol), DIPEA (135.20 μL, 775.11 μmol), **13a** (57.8 mg, 193.78 μmol) in CHCl₃ (1 mL), 40°C. Yield: 54.57 mg (68%). Analysis by ESI+ (Expected [M+H]⁺ = 513.21 Observed [M+Na]⁺ = 535.02) ¹H NMR (300 MHz, CDCl₃) δ 7.28-7.36 (m, 5H), 5.56-5.68 (m, 2H), 4.88 (s, 2H), 4.46-4.52 (m, 1H), 4.10-4.19 (m, 1H), 3.27-3.31 (m, 2H), 2.79-2.94 (m, 1H), 2.03-2.09 (m, 1H), 1.88-1.99 (m, 2H), 1.60-1.68 (m, 1H), 1.23 (d, J = 3.3 Hz, 3H), 1.19 (s, 9H), 1.17 (d, J = 2.7 Hz, 6H). ³¹P NMR (121 MHz, CDCl₃) δ 29.45 (1P), 27.22 (1P).

(((1-hydroxy-2-oxopiperidin-3-yl)(methylamino)phosphoryl)oxy)methyl pivalate (CDP25).

Following the procedure G3, the following quantities were used: **16b** (41.48 mg, 83.87 μ mol), MeOH (3 ml), THF (2 ml). Yield: 41 mg (98%). Analysis by ESI+ (Expected $[M+H]^+ = 423.42$ Observed $[M+Na]^+ = 445.00$). **1H NMR** (300 MHz, $CDCl_3$) δ 5.61-5.74 (m, 2H), 5.00-5.07 (m, 2H), 4.01-4.67 (m, 1H), 3.65-3.69 (m, 2H), 2.97-3.35 (m, 1H), 2.20-2.29 (m, 1H), 1.97-2.82 (m, 2H), 1.83-1.97 (m, 2H), 1.42-1.49 (m, 1H), 1.22-1.29 (m, 1H). **^{13}C NMR** (75 MHz, $CDCl_3$) 177.00 (s, 1C), 173.76 (d, $J=3.25$ Hz, 1C), 160.40 (s, 1C), 116.93 (s, 1C), 113.13 (s, 1C), 81.50 (d, $J=7.50$ Hz, 1C), 69.25 (s, 1C), 50.29 (s, 1C), 49.68 (s, 1C), 42.97 (s, 1C), 41.22 (s, 1C), 38.75 (s, 1C), 26.89 (s, 3C), 21.66 (s, 1C). **^{31}P NMR** (121 MHz, $CDCl_3$) δ 29.06 (1P).

Synthesis of CDP22

***N*-dodecyl-P-(1-hydroxy-2-oxopiperidin-3-yl)phosphonamidic acid (17a).** To a solution of triphenylphosphine (96 mg, 350.59 μ mol) in DCM (4 mL), DIAD (68.17 μ L, 350.59 μ mol) were added with stirring at 0°C for 30 min. Separately, a solution containing BnHEX (50 mg, 175.29 μ mol), dodecylamine (74.69 μ L, 350.59 μ mol), and DBU (52.33 μ L, 350.59 μ mol) in DCM (1 mL) was prepared and added dropwise to the betaine solution. The reaction mixture was allowed to warm to room temperature over 30 minutes. The crude mixture was evaporated and the resulting yellowish solid triturated with MeCN multiple times to obtain the pure title compound. Yield: 44.1 mg (55%) **1H NMR** (300 MHz, $CDCl_3$) δ 7.37-7.44 (m, 5H), 3.55-3.63 (m, 2H), 2.85-2.93 (m, 4H), 2.12-2.17 (m, 1H), 1.96-2.03 (m, 2H), 1.76-1.81 (m, 2H), 1.56-1.66 (m, 2H), 1.41-1.51 (m, 2H), 1.18 (m, 36H), 0.79-0.83 (t, $J=6.0$ Hz). **^{31}P NMR** (121 MHz, $CDCl_3$) δ 31.14 (1P), 22.54 (1P).

***N*-dodecyl-P-(1-hydroxy-2-oxopiperidin-3-yl)phosphonamidic acid (CDP22).** Following the procedure G3, the following quantities were used: **17b** (44.1 mg, 97.22 μ mol), MeOH (3 ml), THF (2 ml). Yield: 32.1 mg (92%). Analysis by ESI+ (Expected $[M+H]^+ = 363.24$. Observed $[M+H]^+ = 362.98$). **1H NMR** (300 MHz, $CDCl_3$) 3.55-3.63 (m, 2H), 2.85-2.93 (m, 4H), 2.12-2.17 (m, 1H), 1.96-2.03 (m, 2H), 1.76-1.81 (m, 2H), 1.56-1.66 (m, 2H), 1.41-1.51 (m, 2H), 1.18 (m, 36H), 0.79-0.83 (t, $J=6.0$ Hz). **^{13}C NMR** (75 MHz, $CDCl_3$) 167.23 (s, 1C), 50.66 (s, 1C), 42.54 (s, 1C), 39.97 (s, 1C), 32.88 (d, $J = 7.5$ Hz, 1C), 31.93 (s, 2C), 29.25-29.70 (m, 12C), 29.02 (s, 1C), 27.74 (s,

2C), 26.78 (s, 2C), 23.44 (s, 1C), 22.70 (s, 2C), 14.12 (s, 2C). **³¹P NMR** (121 MHz, CDCl₃) δ 31.14 (1P), 22.54 (1P).

CHAPTER 4. NITROHETEROCYCLE PRODRUGS OF AN ENOLASE INHIBITOR EXHIBIT INCREASED POTENCY UNDER HYPOXIC CONDITIONS

A continuation of Case Study 1.

This chapter has been published in (permission granted)

Yan VC, Yang KL, Ballato ES, Khadka S, Shrestha P, Arthur K, Georgiou DK, Washington M, Tran T, Poral AH, Pham C-D, Yan MJ, Muller FL. 2020. Bio-reducible Phosphonoamidate Pro-drug Inhibitor of Enolase: Proof of Concept Study. ACS Med Chem Lett 11:1484–1489.

4.1 Abstract

Glycolysis inhibition remains aspirational in cancer therapy. We recently described a promising phosphonate inhibitor of enolase for cancers harboring homozygous deletions of *ENO1*. Here, we describe the application of a nitroheterocycle phosphonoamidate pro-drug pair to capitalize on tumor hypoxia. This bio-reducible prodrug exhibits greater-than 2-fold potency under hypoxic conditions compared to normoxia and exhibits robust stability in biological fluids. Our work provides strong *in vitro* proof-of-concept for using bio-reduction as a prodrug delivery strategy in the context of enolase inhibition.

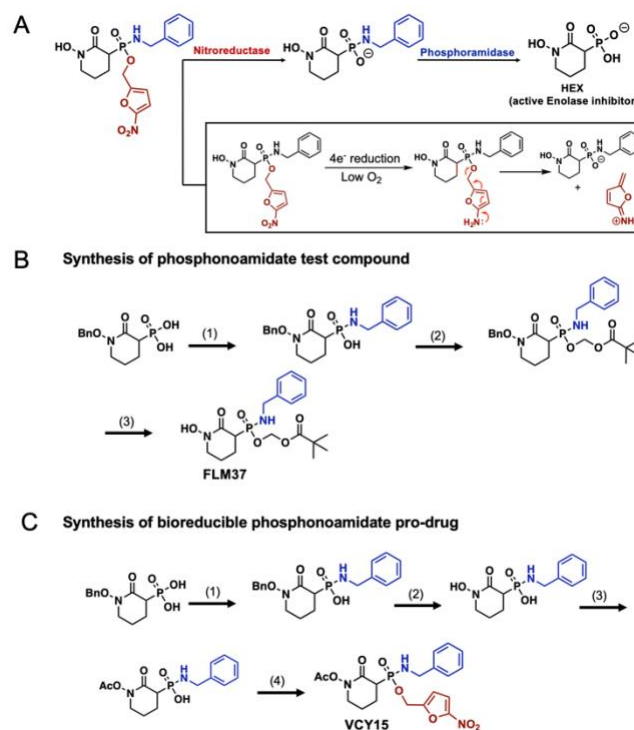
4.2 Hypothesis

Nitroheterocycle promoieties are viable first promoieties on phosphonate drugs that are preferentially removed under low oxygen conditions.

4.3 Introduction

GBM is a highly aggressive form of brain cancer, with few patients surviving beyond 2.5 years (135). Targeting vulnerabilities in cellular metabolism represents a promising, emergent strategy in precision oncology. We previously described one such vulnerability in glycolysis, in which the gene encoding for the enzyme enolase, *ENO1*, undergoes homozygous deletion in a subset of GBMs (4, 5). Cancers harboring the homozygous deletion *ENO1* remain metabolically active and viable through redundant action of its paralogue, ENO2. Inhibition of ENO2 in *ENO1*-deleted cancers results in cancer-specific killing, leaving non-malignant tissue unperturbed (6, 29).

A central challenge to developing a therapeutically relevant enolase inhibitor concerns the highly polar nature of glycolysis metabolites, resulting in highly polar inhibitor structures. To this end, we recently reported the design and synthesis of a phosphonate-containing ENO2-inhibitor, termed “HEX” (29). Because phosphonates are negatively charged at physiological pH, a pivaloyloxymethyl (POM) prodrug derivative, “POMHEX,” was initially synthesized to improve cell permeability (29). While POMHEX shows excellent, preferential potency against *ENO1*-deleted cells *in vitro* and can eradicate *ENO1*-deleted tumors in preclinical murine models, it suffers from poor pharmacokinetics. Rapid, extracellular cleavage of the first POM group by high concentrations of carboxylesterases exposes the negatively charged phosphonate monoester—reintroducing cell and BBB permeability issues (29).



Scheme 3. Bioactivation and synthesis of bioreducible phosphonoamidate pro-drugs. (A) Mechanism of bioactivation. (B) Reaction conditions: 1.) BnNH₂, DBU, PPh₃/DIAD (2 equiv. ea.), 1 h, 2.) POMCl (1.5 equiv.), MeCN, 50°C, 1 h, 3.) H₂, 10% Pd/C, THF/MeOH, 2 h. (C) Reaction conditions: 1.) BnNH₂, DBU, PPh₃/DIAD (2 equiv. ea.), 1 h 2.) H₂, 10% Pd/C, THF/MeOH, 2 h, 3.) Ac₂O, MeCN, 50°C, 1 h, 4.) 2-(bromomethyl)-5-nitrofurane (2 equiv.), MeCN, 50°C, 12 h. For full synthesis procedures, see Section 4.6.

The most optimal prodrug delivery system avoids premature extracellular cleavage and enables selective release of the active agent within the tumor. A common feature of many tumors, especially GBM, is the presence of highly hypoxic regions (136) in which median oxygen levels may be as low as ~2%, as compared to ~7% in normal tissue (137). At present, hypoxia is visualized clinically using agents such as ¹⁸F-AZA and histologically via pimonidazole (138, 139). Common to both probes is the inclusion of a nitroaromatic moiety, which can be reduced under hypoxic condition through nitroreductases (NADH dehydrogenases), to reveal the active agent

(140). Taking the necessity for two pro-drug groups to protect phosphonate drugs into account, we herein provide proof-of-concept for the feasibility of using both a nitroaromatic and benzylamine moieties for delivery of a phosphonate glycolysis inhibitor (**Scheme 3**).

4.4 Results and Discussion

The polyprotic nature of phosphates warrants the attachment of two prodrug protecting groups for efficient cell permeation. While nitroreductases can facilitate the removal of the first prodrug moiety, hydrolysis of the second pro-drug is limited to enzymes that can tolerate the presence of an anionic substrate. We recognized phosphoramidases (97) as a class of enzymes fulfilling this requirement and thus sought to synthesize mixed phosphonoamidate esters. To the best of our knowledge, the only similar example in the literature of a similar pro-drug is the alkylating agent TH-302 (141, 142), wherein nitrogen mustards and nitroimidazole moiety are attached to the phosphate to form the bio-reducible phosphoramidate. However, where the active alkylating agent of TH-302 preserves the P-N phosphoramidate bond, we sought to generate a labile amine pro-drug so that the active enolase inhibitor may be released. The most prominent example in the literature using phosphoramidases for prodrug bioactivation is the McGuigan (ProTide®) prodrugs (118), which use N-linked amino acid alkyl esters in phosphate/phosphonate nucleotide analogues. Another example of a phosphoramidase-labile pro-drug is the liver-specific anti-viral nucleotide IDX-184 (97), in which the phosphate is protected by both a thioester and a benzylamine. Due to the interdependent bioactivation mechanism of the amino acid ester in the context of glioma cells. Given that IDX-184 is a liver-specific anti-viral pro-drug (132), it was initially unclear whether benzylamine would be an effective delivery moiety in the context of glioma. We thus began our study by preparing a cell-permeable, esterase-labile phosphonoamidate pro-drug (**Scheme 3b**, **FLM37**) and examining its efficacy as a pro-drug moiety *in vitro*.

Benzyl-protected HEX (BnHEX), was prepared according to previously published procedures (29). First, BnHEX was coupled with benzylamine using a novel mono-amidation procedure we developed (129) to generate the intermediate phosphonoamidate (**Scheme 3b**). To establish the efficacy of using benzylamine as a pro-drug moiety in the context of glioma cells, we first generated the esterase-labile POM ester through reaction with the free phosphonoamidate

intermediate (**Scheme 3b, step 2**). Finally, we performed reductive hydrogenation to liberate the hydroxamate, generating the POM/benzylamine test compound (**Scheme 3b, FLM37**).

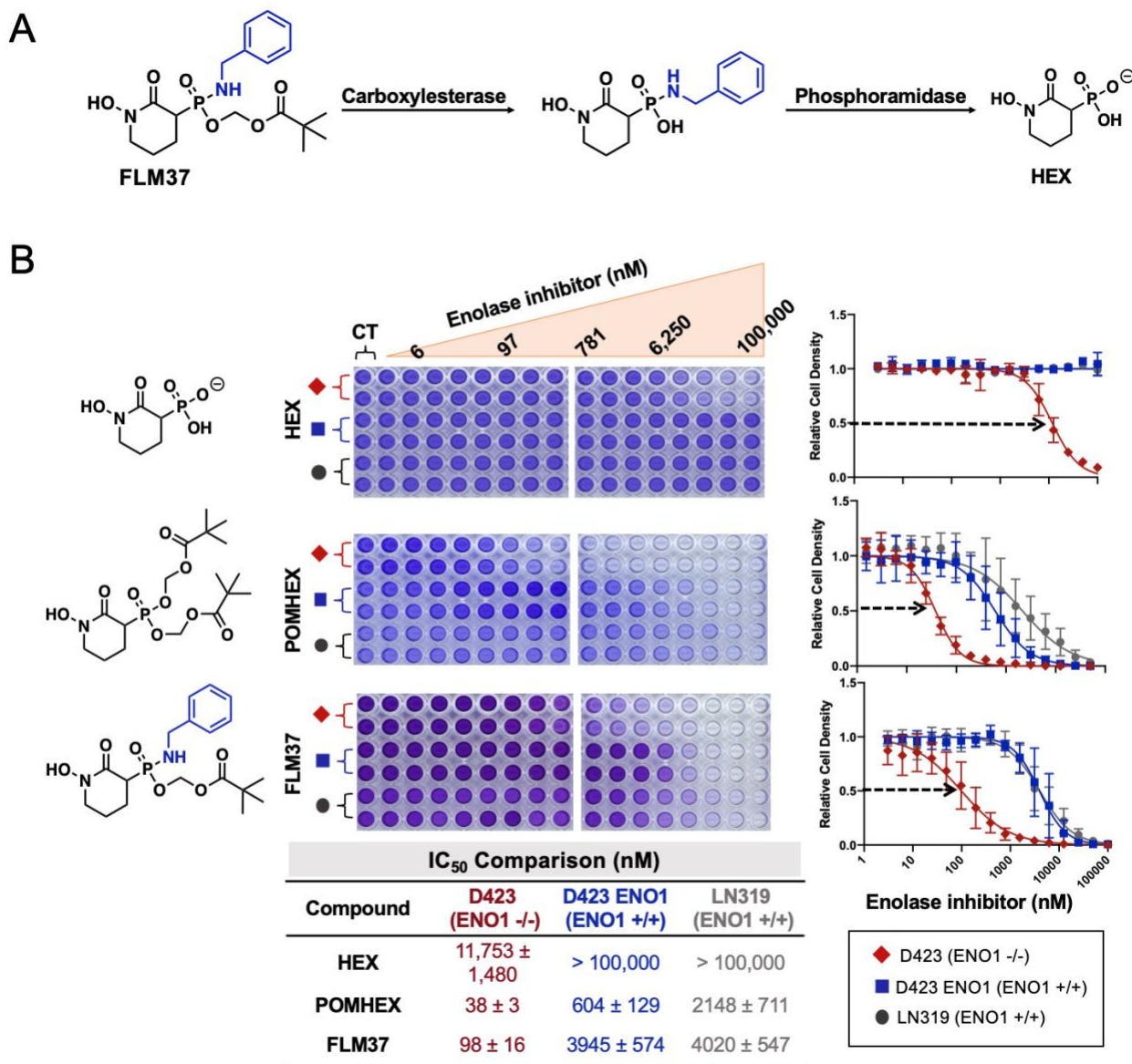


Figure 24. Benzylamine is a viable pro-drug group in the context of glioma. (A) Proposed mechanism of bioactivation for FLM37. (B). Proliferation assay comparing the activity of FLM37 (bottom) to the esterase prodrug POMHEX (middle) and the free phosphonate HEX (top) *in vitro*. Cells were incubated with inhibitor for 5 days before being fixed, stained with crystal violet and quantified spectroscopically at 590 nm. Cell density is plotted as a function of inhibitor concentration. FLM37 exhibits more than 30-fold greater potency compared to HEX, indicating the ability for glioma cells to cleave benzylamine.

We and others have documented the ability for the POM group to undergo rapid hydrolysis by ubiquitously expressed esterases in cells (29, 143). Thus, we can infer that the predominant *in vitro* potency effects observed from FLM37 treatment arise from the lability of benzylamine (**Figure 24a**). Congruent with our general therapeutic framework, we tested FLM37 on a panel of 3 cell lines: D423 (*ENO1*-deleted), D423 *ENO1* (*ENO1* overexpressing), and LN319 (WT control). Cells were treated with FLM37 for 5 days. FLM37 demonstrated select toxicity against *ENO1*-deleted cells in the nanomolar range, indicating the ability for benzylamine to be cleaved in glioma cells to release the active *ENO2* inhibitor, HEX (**Figure 24b**). Compared to the esterase pro-drug POMHEX, FLM37 exhibited less potency against *ENO1*-deleted cells but was still significantly more potent compared to the free phosphonate, HEX (**Figure 24b**).

Having established the feasibility of using benzylamine as a second pro-drug group, we then sought to synthesize the nitroaromatic phosphonoamidate prodrugs. Returning to the benzyl-protected phosphonoamidate intermediate (**Scheme 3c**), we performed reductive hydrogenation to remove the benzyl ether on the hydroxamate; this was then re-protected with an acetyl group. Though circuitous, we found these deprotection-reprotection steps to be necessary due to the incompatibility of hydrogenation with the nitroaromatics. Due to the nucleophilic nature of the hydroxamate, direct reaction with the nitroaromatics was not possible without addition to the hydroxamate.

To examine the relationship between standard reduction potential and sensitivity to hypoxia, we compared the nitrofuran phosphonoamidate pro-drug (**Scheme 3c**, **VCY15**) to TH-302, a nitroimidazole-containing alkylating agent known to exhibit greater potency under hypoxic conditions (144). VCY15 was prepared by simple S_N2 reaction with the phosphonoamidate intermediate and 2-(bromomethyl)-5-nitrofuran (**Scheme 3c**). Previous studies have shown that nitroreductases facilitate the removal of nitroaromatics under hypoxic conditions through a 4-electron reduction mechanism (140). It thus followed that the ease of reduction between VCY15 and TH-302 would depend on the standard reduction potentials of the nitroheterocycles. We hypothesized that the fold-change in potency between normoxic and hypoxic conditions would correlate with the standard reduction potentials of the nitrofuran and nitroimidazole, respectively. Nitrofurans have been reported to have a standard reduction potential of -257 mV (145) while

nitroimidazoles have a reported standard reduction potential of -398 mV (145). Accordingly, both VCY15 and TH-302 would show improved potency under low oxygen conditions, with the latter exhibiting a more dramatic potency increase under hypoxia.

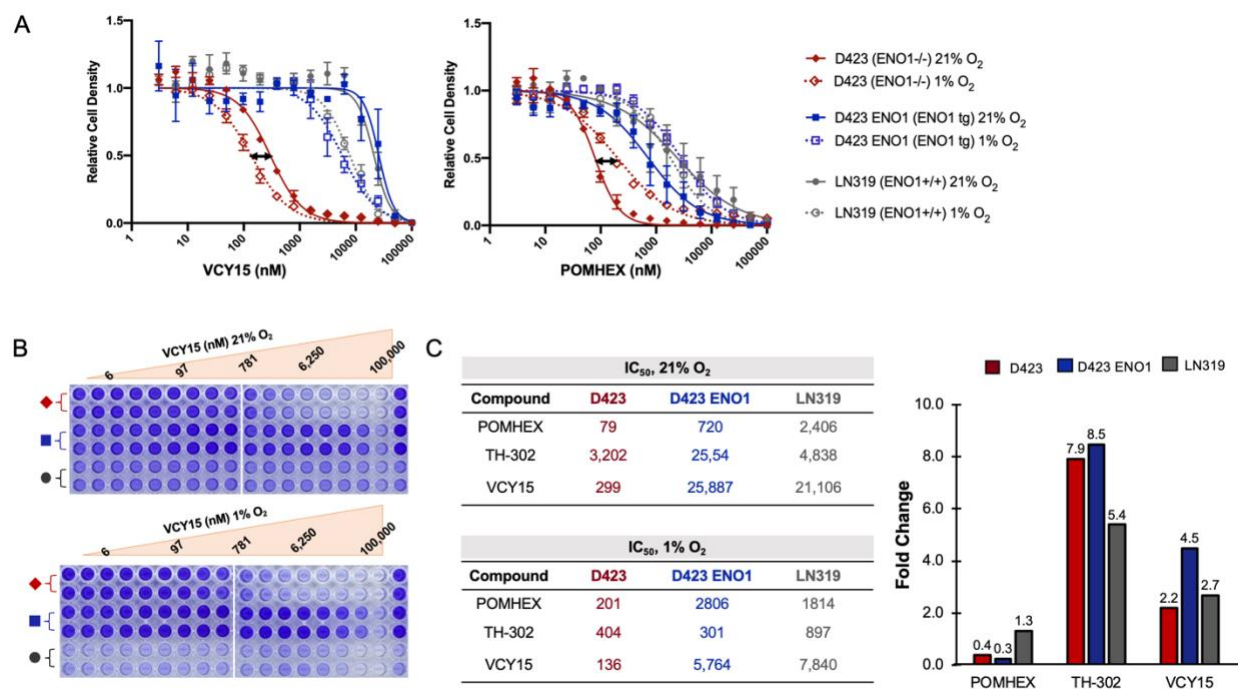


Figure 25. Nitroaromatic benzylamine pro-drug exhibits greater potency under hypoxic conditions. (A) VCY15 contains a bioreducible nitrofuranyl pro-drug moiety that exhibits greater potency at 1% O₂ against a panel of 3 glioma cell lines. In contrast, POMHEX exhibits a decrease in potency at 1% O₂ across the same set of cell lines. (B) Representative plates for cells treated with VCY15 at 21% O₂ and 1% O₂ after a 5-day treatment course. (C) IC₅₀ values for cells treated with either POMHEX, TH-302, or VCY15 and corresponding fold-changes for *ENO1*-deleted cells (n=4). Bioreducible pro-drugs increase in potency at 1% O₂.

To test this hypothesis, we performed *in vitro* cell culture experiments under both normoxia (21% O₂) and hypoxia (1% O₂). We note that while the physiological oxygen concentration (“physioxia”) is about 7% O₂ (146), we saw no significant difference in cytotoxicity measurements between 21% O₂ and 7% O₂ (Figure 25). All three compounds were tested against the same three cell lines aforementioned. Cells were incubated with either VCY15, TH-302 (positive control), or POMHEX (negative control) at 21% O₂ or 1% O₂. After 5 days, cells were then fixed, stained with crystal violet, and quantified spectroscopically. As anticipated, VCY15 showed selectivity for D423 cells, indicating selective inhibition of enolase through release of the active agent, HEX. Importantly, VCY15 also showed markedly improved potency under hypoxic conditions compared to

POMHEX, which contains no bio-reducible moieties (**Figure 25a-c**). At 21% O₂, VCY15 showed an average an IC₅₀ of 299 nM and 136 nM at 1% O₂ against D423 cells. Concurrent with our predictions, the potency changes from normoxia to hypoxia correlated with the standard redox potentials of each nitroaromatic pro-drug. From 21% to 1% O₂, VCY15 (nitrofuran) exhibited a 2-fold increase in potency against D423 cells while TH-302 exhibited an 8-fold increase in potency against the same cell line (**Figure 25c**). In support of the hypoxia-mediated activation for VCY15, we found that POMHEX exhibited a 2-fold *decrease* in potency at 1% O₂ compared to normoxia.

It is generally understood that sensitivity to glycolysis inhibition should increase under hypoxia (147), as capacity for ATP production by oxidative phosphorylation decreases. However, as ENO2 is a HIF-transcription factor that is inducible by hypoxia (147), it is highly upregulated under low oxygen conditions. Prior studies have shown that, compared to ENO1 which exhibits a 2-fold increased induction under hypoxia, ENO2 exhibits a greater-than-5-fold increase across a broad panel of glioma cell lines (147). As the sensitivity of *ENO1*-deleted cells to Enolase inhibition is dependent on residual ENO2 activity (4), upregulation of ENO2 under mild hypoxic conditions paradoxically *decreases* the sensitivity of *ENO1*-deleted cells to Enolase

inhibitors. Within this context, the sensitivity of *ENO1*-deleted cells to VCY15 is thus particularly impressive. That sensitivity to VCY15 is increased at 1% O₂ while that of POMHEX is decreased, suggests that the net increase in nitrofuran pro-drug bioactivation from 21% O₂ to 1% O₂ is actually higher than the 2-fold inferred by the IC₅₀ shift alone. Combined, these results suggest a correlation

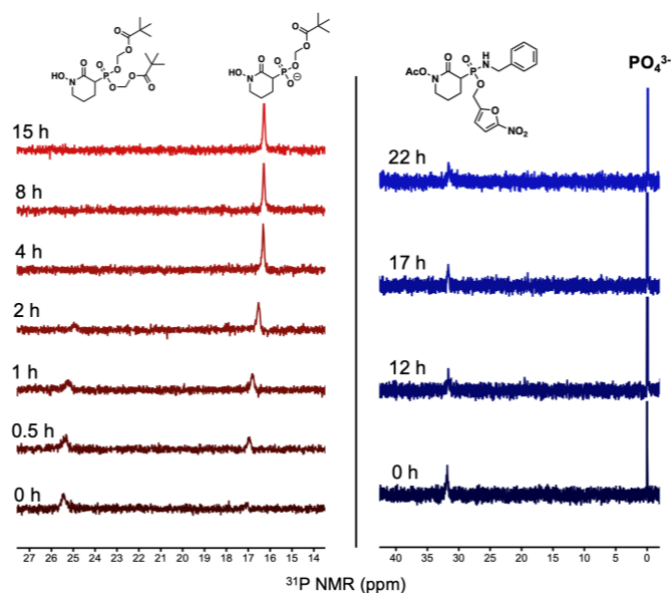


Figure 26. Nitroaromatic benzylamine pro-drugs exhibit robust stability in human plasma.

³¹P NMR scans (121 MHz) of esterase-labile pro-drug, POMHEX (left, red) and VCY15 (right, blue) were taken in 80% human plasma with 20% D₂O for signal lock; ns = 1000. Where POMHEX degrades to its hemi-ester form after 4 hours, VCY15 remains stable for over 22 hours.

between cytotoxicity and pro-drug sensitivity to O₂; this corresponds with earlier studies on various nitroaromatic derivatives conjugated to alkylating agents (148) or radiosensitizers (149).

Finally, we sought to examine the stability of these nitroheterocycle pro-drugs in human plasma. We reasoned that VCY15 should experience little to no degradation, as nitroreductases are found exclusively within the cell and intracellular phosphoramidases require the presence of a negative charge for hydrolytic activity. To examine stability, we assayed VCY15 at various timepoints in human plasma using ³¹P NMR (**Figure 26**). In sharp contrast to POMHEX, which begins to hydrolyze to its monoester form in less than 30 minutes (**Figure 26, left**), all nitroheterocycle prodrugs were stable for over 22 hours (**Figure 26, right**), as indicated by a constant peak at ~32 ppm.

4.5 Conclusions

We have prepared a bio-reducible prodrug inhibitor of enolase containing a nitrofuran and benzylamine that confers improved specificity and stability towards cancer cells. Our data suggest that this delivery mechanism may be specific to tumors, in which extended hypoxia is a unique characteristic (45). Further *in vivo* studies are ongoing. While nitroaromatic prodrugs have previously been reported in other drug delivery contexts, this combination of a nitroaromatic and benzylamine is, to the best of our knowledge, the first of its kind. Benzylamine has previously been reported to be a suitable pro-drug substrate for phosphoramidases in the context of liver diseases (150), however, its efficacy in the context of GBM has not been disclosed in the literature. Our laboratory is actively investigating the tunability of the nitroaromatic prodrug in relation to its hypoxia sensitivity. Preliminary data have shown that nitrothiophene pro-drug (standard reduction potential of -277 mV (145)) and nitroimidazole phosphonoamidate pro-drugs of HEX are also hypoxia-labile moieties. Initial comparison between VCY15 and the nitrothiophene and nitroimidazole derivatives concur with our observed relationship between standard reduction potential and fold-change in potency between normoxic and hypoxic conditions (151). Given the challenge of synthesizing this class of compounds, further optimization and *in vitro* assessments are ongoing.

4.6 Experimental

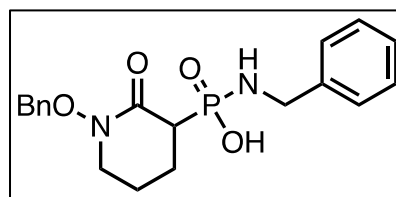
General synthetic procedures. All solvents and reagents were purchased from Sigma-Aldrich at the highest commercially available purity and were used without further purification. ^1H , ^{13}C , and ^{31}P NMR spectra were recorded on a Bruker Avance 500 MHz or 300 MHz spectrometer, as indicated. BnHEX was initially synthesized according to previously published procedures (29); subsequent syntheses were contracted to WuXi AppTec, Shanghai, China. Final compounds were purified via HPLC (Phenomenex Luna-C18. 0-3 min 10% Buffer B, 21-24 min 100% Buffer B, 27-30 min, 10% Buffer B; Buffer A= H_2O + 0.1% TFA, Buffer B= MeCN + 0.01% TFA). See Scheme 3 for a representative synthesis scheme.

Cell viability assay. Cell culture experiments were performed using the D423-MG cell line. The D423-MG cell lines is 1p36 homozygous deleted from *CAMTA1* to *SLC25A33*; this includes *ENO1*. Isogenic *ENO1* ectopically rescued lines were described previously (pCMV *ENO1* 5X) (4). An *ENO1*-intact cell line (LN319) was used as a control for sensitivity to enolase inhibitors. Cells were regularly cultured in Dulbecco's modified Eagle's medium supplemented with 10% fetal bovine serum. Cell viability was determined by crystal violet staining, as previously described (6, 29, 134, 152). The cell lines used were D423 (*ENO1*-deleted), D423 *ENO1* (overexpressing *ENO1*) and LN319 (control). Glioma cells were seeded in 96-well plates and treated with varying concentrations of the inhibitors described above for 7 days. Cells were then washed with PBS, fixed with 10% formalin and stained with 0.05% crystal violet. Washed and dried plates were dye-extracted using 10% acetic acid, and absorbance was measured at 595 nm using Omegastar Plate Reader (BMG Labtech). To test the efficacy of the synthesized under hypoxic conditions, 1×10^4 cells were plated in 96-well plates, treated with inhibitor and incubated for 3 days in a hypoxia station (Don Whitley Scientific, Shipley, UK) set at 1% O_2 and 5% CO_2 . Crystal violet staining was then performed as described above.

Synthesis of FLM37

N-benzyl-P-(1-(benzyloxy)-2-oxopiperidin-3-

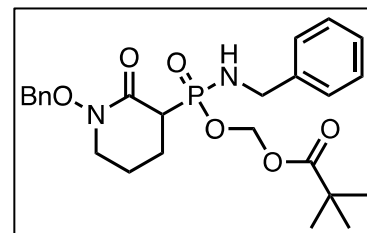
yl)phosphonamidic acid (**1**). Intermediate **1** was prepared using methods describes in *Chapter 2* (129). To a solution of triphenylphosphine (275.87 mg, 1.06 mmol) in DCM (15 mL), DIAD (204.50 μL , 1.06 mmol) were added with stirring at 0°C



for 30 min. Separately, a solution containing BnHEX (150 mg, 527.74 μmol), benzylamine (115.18 μL , 1.06 mmol), and DBU (157.54 μL , 1.06 mmol) in DCM (2 mL) was prepared and added dropwise to the betaine solution. The reaction mixture was allowed to warm to room temperature over 30 minutes. Then, 1 volume of water was added to the crude mixture. After vigorous shaking and partitioning via centrifugation (2 min at 4°C, 4000 rpm), the aqueous layer was isolated and lyophilized to a clear solid. Analysis by ESI+ ($\text{C}_{19}\text{H}_{23}\text{N}_2\text{O}_4\text{P}$ Expected $[\text{M}+\text{H}]^+=375.38$. Observed $[\text{M}+\text{H}]^+=375.35$). **^1H NMR** (500 MHz, D_2O) δ 7.32-7.53 (m, 10 H), 4.91-4.96 (m, 2H), 4.02-4.11 (m, 2H), 3.46-3.57 (m, 2H), 2.80-2.87 (dt, $J=21.52$ Hz, $J=21.70$ Hz, 1H), 2.07-2.13 (m, 1H), 1.92-1.98 (m, 2H), 1.72-1.79 (m, 1H). **^{13}C NMR** (125.7 MHz, D_2O) δ 167.97 (d, $J=4.72$ Hz, 1C), 141.25 (d, $J=7.36$ Hz, 1C), 134.52 (s, 1C), 129.92 (s, 2C), 129.15 (s, 1C), 128.73 (s, 2C), 128.60 (s, 2C), 127.59 (s, 1C), 127.00 (s, 1C), 75.54 (s, 1C), 50.11 (s, 1C), 45.28 (s, 1C), 43.64 (d, $J=111.12$ Hz, 1C), 22.33 (d, $J=3.65$ Hz, 1C), 21.65 (d, $J=7.23$ Hz, 1C). **^{31}P NMR** (202 MHz, D_2O) δ 20.91

(((Benzylamino)(1-(benzyloxy)-2-oxopiperidin-3-

yl)phosphoryl)oxy)methyl pivalate (2). To a solution of (1) (36.50 mg, 97.24 μmol) in anhydrous MeCN (1 mL), chloromethyl pivalate (21.02 μL , 145.86 μmol) and DIPEA (2 μL , 11.51 μmol) were added. The reaction was allowed to stir for 15 h at 50°C. Then, the

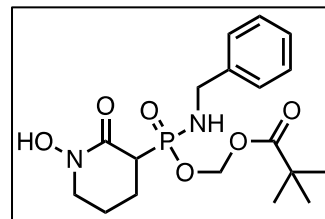


crude mixture was concentrated under reduced pressure to a yellow oil and purified via reverse-phase HPLC (Agilent G1361A 1260 Infinity) using a stepwise gradient (5-90% Buffer B over 10 minutes, 90-100% Buffer B over 7 minutes, 100% Buffer B over 8 minutes, 100-5% Buffer B over 5 minutes; Buffer A: dH_2O with 0.1% TFA, Buffer B: CH_3CN + 0.1% TFA). The desired compound was obtained after 10 minutes and lyophilized to a white powder. Analysis by ESI+ ($\text{C}_{25}\text{H}_{33}\text{N}_2\text{O}_6\text{P}$ Expected $[\text{M}+\text{H}]^+=490.51$. Observed $[\text{M}+\text{H}]^+=490.41$). **^1H NMR** (500 MHz, CDCl_3) δ 8.81 (d, $J=4.77$ Hz, 1H), 8.24-8.27 (t, $J=7.80$, 7.87 Hz, 1H), 7.90-7.92 (d, $J=7.99$ Hz, 1H), 7.69-7.71 (t, $J=6.44$, 6.75 Hz, 1H), 7.33-7.40 (m, 5H), 5.61-5.68 (m, 2H), 4.90 (d, $J=2.22$ Hz, 2H), 4.64-4.80 (t, $J=9.91$, 9.91 Hz, 2H), 3.35-3.37 (m, 2H), 3.12-3.20 (dt, $J=23.65$ Hz, 1H), 2.09-2.15 (m, 1H), 1.94-2.05 (m, 2H), 1.69-1.75 (m, 1H), 1.18 (s, 9H). **^{13}C NMR** (125 MHz, CDCl_3) δ 177.48 (d, $J=7.39$ Hz, 1C), 163.53 (d, $J=4.81$ Hz, 1C), 156.93 (d, $J=4.22$ Hz, 1C), 145.22 (s, 1C), 143.48 (s, 1C), 130.13 (s, 2C), 130.03 (s, 1C), 129.42 (s, 1C), 129.03 (s, 2C), 126.04 (s, 1C),

125.18 (s, 1C), 81.58-81.64 (d, J=7.40 Hz, 1C), 76.40 (s, 1C), 43.73-44.77 (d, J=132.02 Hz, 1C), 43.05 (s, 1C), 22.43-22.47 (d, J=4.61 Hz, 1C), 21.91-21.94 (d, J=4.32 Hz, 1C); quaternary sp³ carbon not observed. ³¹P NMR (202 MHz, CDCl₃) δ 29.81 (s, 1P), 29.11 (s, 1P) (*isomers*).

(((Benzylamino)(1-hydroxy-2-oxopiperidin-3-

yl)phosphoryl)oxy)methyl pivalate (3, FLM37). Palladium on carbon (10 wt. %, 100 mg) was mixed with THF (2 mL) and MeOH (3 mL) with stirring. Hydrogen in a balloon was then allowed to flow through the reaction for 1 minute with venting. Then, a second balloon

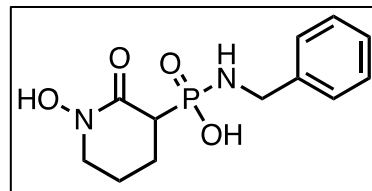


with hydrogen was added to the reaction and the mixture was allowed to stir and saturate with hydrogen for 1 hour. Next, to a separate vial, (**2**) was dissolved in MeOH (2 mL) and injected into the hydrogen-charged flask. The reaction stirred at room temperature for 1 hour. Then, the palladium was filtered, and the reaction was concentrated under reduced pressure to a pale-yellow oil. The crude product was purified via reverse-phase HPLC (Agilent G1361A 1260 Infinity) using a stepwise gradient (1-60% Buffer B over 25 minutes, 60-100% Buffer B over 10 minutes, 100% Buffer B over 5 minutes, 100-0% Buffer B over 1 minutes; Buffer A: dH₂O with 0.1% TFA, Buffer B: CH₃CN + 0.1% TFA). Product-containing fractions were combined and lyophilized to a pale-yellow solid. Analysis by ESI+ (C₁₈H₂₇N₂O₆P Expected [M+H]⁺=399.40. Observed [M+H]⁺=399.35). ¹H NMR (500MHz, CDCl₃) δ 7.22-7.39 (m, 5H), 5.59-5.66 (dd, J=12.32Hz, 2H), 5.54-5.59 (ds, J=12.66Hz, 2H), 4.29-4.36 (t, J=11.71Hz, 2H), 4.25-4.32 (t, J=11.29Hz, 2H), 3.01-3.10 (dt, J=22.99Hz, 1H), 2.86-2.95 (dt, J=22.79Hz, 1H), 2.08-2.13 (m, 2H), 1.83-2.08 (m, 2H), 1.20 (s, 9H), 1.19 (s, 9H). ¹³C NMR (125.7MHz, CDCl₃) δ 177.26 (s, 1C), 177.23 (s, 1C), 160.33-160.43 (d, 1.29Hz, 1C), 160.17-160.31 (d, J=2.96Hz, 1C), 139.94 (d, J=2.72Hz, 1C), 139.4-139.52 (d, 2.53Hz, 1C), 127.27-128.70 (m, 5C), 81.26-81.45 (d, J=3.11Hz, 1C), 80.87-81.05 (d, J=3.60Hz, 1C), 48.67 (s, 1C), 40.89-41.21 (d, J=31.86Hz, 1C), 26.81-26.90 (s, 3C), 21.43-21.85 (m, 2C). ³¹P NMR (202 MHz, CDCl₃) δ 28.76 (s, 1P), 29.63 (s, 1P) (*isomers*)

Synthesis of VCY15

N-benzyl-P-(1-hydroxy-2-oxopiperidin-3-yl)phosphonamidic

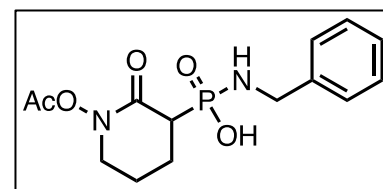
acid (4). A solution of 10% Pd/C (200 mg) in anhydrous THF/MeOH (2:3) was stirred at 25°C. A balloon of H₂ was added and the solution vented for 10 minutes. A second balloon of H₂ was



then added, and the solution stirred for 1 h. Then, this slurry was transferred to a vial containing BnFLM38 (250 mg, 668 mmol) and was allowed to stir for 1 h. The reaction was filtered and concentrated to a yellow oil. Analysis by ESI+ (C₁₂H₁₆N₂O₆P Expected [M+H]⁺=285.25 Observed [M+H]⁺=285.30).

P-(1-acetoxy-2-oxopiperidin-3-yl)-N-benzylphosphonamidic

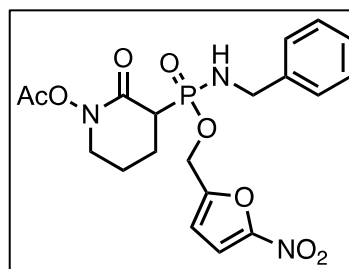
acid (5). To a solution of (4) (65 mg, 229 μmol) in anhydrous MeCN (500 μL), Ac₂O (65 μL, 668 μmol) was added. The reaction stirred for 3 h at 25°C. Then, the reaction was concentrated and lyophilized



for 2 days. Analysis by ESI+ (C₁₄H₁₈N₂O₆P Expected [M+H]⁺=327.29 Observed [M+H]⁺=327.32). ¹³C NMR (75 MHz, CDCl₃) δ 168.01 (s, 1C), 161.65 (d, J=6.32 Hz, 1C), 141.92 (d, J=6.96 Hz, 1C), 128.22 (s, 2C), 127.55 (s, 2C), 126.54 (s, 1C), 51.63 (s, 1C), 43.24 (s, 1C), 36.42-35.29 (d, J=170.11 Hz, 1C), 25.48 (s, 1C), 25.14 (5.93 Hz, 1C), 22.13 (d, J=7.06 Hz, 1C). ³¹P NMR (121 MHz, CDCl₃) δ 17.50 (s, 1P).

3-((benzylamino)((5-nitrofuran-2-yl)methoxy)phosphoryl)-2-

oxopiperidin-1-yl acetate (6, VCY15). To a solution of (5) (73 mg, 224 mmol) in anhydrous acetonitrile, 2-(bromomethyl)-5-nitrofurane (138.26 mg, 671 mmol) were added. The reaction was allowed to stir at 50°C for 20 h. The solvent was then removed and



the reaction was purified via reverse-phase HPLC (1-60% Buffer B over 25 minutes, 60-100% Buffer B over 10 minutes, 100% Buffer B over 5 minutes, 100-0% Buffer B over 1 minutes; Buffer A: dH₂O with 0.1% TFA, Buffer B: CH₃CN + 0.1% TFA). Product-containing fractions were combined and lyophilized to a yellow solid. Analysis by ESI+ (C₁₉H₂₂N₃O₈P Expected [M+H]⁺=452.37. Observed [M+H]⁺=452.42). ¹H NMR (300 MHz, CDCl₃) 7.26-7.23 (m, 6H), 7.17-7.12 (d, J=3.82 Hz, 1H), 6.49 (d, J=7.12 Hz, 2H), 4.89 (m, 2H), 4.36 (d, J=3.22 Hz, 2H), 4.22

(d, $J=5.92$ Hz, 2H), 3.62 (m, 2H), 3.04 (dt, $J=23.40, 7.58$ Hz, 1H), 2.13 (s, 3H), 1.96 (s, 2H), 1.18 (s, 2H). **^{13}C NMR** (75 MHz, CDCl_3) δ 170.19 (s, 1C), 167.26 (d, $J=15.44$ Hz, 1C), 153.35 (d, $J=9.55$ Hz, 1C), 152.60 (s, 1C), 140.09 (d, $J=2.07$ Hz, 1C), 128.83-127.24 (m, 5C), 112.62-111.99 (m, 2C), 57.39 (s, 1C), 51.37 (s, 1C), 44.46 (s, 1C), 43.61 (d, $J=62.07$ Hz, 1C), 22.52 (d, $J=6.32$ Hz, 1C), 20.67 (d, $J=2.58$ Hz, 1C), 18.2 (s, 1C). **^{31}P NMR** (121 MHz, CDCl_3) δ 29.49 (s, 1P), 29.37 (s, 1P) (*isomers*).

CHAPTER 5. PRODRUG IDENTITY INFLUENCES CELL- AND TISSUE-SPECIFIC LOCALIZATION

Part of this chapter has been published in (permission granted)

Yan VC, Butterfield HE, Poral AH, Yan MJ, Yang KL, Pham C-D, Muller FL. 2020. Why Great Mitotic Inhibitors Make Poor Cancer Drugs. *Trends in Cancer* 6:924–941.

7.1 Hypothesis

The rate of prodrug removal is largely influenced by the expression of the corresponding prodrug activating enzyme in a given tissue or cell type. Prodrugs will be preferentially activated in tissues and cell types with high expression of prodrug activating enzyme.

7.2 Introduction

Two prodrug motifs dominate the landscape of FDA-approved drugs: bis-ester (Farquhar) prodrugs (*Section 1.2.1*) and McGuigan prodrugs (*Section 1.2.2*). While alternative prodrugs (*Section 1.2.3*) have been developed and explored, most have remained in preclinical development (16); efforts on this front are nonetheless ongoing (16, 153). Amongst the phosph(on)ate prodrug motifs that have been published, the most popular motif is the McGuigan prodrug; this is largely due to the success of FDA-approved drugs such as SOF and TAF. In the latter case, the development of TAF was seen as an improvement over its bis-ester predecessor, TDF (154). As a result, the McGuigan prodrug motif has been applied to a number of phosph(on)ate-containing drugs and molecules (117)—seemingly without serious consideration of whether such a strategy is appropriate in the context of a given pathology. The prevalence of McGuigan prodrugs in pathological contexts that would seem to disfavor such an approach (102) is perhaps illustrative of how the phosph(on)ate prodrug field overlooks: 1.) the relationship between prodrug structure and expression of the corresponding bioactivating enzyme(s) in the cell type of a given pathology and 2.) the PK properties of the intact prodrug and the effects of extracellular plasma enzymes on prodrug metabolism. This oversight is exacerbated by modern (over)reliance and misconception that cell culture models are reliable indicators of a phosph(on)ate prodrug's efficacy *in vivo*. While my critique on the over-application of McGuigan prodrugs serves as a convenient, modern, and relevant example of some of the field's oversights, it is not the only class of phosph(on)ate prodrug that is illustrative of—what I perceive to be—a gap between chemists and biologists. In this section, I briefly discuss 2 examples of different phosphate prodrugs indicated for 2 different diseases to

illustrate the relationship between promoiety structure and cell- and tissue-specific metabolism towards the active pharmacophore. These examples provide concrete insight into situations when phosphate prodrugs work well and afford (a sufficient level) of specificity for the target cell population. In the next chapter, I will describe a situation where scientific disregard of the relationship between bioactivation of the McGuigan prodrug RDV and localization to the cell population of interest results in suboptimal delivery of the active pharmacophore to the SARS-CoV-2-infected pneumocytes. The seemingly contrarian rationale that I will present in the next chapter with the RDV/GS-441524 paradigm is a foil to that of SOF, described here in *Section 7.4.1*.

7.3.1 Case Study 2: Cyclophosphamide achieves a therapeutic window through preferential formation of the active metabolite in tumors versus normal tissue.

While conventional cytotoxic chemotherapies do not often receive much of a spotlight in an era preferring molecular targeted therapies, chemotherapy can succeed sufficiently well to impart clinically meaningful—if not even transformative results at times (155, 156). Combinations of various chemotherapies have been central to cancer treatment, with a considerable number of patients across a range of cancers being effectively cured by such combinations (157, 158). While this is not well appreciated in the cancer research community, many key chemotherapeutic drugs from diverse classes are prodrugs; their therapeutic windows arise from preferential bioactivation in cancerous versus normal tissues. A classic and elegant example of this theme is captured by the bioactivation of cyclophosphamide (**Figure 27**).

Cyclophosphamide is an intricate prodrug of a nitrogen mustard (159): the nitrogen derivative of the sulfur mustards used during WWII. Direct application of nitrogen mustards to patients suffering from cancer such as lymphomas and leukemias yielded hints of anti-neoplastic activity in model systems and in the clinic (160–165), but intolerable adverse effects (156, 166–170) precluded further clinical utility. Structurally, the severity of these adverse events may be attributed to the electrophilic, aliphatic nature of the first clinically-deployed mustards (168–170). To temper the indiscriminate toxicity of the aliphatic nitrogen mustard (**Figure 24**), a concerted effort to reduce the electrophilicity of the mustard was made in the 1950s. It was then that the very first pro-drug iterations of the nitrogen mustard arose, with the FDA approving chlorambucil in

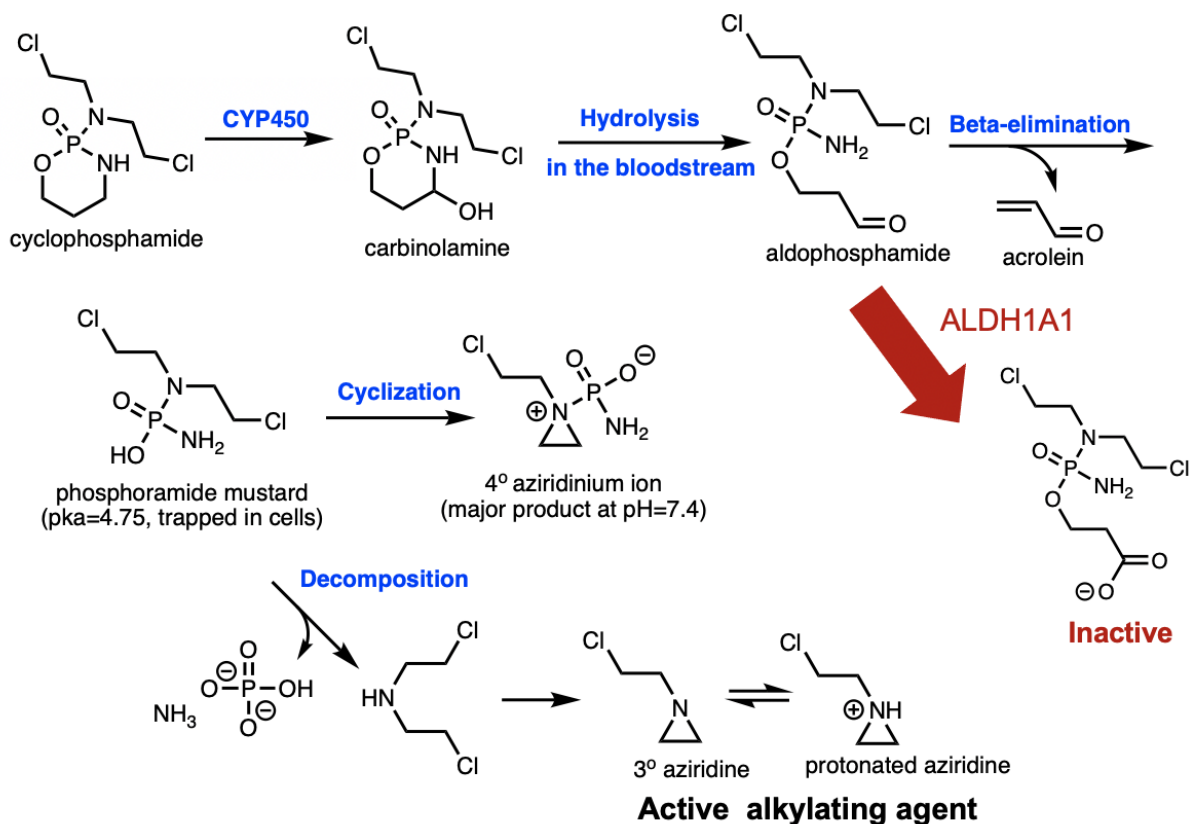


Figure 27. Cyclophosphamide mechanism of bioactivation. ALDH oxidizes the aldophosphamide intermediate to a negatively charged carboxylate, which is inactive. In cancer cells lacking ALDH, beta-elimination of the aldophosphamide occurs. A narrow therapeutic window between many rapidly proliferating normal tissue and cancerous tissue arises from the presence versus absence of ALDH(1A1).

1957. Unlike the previously administered aliphatic nitrogen mustards, chlorambucil contained an aromatic pro-drug group, which reduced electrophilicity and—by extension—its reactivity with DNA. More sophisticated efforts to modulate the reactivity of the mustard while increasing specificity for tumors followed after the inception of perhaps the most iconic nitrogen mustard pro-drug, cyclophosphamide. Cyclophosphamide is a DNA cross-linking agent that exhibits selectivity for cancer cells over rapidly proliferating cells such as the bone marrow by exploiting differences in aldehyde dehydrogenase (ALDH) expression to yield a narrow but sufficient therapeutic window to impart its therapeutic effects (171). The mechanism of bioactivation begins with hydroxylation of the carbon alpha to the amine by cytochrome P450 in the liver to generate the carbinolamine. The instability of this pseudo-enol renders its hydrolysis and subsequent tautomerization to the aldophosphamide species. Because many cancer cells exhibit diminished expression of ALDH1A1 (172–175) they are unable to oxidize the free aldehyde to the

corresponding carboxylate. In normal tissue and especially stem cells, high expression of ALDH1A1 (172) (and consequent conversion to the anionic carboxylate prevents effectively nullifies the acidity of the proton on the alpha carbon, thereby preventing beta-elimination (which is favored in a Lewis basic environment which may also be favored in cancer cells) and subsequent trapping of the phosphoramidate mustard in cells. In contrast, this oxidation of the free aldehyde is diminished in cancer cells due to downregulated ALDH. Trapping of the aldophosphoramidate mustard and beta-elimination to yield active nitrogen mustard are thus sufficiently cancer-specific to yield a narrow therapeutic window between prolific normal and cancerous tissue. Sufficient target-specific killing is contingent upon loss of ALDH expression in cancer, allowing activation, but retention of ALDH in stem cells, yielding protection (173). Contrary to the non-specific characteristic of rapid rates of proliferation, lowered ALDH expression is an attribute specific to cancer cells. This leaves many rapidly proliferating, non-malignant cells unperturbed. Cells expressing high levels of ALDH, such as bone marrow-derived stem cells and skin cells, are able to detoxify the aldophosphoramidate intermediate into the inactive carboxylate-cyclophosphamide species (58, 59).

7.3.1 Case Study 3: Sofosbuvir is an orally administered McGuigan prodrug for the treatment of HCV.

As introduced in *Section 1.5*, SOF is an iconic, orally administered prodrug nucleotide analogue of the McGuigan class that is FDA-approved for the treatment of HCV (42). The active NTP of SOF is a UTP analogue; the nucleoside of SOF is a uracil analogue. While the active nucleoside triphosphate (NTP) is a somewhat potent inhibitor of the NS5B polymerase, with a K_i of 0.42 ± 0.04 μM (14, 60, 61), the nucleoside of sofosbuvir (RO2433, uridine analogue) is inefficiently phosphorylated by intracellular nucleoside kinases (deoxycytidine kinase dCK, uridine kinase UCK, or thymidine kinase TK) to the corresponding monophosphate (**Figure 9**) (61). As described in *Section 1.2.2*, McGuigan prodrugs such as SOF are bioactivated through CES1/CTSA and HINT1, which are highly expressed in the liver (**Figure 9**). Because SOF is administered orally and must go through first pass metabolism through the liver, there is high hepatic extraction of intact SOF; its McGuigan promoieties are quickly removed and the resulting nucleoside monophosphate is trapped within hepatocytes (65). The monophosphate is then subject to phosphorylation by nucleotide kinases to the active triphosphate inhibitor; alternatively, it could

be dephosphorylated to the inactive nucleoside (RO2433), which can diffuse out of the cell and into circulation (33, 34, 88). Inactivation of the intact prodrug to the parent nucleoside RO2433 is essentially innocuous to visceral organs for two reasons: 1.) the majority of SOF undergoes rapid hepatic extraction (65, 88) and 2.) the parent nucleoside is very inefficiently metabolized to the corresponding monophosphate (14, 60) For a liver-specific pathology such as HCV, this paradigm is ideal as any remaining release of RO2433 is essentially innocuous due to its inability to be efficiently converted to the bioactive NTP in visceral organs.

CHAPTER 6. GS-441524 IS THE PARENT NUCLEOSIDE OF REMDESIVIR WITH MORE FAVORABLE PHARMACOKINETIC PROPERTIES FOR COVID-19 TREATMENT

A foil to sofosbuvir

Part of this chapter has been published in (permission granted)

Yan VC, Muller FL. 2020. Advantages of the Parent Nucleoside GS-441524 over Remdesivir for Covid-19 Treatment. ACS Med Chem Lett 11:1361–1366.

Yan VC, Muller FL. 2020. Captisol and GS-704277, but not GS-441524, are credible mediators of remdesivir's nephrotoxicity. Antimicrob Agents Chemother 64:01920–1920.

8.1 Abstract

While RDV has garnered much hope for its moderate anti-COVID-19 effects, its parent nucleoside, GS-441524, has been overlooked. Pharmacokinetics analysis of RDV evidences premature serum hydrolysis to GS-441524 (41, 67, 85); GS-441524 is the predominant metabolite in circulation, following IV administration of RDV. In contrast to RDV, which is a McGuigan prodrug (*Section 1.2.2*) that is preferentially bioactivated in tissues such as the liver, GS-441524 is activated by enzymes that are broadly expressed in all tissue types and exhibits an excellent safety profile (66, 89, 92, 176, 177). Given the pneumocyte-centric nature of COVID-19, we contend that GS-441524 is superior to RDV due to its synthetic simplicity (35, 66, 73), *in vivo* safety and efficacy, and ability to be administered orally.

8.2 Hypothesis

In contrast to RDV, GS-441524 is bioconverted by enzymes that are broadly expressed across cell- and tissue-types in the body, including the pneumocytes. Thus, direct administration of GS-441524 would be more effective than RDV due to its safety and distribution profile *in vivo*.

8.3 Introduction

RDV has been FDA-approved for the treatment of COVID-19 (38) on the basis of one NIH/NIAID-sponsored placebo controlled, randomized control trial (RCT; ACTT-1 Trial) demonstrating a reduction in average hospitalization time from 15 days to 11 days in patients with

severe COVID-19 (178). However, preliminary results from a larger RCT (not placebo-controlled) conducted by the WHO (Solidarity Trial) have thus far not found a significant difference in mortality between patients treated with RDV versus local standard-of-care (SOC) (179); it should be noted that the primary endpoints of ACTT-1 and Solidarity are different. Nonetheless, these preliminary results from the Solidarity Trial have caused many to question the efficacy of RDV (180). These issues have been exacerbated by RDV's obligatory IV administration requiring an inpatient setting (38), inability to be dosed higher due to liver and kidney-related DLTs (181, 182), and difficult synthesis (35, 77, 183)—all of which hamper its broad translational applicability.

We recently described in a general audience publication the advantages that the parent nucleoside of RDV, GS-441524, has over remdesivir itself for the treatment of COVID-19 (90). Investigation into the metabolism of remdesivir evidences premature serum hydrolysis of its phosphate prodrug, followed by dephosphorylation. As a result, the major metabolite circulating in the bloodstream is the parent nucleoside, GS-441524, even though RDV (monophosphoramidate prodrug) was the species initially administered. Accounting for this broader pharmacokinetic (PK) rationale, we herein provide a detailed analysis of the literature that supports the use of GS-441524 over remdesivir for the treatment of COVID-19.

8.4 Results and Discussion

8.4.1 The phosphate prodrug on remdesivir is not intended for pneumocyte-specific delivery.

Remdesivir is a structural analogue of adenosine monophosphate (AMP) that interferes with the SARS-CoV-2 RNA-dependent RNA polymerase (RdRp) (78). The anionic phosphate moiety on remdesivir is masked by McGuigan prodrug moieties (117), (phenol and L-alaninate ethylbutyl ester, *Section 1.2.2*) to enhance cell permeability. In principle, these prodrug moieties would be removed intracellularly—first by esterases (cathepsin A/carboxylesterase 1) and then by phosphoramidases (HINT1) (32) to release the monophosphorylated nucleotide. This would then be phosphorylated twice to give the active NTP (32, 78) (**Figure 26**), which is substrate-competitive with ATP for incorporation by viral RdRp and inhibition of viral RNA synthesis via chain termination at the i+3 position (78) or via template-dependent inhibition (79). The McGuigan phosphate prodrug was partly developed to overcome the perceived rate-limiting first

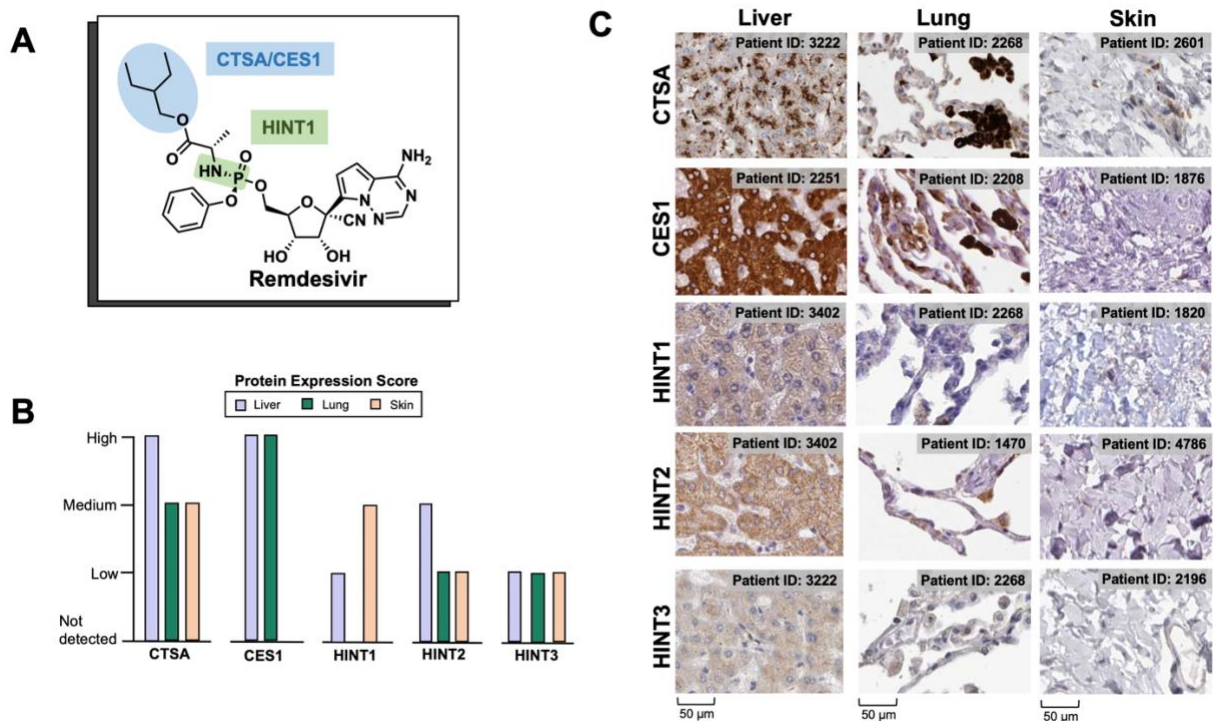


Figure 28. McGuigan prodrugs on remdesivir are preferentially bioactivated in the liver. (A) Labile prodrug moieties on remdesivir with corresponding bioactivation enzymes. (B) Relative tissue mRNA expression of initial prodrug bioactivating enzymes for RDV (CES1/CTSA/HINT1) adapted from the HPA dataset on the Human Protein Atlas reported as median-centered protein-coding transcripts per million (pTPM). Overall, McGuigan prodrug bioactivating enzymes are more highly expressed in the liver than in the lungs. (C) Immunohistochemistry (IHC) images from the Human Protein Atlas indicating expression for ProTide bioactivating enzymes. Brown regions indicate enzyme expression while blue regions indicate absent expression. For the lung, pneumocytes—cells frequently infected by COVID-19—are characterized by a threadlike appearance. Expression in the liver is generally higher compared to lung for all enzymes. For CTSA, darkly stained regions are associated with macrophages. IHC images for the skin are included to show lack of enzyme expression.

phosphorylation step towards the active tri-phosphorylated species (184). Bioactivation of the prodrug first involves CSE1 and CTSA, followed by HINT1 (**Figure 10**) (32, 131, 185). Protein expression data from the Human Protein Atlas show that these enzymes (CES1, CTSA, HINT1-3) all have high expression in the liver, with minimal expression in alveolar type 2 (AT2) in the lung (186) (**Figure 26**). For the HINT family of phosphoramidases, there is some slight variation in each isoform's tissue-specific expression (**Figure 26b, c**); however, all 3 isoforms show high expression in the GI tract, liver, and kidneys. From the pattern of bioactivation for McGuigan prodrugs, it follows that the most significant accumulation active NTP will be in cell types with high expression of CES1/CTSA/HINT1-3, such as the liver. Preferential bioactivation of

McGuigan prodrugs such as remdesivir could explain the Grade 3/4 adverse events related to liver and kidney damage in COVID-19 patients treated with remdesivir (187) and grade 2 elevations of ALT/AST in healthy human volunteers treated with 150 mg of RDV daily for 7 or 14 days (41). Seeing that the enzymes involved in McGuigan prodrug hydrolysis are hardly expressed in the lungs undermines its utility in the context of a primarily respiratory disease such as COVID-19.

8.4.2 GS-441524 is the predominant metabolite in the bloodstream when remdesivir is administered IV.

Hydrolytic enzymes are ubiquitous in serum (188). This is one physiological factor that, especially for prodrugs (189), prevents direct extrapolation of bioactivation mechanisms observed *in vitro* to the *in vivo* setting. For example, esterases and phosphatases are abundantly present in serum across species (30, 190). Premature serum hydrolysis of the McGuigan prodrug on RDV is thus unsurprising (**Figure 10b**). Multiple studies have demonstrated that the nucleoside, GS-441524, is the predominant species in serum after RDV is administered (**Figure 10b, c**) (39, 40, 82). All studies that have investigated the PK of RDV in non-human primates (NHP) have concluded that intact RDV exhibits a short plasma half-life of about 0.4 hours in serum, with “persistence” of the downstream nucleoside, GS-441524 (**Figure 10c**) (40, 82). IV injection of remdesivir in NHP results in GS-441524 being present in serum at concentrations 1,000-fold higher than RDV throughout a 7-day treatment course (40) (**Figure 10b**). This recurring phenomenon can first be explained by the abundance of plasma esterases, as the phosphoramidases (HINT1) involved in removal of the L-alanine have a strictly intracellular presence (see Human Protein Atlas HINT1). Inadvertent biotransformation of remdesivir to GS-441524 can be explained by the following sequence: 1.) esterase removal of the L-alaninate ester, 2.) intramolecular cyclization, displacement of the phenolate, followed by re-opening of the ring, 3.) cleavage of the phosphate ester by serum phosphatases or nucleosidases (**Figure 10b**). The proposed serum bioactivation mechanism accounts for the general substrate constraints for each class of enzyme. For instance, CES1 is named as one of the enzymes involved in McGuigan prodrug hydrolysis (32, 33). However, this does not preclude other esterases from acting on its L-alaninate ester. A study conducted by Sheahan and colleagues specifically investigated the PK of remdesivir in carboxylesterase 1c deficient mice (*Ces1c*^{-/-}) (39). Even in this *Ces1c*^{-/-} model, the half-life of remdesivir was still short ($T_{1/2}$ ~25 minutes), supporting the notion that other esterases are capable

of performing the initial hydrolysis reaction. Thus, the abundance of hydrolytic enzymes in serum explains the persistent, multi-species observation that GS-441524 is the predominant metabolite when remdesivir is administered (39, 40, 82). For the fleeting duration of time that remdesivir is in the blood (prior to hydrolysis to GS-441524), the expression of bioactivating enzymes for McGuigan prodrugs suggests that the highest concentrations of NTP formation by remdesivir—rather than GS-441524—would occur in cell types with high expression of CES1/CTSA/HINT1. This largely favors the liver over the lungs (**Figure 28**). Differential expression of prodrug bioactivating enzymes likely explains the wide range of EC₅₀ values with remdesivir *in vitro* (75, 84, 191). A study investigating the PK and tissue distribution of RDV following IV injection in mice (20 mg/kg) found that the AUC_{0-t} of RDV was approximately 5-fold higher in the liver compared to the lungs, AUC_{0-t} (last observable timepoint) of the monophosphate was approximately 1,000-fold higher in the liver compared to lungs, and that the AUC_{0-t} of the active NTP was approximately 1.6-fold higher in liver compared to lungs (192). At first glance, it may seem that formation of active NTP is only slightly higher in the liver compared to lungs; however, it is important to consider that the AUC values were taken from T=0 to the last timepoint when the species of interest was detected. GS-443902 (active NTP) has an intracellular T_{1/2} of over 35 h in peripheral blood mononuclear cells (PBMCs) (193) and over 7 days in RBCs (Peter Anderson, CU Boulder, personal correspondence). Considering that the T_{1/2} of GS-441524 is >24 h following IV injection of RDV (41, 85) and that GS-441524 is capable of being converted to GS-443902 (81, 84, 92), the narrower gap between the concentration of active NTP in the liver versus lungs can likely be explained by the formation of active NTP by GS-441524 in the lungs.

Finally, due to the exceedingly short T_{1/2} of RDV, the influence of duration of drug exposure to the cell and tissue-types of interest is poorly modeled in cell culture-based experiments. In stark contrast to the < 1 h systemic exposure to RDV *in vivo*, cells in culture are typically subjected to 48-72 h of continuous drug exposure (35, 75, 81, 84). A key experiment conducted by Wang and colleagues inadvertently revealed the significance of duration of RDV drug exposure *in vitro* through pulsed (2 h treatment with drug-containing media, then replace with fresh media and incubate for 48 h) versus continuous treatment (drug-containing media for 48 h) in VeroE6 cells infected with SARS-CoV-2 (194). Wang and colleagues showed that, in contrast to cells continuously exposed to drug media where RDV showed inhibition of viral replication, no

inhibition of viral replication was observed in cells given pulsed treatment (194). These results demonstrate the shortcomings of traditional cell culture experimental approaches when attempting to extrapolate efficacy to the *in vivo* situation with phosph(on)ate prodrugs.

8.4.3 GS-441524 is exceptionally effective and well-tolerated against clinical presentations of feline coronavirus.

There are currently no published studies that have compared the antiviral activities of remdesivir and GS-441524 *in vivo* (see *Section 8.4.4*), with most focusing exclusively on remdesivir. Where GS-441524 has been investigated *in vivo* is in the veterinary setting (176, 177, 195). Cats infected with feline coronavirus (FCoV) present with a serious disease known as feline infectious peritonitis (FIP). While long considered fatal in its severe manifestations (196), a study conducted by Pedersen and colleagues showed that GS-441524 is capable of treating cats suffering from FIP with a 96% cure rate (176). Pedersen noted the “impressive” safety profile of GS-441524, with no systemic signs of toxicity observed when administered subcutaneously at 4 mg/kg (176). In a more recent study, Pedersen and colleagues escalated the dose of GS-441524 (5-10 mg/kg) to treat neurological manifestations of FIP; without accounting for species differences in drug absorption this translates to about 350-700 mg in a 70 kg human, greatly exceeding the dose currently given to patients treated with RDV (200 mg loading, then 100 mg) (187, 197). Even at these higher doses, they found that GS-441524 treatment resulted in the long-term resolution of neurological FIP with an excellent safety profile: minimal dose-related toxicities were observed (177).

8.4.4 GS-441524 and remdesivir are equally capable of reducing viral titers in the lungs in pre-clinical models of SARS-CoV-2.

Gilead Sciences has shared data with us from a head-to-head comparison study between GS-441524 and RDV in non-human primates (NHP; African green monkeys) infected with SARS-CoV-2. NHP were treated IV with either RDV (10 mg/kg loading, then 5 mg/kg daily maintenance), GS-441524 (7.5 mg/kg) or GS-441524 (20 mg/kg) for 6 days (N=6 per group). NHP were sacrificed for PD examination in the lungs at 24 h and bronchial alveolar lavage (BAL) was performed daily to measure viral titers in the upper airway by qPCR. GS-441524 at 20 mg/kg and RDV were essentially equal in their abilities to reduce viral titers over 5 days. When administered at 7.5 mg/kg/day, GS-441524 was less effective than RDV but was still able to reduce the viral

titers to similar levels as RDV in 3/6 of the NHP (compared to 2/6 in untreated CT). No gross observations were observed in any group. Another study by Li and colleagues examined the efficacy of GS-441524 in mice transduced with an adenovirus associated virus (AAV) expressing hACE2 and infected with SARS-CoV-2 (92); this is because mice are not susceptible to infection via mouse ACE2. AAV-hACE2 mice administered 25 mg/kg/8 days GS-441524 IP demonstrated 100-fold reduction in viral titers at 2 days post infection (dpi) and maintained body weight compared to untreated controls, highlighting its antiviral efficacy and safety. Both studies provide *in vivo* proof-of-principle of the safety and efficacy of GS-441524 against SARS-CoV-2 *in vivo*.

Due to species differences in drug metabolism and absorption, Gilead had informed us that the routinely used dosing schedule with RDV in NHP (10 mg/kg loading, then 5 mg/kg maintenance) approximately translates to the recommended clinical dose in humans (200 mg loading, then 100 mg maintenance) (38). This is particularly intriguing because direct translation of the NHP dose in a 70 kg human would result in a 700 mg loading, then 350 mg maintenance, which is evidently prohibitive due to liver DLTs that have already been observed at repeated doses of 150 mg in healthy human volunteers (41). We suspect that NHPs are capable of tolerating such a dose due to reduced hepatic extraction of McGuigan prodrugs compared to that observed in humans; this is because a 15-day study with RDV at 10 mg/kg (starting 3 dpi) did not result in elevations in ALT/AST (67). PK analysis of RDV following rapid bolus injection in NHP also demonstrates shows a slightly longer $T_{1/2}$ in of the intermediate L-Ala metabolite (GS-704277) in plasma (67). This species difference in drug metabolism between NHP and humans is important because it likely explains the inability to dose RDV higher in humans, even with its questionable efficacy, due to liver-related DLTs (41). Inability to dose higher results in the inability to increase concentrations of both RDV and GS-441524—both of which are able to form active NTP (84). The significance of increasing the concentration of GS-441524 has been alluded to in the cases studies where patients with end-stage renal disease (ESRD) have been treated with RDV (86). To offset the recommendation against using RDV in patients with severe kidney disease, Davis and colleagues also performed hemodialysis on the 3 patients treated with RDV. All 3 patients receiving RDV treatment also had other co-morbidities, such as hypertension and diabetes. While the results from this study should be interpreted cautiously, it is interesting to note that, because GS-441524 is renally excreted, these 3 patients with ESRD had C_{max} concentrations of GS-441524

in plasma between 5-10-fold higher than that reported in healthy human volunteers (86). Patient 3 achieved a 5 μ M C_{\max} value of GS-441524 in plasma by day 5 of treatment, which is likely due to accumulation of GS-441524 in plasma. Notably, all 3 patients successfully recovered even while being part of populations with high morbidity rates (198). Again, such results are observational but do warrant further investigations into increasing concentrations of active NTP in the lungs/pneumocytes; this is possible with GS-441524 due to its safety profile (89, 176, 177), but not with RDV because, again, it is hepatotoxic at higher doses (41).

8.4.5 GS-441524 has the potential to be administered orally

McGuigan prodrugs such SOF can be administered orally because the promoieties are intended to be rapidly removed in the liver in the context of HCV; however, this is not the case for RDV and COVID-19, in which RDV is supposed to facilitate the delivery of active NTP to the lungs (AT2 cells). High hepatic extraction of RDV by human hepatocytes (38, 41, 184) would result in negligible amount of intact RDV that would survive first-pass metabolism to reach the target cell population. As a result, oral administration of RDV is not feasible. In sharp contrast, GS-441524 is not susceptible to first-pass metabolism and hepatic extraction, making it amenable to oral administration.

On August 20, 2020, we wrote and co-signed a letter with Public Citizen addressed to Drs. Francis Collins (NIH Director), Anthony Fauci (NIH/NIAID), Stephen Hahn (FDA), Gary Disbrow (BARDA), and Daniel O'Day (CEO, Gilead Sciences) to urge further investigation of GS-441524. In response, Dr. Christopher Austin (Director, NCATS) wrote that NCATS finds the hypothesis worthy of further investigation and that NCATS will conduct the necessary studies to support clinical investigation of GS-441524 (199). As of December 11, NCATS has thus far performed single dose safety and toxicity studies in mice, rats, dogs, and cynomolgus monkeys with GS-441524 both IV and PO (**Table 3**). Range finding studies and confirmatory GLP toxicity studies are currently ongoing (NCATS OpenData Portal).

It is striking to note the large variation in F% across preclinical species (**Table 3**). While GS-441524 exhibits high oral bioavailability in dogs (85%), the oral bioavailability is significantly lower in NHP (8.3%). These results are consistent with those later shared with us by Gilead (private

communication). Systematic comparison of the oral bioavailabilities of various nucleoside analogues generally show that dogs tend to overestimate whereas NHP tend to underestimate F% in humans (200). High F% in dogs can likely be attributed to the presence of a paracellular nucleoside transporter that is absent in other species such as humans and NHP (201). Low F% in NHP may be explained by the tendency for gastrointestinal (GI) pH in NHP to be in the neutral/slightly alkaline range for longer durations after food consumption compared to in humans (202, 203). This key difference between NHP and humans, coupled with the absence of a paracellular nucleoside transporter in NHP, could explain the general observation that NHP tend to underpredict the F% of nucleoside analogues and other drugs in humans (204). Considerations of GI pH in the context of species differences in drug absorption are particularly important for GS-441524 due to its odd solubility properties. While GS-441524 is considerably more hydrophilic than RDV, it is only soluble in water at acidic pH (pH < 1.5-2). At the same time, GS-441524 is poorly soluble in most organic solvents, somewhat soluble in DMF and NMP (~2 mg/mL) and readily soluble in DMSO. These rather odd solubility properties make considerations of species differences in GI pH particularly important when evaluating the F% of GS-441524 in preclinical species. Interestingly, the F% of GS-441524 are quite similar to the F% of acyclovir (**Table 3 vs. Table 4**). These data collectively indicate that, while the oral bioavailability of GS-441524 is unlikely to be as high as that observed in dogs, it will likely be higher than that projected by NHP.

Species	GS-441524 IV*				GS-441524 PO**				
	C _{max} (ng/mL)	T _{max} (h)	AUC (ng*h/mL)	T _{1/2} (h)	C _{max} (ng/mL)	T _{max} (h)	AUC (ng*h/mL)	T _{1/2} (h)	F (%)
Mouse	4340	0.083	2540	3.3	582	1.5	2540	3.9	39
Rat	2703	0.083	2888	2.7	193	3.8	2170	3.4	33
Dog	4567	0.083	7588	4.0	6010	0.28	8320	4.1	85
Cynomolgus monkey	4597	0.083	2775	2.4	59.3	2.0	734	7.7	8.3

Table 3. Oral bioavailability of GS-441524 and acyclovir across species. Single dose PK of GS-441524 in preclinical species. Studies were conducted by NCATS. *IV doses: 5 mg/kg for mouse, rat; 2 mg/kg for dog, NHP. **PO doses: 10 mg/kg for mouse/rat; 5 mg/kg for dog, NHP.

Species differences in oral bioavailability of acyclovir		
Species	F%	Reference
Human	10-20	FDA (205)
Monkey	3.7	Laskin et al. Clin. Pharm. (1983) (206)
Dog	54-90	Kransy et al. J. Pharm. Exp. Ther. (1981) (207)

Table 4. Oral bioavailability acyclovir across species. Oral bioavailability of acyclovir in preclinical species is similar to that for GS-441524.

8.5 Conclusions

While RDV has demonstrated some efficacy in patients with advanced COVID-19 (187), its phosphate prodrug is fundamentally not designed for lung-specific delivery. Enzymes that activate the McGuigan prodrug are preferentially expressed in tissues such as the liver (*Section 1.2.2*), which results in uneven distribution of active NTP formation via remdesivir that disfavors the pneumocytes. Practically, the structural complexity of the McGuigan prodrug (208) adds unnecessary synthetic difficulty that hampers mass production and impedes distribution (209). Above all else, premature hydrolysis of the McGuigan prodrug, followed by dephosphorylation in serum such that GS-441524 is the predominant metabolite (39, 40, 82) compels studies investigating its utility in patients with COVID-19. In contrast to the prodrug activating enzymes that activate RDV, bioactivation of GS-441524 relies on expression of the kinase responsible for initial phosphorylation (likely adenosine kinase, ADK). According to the Human Protein Atlas, ADK is moderately expressed across all tissues, suggesting that administration of GS-441524 would result in even distribution across tissues. The remarkable safety profile of GS-441524, indicated by selectivity indices *in vitro* (EC_{50}/CC_{50} ratio) (35, 66, 75) and by clinical observations in cats (176, 177, 195), suggest that higher dosing and pneumocyte NTP loading could be achieved with GS-441524 without encountering serious adverse effects. GS-441524 is also a structurally simple molecule that is easier to synthesize compared to RDV (35), which would ease mass production and distribution. Especially amidst the documented premature serum hydrolysis of remdesivir to GS-441524 (39, 40, 82), there are several advantages to using GS-441524 over remdesivir for patients with COVID-19. Further investigations into the anti-COVID-19 utility of GS-441524 are thus ongoing and imperative.

8.6 Experimental

Tissue dependent expression of RDV bioactivating expression. Lung, liver, and skin (negative CT) stained for CES1, CTSA, and HINT1-3 were compiled from the Human Protein Atlas; Patient IDs are indicated in Figure 26. Antibodies used: CTSA (CAB024930), CES1 (HPA046717), HINT1 (HPA044577).

Single dose IV and PO PK of GS-441524. Studies were conducted by NIH/NCATS and made publicly available through the NCATS OpenData Portal

REFERENCES

1. Westheimer FH. 1992. The Role of Phosphorus in Chemistry and Biochemistry: An Overview. American Chemical Society (ACS).
2. Chu MY, Zuckerman LB, Sato S, Crabtree GW, Bogden AE, Lim MI, Klein RS. 1984. 9-Deazaadenosine-A new potent antitumor agent. *Biochem Pharmacol* 33:1229–1234.
3. Vander Heiden MG. 2011. Targeting cancer metabolism: A therapeutic window opens. *Nat Rev Drug Discov* 10:671–684.
4. Muller FL, Colla S, Aquilanti E, Manzo VE, Genovese G, Lee J, Eisenson D, Narurkar R, Deng P, Nezi L, Lee MA, Hu B, Hu J, Sahin E, Ong D, Fletcher-Sananikone E, Ho D, Kwong L, Brennan C, Wang YA, Chin L, Depinho RA. 2012. Passenger deletions generate therapeutic vulnerabilities in cancer. *Nature* 488:337–343.
5. Muller FL, Aquilanti EA, DePinho RA. 2015. Collateral Lethality: A New Therapeutic Strategy in Oncology. *Trends in Cancer* 1:161–173.
6. Leonard PG, Satani N, Maxwell D, Lin Y-H, Hammoudi N, Peng Z, Pisaneschi F, Link TM, Lee GR, Sun D, Prasad BAB, Di Francesco ME, Czako B, Asara JM, Wang YA, Bornmann W, DePinho RA, Muller FL. 2016. SF2312 is a natural phosphonate inhibitor of enolase. *Nat Chem Biol* 12:1053–1058.
7. Boulard-Heitzmann P, Boulard M, Tallineau C, Boivin P, Tanzer J, Bois M, Barriere M. 1984. Decreased red cell enolase activity in a 40-year-old woman with compensated haemolysis. *Scand J Haematol* 33:401–404.
8. Stefanini M. 1972. Chronic Hemolytic Anemia Associated with Erythrocyte Enolase Deficiency Exacerbated by Ingestion of Nitrofurantoin. *Am J Clin Pathol* 58:408–414.
9. Rautio J, Meanwell NA, Di L, Hageman MJ. 2018. The expanding role of prodrugs in contemporary drug design and development. *Nat Rev Drug Discov* 17:559–587.
10. Farquhar D, Srivastva DN, Kuttisch NJ, Saunders PP. 1983. Biologically reversible phosphate-protective groups. *J Pharm Sci* 72:324–325.
11. Mehellou Y, Rattan HS, Balzarini J. 2018. The ProTide Prodrug Technology: From the Concept to the Clinic. *J Med Chem* 61:2211–2226.
12. Meier C. 1998. Pro-nucleotides - Recent advances in the design of efficient tools for the delivery of biologically active nucleoside monophosphates. *Synlett* 233–242.
13. Deeks SG, Barditch-Crovo P, Lietman PS, Hwang F, Cundy KC, Rooney JF, Hellmann

- NS, Safrin S, Kahn JO. 1998. Safety, pharmacokinetics, and antiretroviral activity of intravenous 9- [2-(R)-(phosphonomethoxy)propyl]adenine, a novel anti-human immunodeficiency virus (HIV) therapy, in HIV-infected adults. *Antimicrob Agents Chemother* 42:2380–2384.
14. Ma H, Jiang WR, Robledo N, Leveque V, Ali S, Lara-Jaime T, Masjedizadeh M, Smith DB, Cammack N, Klumpp K, Symons J. 2007. Characterization of the metabolic activation of hepatitis C virus nucleoside inhibitor β -D-2'-deoxy-2'-fluoro-2'-C-methylcytidine (PSI-6130) and identification of a novel active 5'-triphosphate species. *J Biol Chem* 282:29812–29820.
 15. Borch RF, Liu J, Schmidt JP, Marakovits JT, Joswig C, Gipp JJ, Mulcahy RT. 2000. Synthesis and Evaluation of Nitroheterocyclic Phosphoramidates as Hypoxia-Selective Alkylating Agents. *J Med Chem* 43:2258–2265.
 16. Pradere U, Garnier-Amblard EC, Coats SJ, Amblard F, Schinazi RF. 2014. Synthesis of Nucleoside Phosphate and Phosphonate Prodrugs. *Chem Rev* 114:9154–9218.
 17. Yan VC, Muller FL. 2020. Advantages of the Parent Nucleoside GS-441524 over Remdesivir for Covid-19 Treatment. *ACS Med Chem Lett* 11:1361–1366.
 18. Schooley RT, Carlin AF, Beadle JR, Valiaeva N, Garretson AF, Smith VI, Murphy J, Hostetler KY. 2020. Rethinking Remdesivir: Synthesis of Lipid Prodrugs that Substantially Enhance Anti-Coronavirus Activity. *bioRxiv* 2020.08.26.269159.
 19. Périgaud C, Gosselin G, Lefebvre I, Girardet JL, Benzaria S, Barber I, Imbach JL. 1993. Rational design for cytosolic delivery of nucleoside monophosphates : “SATE” and “DTE” as enzyme-labile transient phosphate protecting groups. *Bioorganic Med Chem Lett* 3:2521–2526.
 20. Farquhar D, Khan S, Srivastva DN, Saunders PP. 1994. Synthesis and Antitumor Evaluation of Bis[(pivaloyloxy)methyl] 2'-Deoxy-5-fluorouridine 5'-Monophosphate (FdUMP): A Strategy To Introduce Nucleotides into Cells. *J Med Chem* 37:3902–3909.
 21. Annaert P, Kinget R, Naesens L, De Clercq E, Augustijns P. 1997. Transport, uptake, and metabolism of the bis(pivaloyloxymethyl)-ester prodrug of 9-(2-phosphonylmethoxyethyl)adenine in an in vitro cell culture system of the intestinal mucosa (Caco-2). *Pharm Res* 14:492–496.
 22. Benzaria S, Ne Pélicano H, Johnson R, Maury G, Imbach J-L, Aubertin A-M, Obert G,

- Gosselin G. 1996. Synthesis, in Vitro Antiviral Evaluation, and Stability Studies of Bis(S-acyl-2-thioethyl) Ester Derivatives of 9-[2-(Phosphonomethoxy)ethyl]adenine (PMEA) as Potential PMEA Prodrugs with Improved Oral Bioavailability. *J Med Chem* 39:4958–4965.
23. Marcellin P, Chang T-T, Lim SG, Tong MJ, Sievert W, Shiffman ML, Jeffers L, Goodman Z, Wulfsohn MS, Xiong S, Fry J, Brosgart CL. 2003. Adefovir Dipivoxil for the Treatment of Hepatitis B e Antigen–Positive Chronic Hepatitis B. *N Engl J Med* 348:808–816.
 24. Bahar FG, Ohura K, Ogihara T, Imai T. 2012. Species Difference of Esterase Expression and Hydrolase Activity in Plasma. *J Pharm Sci* 101:3979–3988.
 25. Aririlli M, Kim C, Dougherty J, Mulato A, Shaw J, Cundy K, Bischofberger N. 1997. Synthesis, in vitro biological evaluation and oral bioavailability of 9-[2-(phosphonomethoxy)propyl]adenine (PMPA) prodrugs. *Antiviral Chemistry and Chemotherapy*.
 26. Naesens L, Balzarini J, Bischofberger N, De Clercq E. 1996. Antiretroviral Activity and Pharmacokinetics in Mice of Oral Bis(Pivaloyloxymethyl)-9-(2-Phosphonylmethoxyethyl)Adenine, the Bis(Pivaloyloxymethyl) Ester Prodrug of 9-(2-Phosphonylmethoxyethyl)Adenine. *Antimicrob Agents Chemother* 40:22–28.
 27. Food and Drug Administration. 2001. VIREAD® (tenofovir disoproxil fumarate).
 28. Food and Drug Administration. 2002. HEPSERA® (adefovir dipivoxil).
 29. Lin YH, Satani N, Hammoudi N, Yan VC, Barekatain Y, Khadka S, Ackroyd JJ, Georgiou DK, Pham CD, Arthur K, Maxwell D, Peng Z, Leonard PG, Czako B, Pisaneschi F, Mandal P, Sun Y, Zielinski R, Pando SC, Wang X, Tran T, Xu Q, Wu Q, Jiang Y, Kang Z, Asara JM, Priebe W, Bornmann W, Marszalek JR, DePinho RA, Muller FL. 2020. An enolase inhibitor for the targeted treatment of ENO1-deleted cancers. *Nat Metab* 2:1413–1426.
 30. Bahar FG, Ohura K, Ogihara T, Imai T. 2012. Species difference of esterase expression and hydrolase activity in plasma. *J Pharm Sci* 101:3979–88.
 31. McGuigan C, Pathirana RN, Mahmood N, Devine KG, Hay AJ, McGuigan C. 1992. Aryl phosphate derivatives of AZT retain activity against HIV1 in cell lines which are resistant to the action of AZT. *Antiviral Research*.

32. Murakami E, Wang T, Babusis D, Lepist E-I, Sauer D, Park Y, Vela JE, Shih R, Birkus G, Stefanidis D, Kim CU, Cho A, Ray AS. 2014. Metabolism and Pharmacokinetics of the Anti-Hepatitis C Virus Nucleotide Prodrug GS-6620. *Antimicrob Agents Chemother* 58:1943–1951.
33. Murakami E, Tolstykh T, Bao H, Niu C, Micolochick Steuer HM, Bao D, Chang W, Espiritu C, Bansal S, Lam AM, Otto MJ, Sofia MJ, Furman PA. 2010. Mechanism of activation of PSI-7851 and its diastereoisomer PSI-7977. *J Biol Chem* 285:34337–34347.
34. Sofia MJ, Bao D, Chang W, Du J, Nagarathnam D, Rachakonda S, Reddy PG, Ross BS, Wang P, Zhang HR, Bansal S, Espiritu C, Keilman M, Lam AM, Steuer HMM, Niu C, Otto MJ, Furman PA. 2010. Discovery of a fluoro-2'- β -C -methyluridine Nucleotide Prodrug (PSI-7977) for the treatment of hepatitis C virus. *J Med Chem* 53:7202–7218.
35. Siegel D, Hui HC, Doerffler E, Clarke MO, Chun K, Zhang L, Neville S, Carra E, Lew W, Ross B, Wang Q, Wolfe L, Jordan R, Soloveva V, Knox J, Perry J, Perron M, Stray KM, Barauskas O, Feng JY, Xu Y, Lee G, Rheingold AL, Ray AS, Bannister R, Strickley R, Swaminathan S, Lee WA, Bavari S, Cihlar T, Lo MK, Warren TK, Mackman RL. 2017. Discovery and Synthesis of a Phosphoramidate Prodrug of a Pyrrolo[2,1-*f*][triazin-4-amino] Adenine C -Nucleoside (GS-5734) for the Treatment of Ebola and Emerging Viruses. *J Med Chem* 60:1648–1661.
36. Keith KA, Hitchcock MJM, Lee WA, Holy', AH, Kern ER. 2003. Evaluation of Nucleoside Phosphonates and Their Analogs and Prodrugs for Inhibition of Orthopoxvirus Replication. *Antimicrob Agents Chemother* 47:2193–2198.
37. Mayer KH, Molina JM, Thompson MA, Anderson PL, Mounzer KC, De Wet JJ, DeJesus E, Jessen H, Grant RM, Ruane PJ, Wong P, Ebrahimi R, Zhong L, Mathias A, Callebaut C, Collins SE, Das M, McCallister S, Brainard DM, Brinson C, Clarke A, Coll P, Post FA, Hare CB. 2020. Emtricitabine and tenofovir alafenamide vs emtricitabine and tenofovir disoproxil fumarate for HIV pre-exposure prophylaxis (DISCOVER): primary results from a randomised, double-blind, multicentre, active-controlled, phase 3, non-inferiority trial. *Lancet* 396:239–254.
38. Food and Drug Administration. 2020. VEKLURY® (remdesivir).
39. Sheahan TP, Sims AC, Graham RL, Menachery VD, Gralinski LE, Case JB, Leist SR, Pyrc K, Feng JY, Trantcheva I, Bannister R, Park Y, Babusis D, Clarke MO, Mackman

- RL, Spahn JE, Palmiotti CA, Siegel D, Ray AS, Cihlar T, Jordan R, Denison MR, Baric RS. 2017. Broad-spectrum antiviral GS-5734 inhibits both epidemic and zoonotic coronaviruses. *Sci Transl Med* 9.
40. Williamson BN, Feldmann F, Schwarz B, Meade-White K, Porter DP, Schulz J, Van Doremalen N, Leighton I, Yinda CK, Pérez-Pérez L, Okumura A, Lovaglio J, Hanley PW, Saturday G, Bosio CM, Anzick S, Barbian K, Cihlar T, Martens C, Scott DP, Munster VJ, De Wit E. 2020. Clinical benefit of remdesivir in rhesus macaques infected with SARS-CoV-2. *Nature* <https://doi.org/10.1038/s41586-020>.
 41. Humeniuk R, Mathias A, Cao H, Osinusi A, Shen G, Chng E, Ling J, Vu A, German P. 2020. Safety, Tolerability, and Pharmacokinetics of Remdesivir, An Antiviral for Treatment of COVID-19, in Healthy Subjects. *Clin Transl Sci* cts.12840.
 42. Food and Drug Administration. 2013. SOVALDI® (sofosbuvir).
 43. Lee WA, He G-X, Eisenberg E, Cihlar T, Swaminathan S, Mulato A, Cundy KC. 2005. Selective Intracellular Activation of a Novel Prodrug of the Human Immunodeficiency Virus Reverse Transcriptase Inhibitor Tenofovir Leads to Preferential Distribution and Accumulation in Lymphatic Tissue. *Antimicrob Agents Chemother* 49:1898–1906.
 44. Food and Drug Administration. 2015. VEMLIDY® (tenofovir alafenamide).
 45. Yan VC, Butterfield HE, Poral AH, Yan MJ, Yang KL, Pham C-D, Muller FL. 2020. Why Great Mitotic Inhibitors Make Poor Cancer Drugs. *Trends in Cancer* 6:924–941.
 46. Coleman CN. 1988. Hypoxia in tumors: A paradigm for the approach to biochemical and physiologic heterogeneity. *J Natl Cancer Inst. Oxford Academic*.
 47. Yan VC, Yang KL, Ballato ES, Khadka S, Shrestha P, Arthur K, Georgiou DK, Washington M, Tran T, Poral AH, Pham C-D, Yan MJ, Muller FL. 2020. Bio reducible Phosphonoamidate Pro-drug Inhibitor of Enolase: Proof of Concept Study. *ACS Med Chem Lett* 11:1484–1489.
 48. Meier C. 1996. 2-Nucleos-5'-O-yl-4H-1,3,2-benzodioxaphos-phinin-2-oxides-A New Concept for Lipophilic, Potential Prodrugs of Biologically Active Nucleoside Monophosphate. *Angew Chemie Int Ed* 35:70–72.
 49. Peshavaria M, Day INM. 1991. Molecular structure of the human muscle-specific enolase gene (ENO3). *Biochem J* 275:427–433.
 50. Giallongo A, Venturella S, Oliva D, Barbieri G, Rubino P, Feo S. 1993. Structural

- features of the human gene for muscle-specific enolase: Differential splicing in the 5'-untranslated sequence generates two forms of mRNA. *Eur J Biochem.* *Eur J Biochem.*
51. Marangos PJ, Polak JM, Pearse AGE. 1982. Neuron-specific enolase. A probe for neurons and neuroendocrine cells. *Trends Neurosci.* Elsevier.
 52. Poyner RR, Reed GH. 1992. Structure of the Bis Divalent Cation Complex with Phosphonoacetoxyhydroxamate at the Active Site of Enolase. *Biochemistry* 31:7166–7173.
 53. Anderson VE, Weiss PM, Cleland WW. 1984. Reaction Intermediate Analogues for Enolase. *Biochemistry* 23:2779–2786.
 54. Sjövall J, Bergdahl S, Movin G, Ogenstad S, Saarimäki M. 1989. Pharmacokinetics of foscarnet and distribution to cerebrospinal fluid after intravenous infusion in patients with human immunodeficiency virus infection. *Antimicrob Agents Chemother* 33:1023–1031.
 55. Pérez DS, Tapia MO, Soraci AL. 2014. Fosfomycin: Uses and potentialities in veterinary medicine. *Open Vet J* 4:26–43.
 56. Food and Drug Administration. 1959. CYCLOPHOSPHAMIDE Food and Drug Administration.
 57. Mounier N, Briere J, Gisselbrecht C, Emile JF, Lederlin P, Sebban C, Berger F, Bosly A, Morel P, Tilly H, Bouabdallah R, Reyes F, Gaulard P, Coiffier B. 2003. Rituximab plus CHOP (R-CHOP) overcomes bcl-2-associated resistance to chemotherapy in elderly patients with diffuse large B-cell lymphoma (DLBCL). *Blood* 101:4279–4284.
 58. Jones RJ, Barber JP, Vala MS, Collector MI, Kaufmann SH, Ludeman SM, Colvin OM, Hilton J. 1995. Assessment of aldehyde dehydrogenase in viable cells. *Blood* 85:2742–2746.
 59. Kastan MB, Schlaffer E, Russo JE, Colvin OM, Civin CI, Hilton J. 1990. Direct demonstration of elevated aldehyde dehydrogenase in human hematopoietic progenitor cells. *Blood* 75:1947–1950.
 60. Murakami E, Niu C, Bao H, Micolochick Steuer HM, Whitaker T, Nachman T, Sofia MA, Wang P, Otto MJ, Furman PA. 2008. The mechanism of action of β -D-2'-deoxy-2'-fluoro-2'-C-methylcytidine involves a second metabolic pathway leading to β -D-2'-deoxy-2'-fluoro-2'-C-methyluridine 5'-triphosphate, a potent inhibitor of the hepatitis C virus RNA-dependent RNA polymerase. *Antimicrob Agents Chemother* 52:458–464.
 61. Murakami E, Bao H, Ramesh M, McBrayer TR, Whitaker T, Steuer HMM, Schinazi RF,

- Stuyver LJ, Obikhod A, Otto MJ, Furman PA. 2007. Mechanism of activation of β -D-2'-Deoxy-2'-fluoro-2'-C-methylcytidine and inhibition of hepatitis C virus NS5B RNA polymerase. *Antimicrob Agents Chemother* 51:503–509.
62. Perrone P, Daverio F, Valente R, Rajyaguru S, Martin JA, L  v  que V, Le Pogam S, Najera I, Klumpp K, Smith DB, Mcguigan C. 2007. First Example of Phosphoramidate Approach Applied to a 4'-Substituted Purine Nucleoside (4'-Azidoadenosine): Conversion of an Inactive Nucleoside to a Submicromolar Compound versus Hepatitis C Virus. *J Med Chem* 50.
 63. Lawitz E, Hill J, Marbury T, Hazan D, Gruener D, Webster L, Majauskas R, Morrison R, DeMicco M, German P, Stefanidis D, Svaroskaia E, Arterburn S, Ray A, Rossi S, McHutchinson J, Rodriguez-Torres M. 2012. GS-6620, A Liver-Targeted Nucleotide Prodrug, Exhibits Antiviral Activity and Favorable Safety Profile Over 5 Days in Treatment Na  ve Chronic HCV Genotype 1 SubjectsEASL 47th Annual Meeting. EASL 47th Annual Meeting, Barcelona.
 64. Afdhal N, Zeuzem S, Kwo P, Chojkier M, Gitlin N, Puoti M, Romero-Gomez M, Zarski J-P, Agarwal K, Buggisch P, Foster GR, Br  u N, Buti M, Jacobson IM, Subramanian GM, Ding X, Mo H, Yang JC, Pang PS, Symonds WT, McHutchison JG, Muir AJ, Mangia A, Marcellin P. 2014. Ledipasvir and Sofosbuvir for Untreated HCV Genotype 1 Infection. *N Engl J Med* 370:1889–1898.
 65. Wang T, Babusis D, Park Y, Niu C, Kim C, Zhao X, Lu B, Ma B, Muench RC, Sperger D, Ray AS, Murakami E. 2020. Species differences in liver accumulation and metabolism of nucleotide prodrug sofosbuvir. *Drug Metab Pharmacokinet* 35:334–340.
 66. Cho A, Saunders OL, Butler T, Zhang L, Xu J, Vela JE, Feng JY, Ray AS, Kim CU. 2012. Synthesis and antiviral activity of a series of 1'-substituted 4-aza-7,9-didezaadenosine C-nucleosides. *Bioorg Med Chem Lett* 22:2705–2707.
 67. Warren TK, Jordan R, Lo MK, Ray AS, Mackman RL, Soloveva V, Siegel D, Perron M, Bannister R, Hui HC, Larson N, Strickley R, Wells J, Stuthman KS, Van Tongeren SA, Garza NL, Donnelly G, Shurtleff AC, Retterer CJ, Gharaibeh D, Zamani R, Kenny T, Eaton BP, Grimes E, Welch LS, Gomba L, Wilhelmsen CL, Nichols DK, Nuss JE, Nagle ER, Kugelman JR, Palacios G, Doerffler E, Neville S, Carra E, Clarke MO, Zhang L, Lew W, Ross B, Wang Q, Chun K, Wolfe L, Babusis D, Park Y, Stray KM, Trancheva I, Feng

- JY, Barauskas O, Xu Y, Wong P, Braun MR, Flint M, McMullan LK, Chen S-S, Fearn R, Swaminathan S, Mayers DL, Spiropoulou CF, Lee WA, Nichol ST, Cihlar T, Bavari S. 2016. Therapeutic efficacy of the small molecule GS-5734 against Ebola virus in rhesus monkeys. *Nature* 531:381–385.
68. Mulangu S, Dodd LE, Davey RT, Tshiani Mbaya O, Proschan M, Mukadi D, Lusakibanza Manzo M, Nzolo D, Tshomba Oloma A, Ibanda A, Ali R, Coulibaly S, Levine AC, Grais R, Diaz J, Lane HC, Muyembe-Tamfum J-J, the PALM Writing Group. 2019. A Randomized, Controlled Trial of Ebola Virus Disease Therapeutics. *N Engl J Med* 381:2293–2303.
 69. Cho A, Zhang L, Xu J, Lee R, Butler T, Metobo S, Aktoudianakis V, Lew W, Ye H, Clarke M, Doerffler E, Byun D, Wang T, Babusis D, Carey AC, German P, Sauer D, Zhong W, Rossi S, Fenaux M, McHutchison JG, Perry J, Feng J, Ray AS, Kim CU. 2014. Discovery of the First C -Nucleoside HCV Polymerase Inhibitor (GS-6620) with Demonstrated Antiviral Response in HCV Infected Patients. *J Med Chem* 57:1812–1825.
 70. Pollack A, Gale J. BMS Suspends Study of Nucleotide BMS094 Formerly INX189. Bloomberg.
 71. Loughheed K. 2012. Hepatitis C drug trial halted after patient death : News blog. Nat News Blog.
 72. Tao S, Zhou L, Zhang H, Zhou S, Amiralaie S, Shelton J, Ehteshami M, Jiang Y, Amblard F, Coats SJ, Schinazi RF. 2020. Intracellular metabolism and potential cardiotoxicity of a β -D-2'-C-methyl-2,6-diaminopurine ribonucleoside phosphoramidate that inhibits hepatitis C virus replication. *Nucleosides, Nucleotides and Nucleic Acids* 39:204–224.
 73. Butler T, Cho A, Kim C, Saunders OL, Zhang L. October 2009. 1' -Substituted Carba-Nucleoside Analogues for Antiviral Treatment. WO2009132135. World Intellectual Property Organization.
 74. Goldman JD, Lye DCB, Hui DS, Marks KM, Bruno R, Montejano R, Spinner CD, Galli M, Ahn M-Y, Nahass RG, Chen Y-S, SenGupta D, Hyland RH, Osinusi AO, Cao H, Blair C, Wei X, Gaggar A, Brainard DM, Towner WJ, Muñoz J, Mullane KM, Marty FM, Tashima KT, Diaz G, Subramanian A. 2020. Remdesivir for 5 or 10 Days in Patients with Severe Covid-19. *N Engl J Med* <https://doi.org/10.1056/nejmoa2015301>.
 75. Lo MK, Jordan R, Arvey A, Sudhamsu J, Shrivastava-Ranjan P, Hotard AL, Flint M,

- McMullan LK, Siegel D, Clarke MO, Mackman RL, Hui HC, Perron M, Ray AS, Cihlar T, Nichol ST, Spiropoulou CF. 2017. GS-5734 and its parent nucleoside analog inhibit Filo-, Pneumo-, and Paramyxoviruses. *Sci Rep* 7:43395.
76. Gordon CJ, Tchesnokov EP, Woolner E, Perry JK, Feng JY, Porter DP, Götte M. 2020. Remdesivir is a direct-acting antiviral that inhibits RNA-dependent RNA polymerase from severe acute respiratory syndrome coronavirus 2 with high potency. *J Biol Chem.* American Society for Biochemistry and Molecular Biology Inc.
 77. Clarke MONH, Feng JY, Jordan R, Mackman RL, Ray AS, Siegel D. March 2017. Methods For Treating Arenaviridae and Coronaviridae Virus Infections. US 2017/0071964A1. US Patent Application Publication.
 78. Gordon CJ, Tchesnokov EP, Feng JY, Porter DP, Gotte M. 2020. The antiviral compound remdesivir potently inhibits RNA-dependent RNA polymerase from Middle East respiratory syndrome coronavirus. *J Biol Chem jbc.AC120.013056*.
 79. Tchesnokov EP, Gordon CJ, Woolner E, Kocincova D, Perry JK, Feng JY, Porter DP, Gotte M. 2020. Template-dependent inhibition of coronavirus RNA-dependent RNA polymerase by remdesivir reveals a second mechanism of action. *J Biol Chem jbc.AC120.015720*.
 80. Brown AJ, Won JJ, Graham RL, Dinno KH, Sims AC, Feng JY, Cihlar T, Denison MR, Baric RS, Sheahan TP. 2019. Broad spectrum antiviral remdesivir inhibits human endemic and zoonotic deltacoronaviruses with a highly divergent RNA dependent RNA polymerase. *Antiviral Res* 169:104541.
 81. Agostini ML, Andres EL, Sims AC, Graham RL, Sheahan TP, Lu X, Clinton Smith E, Brett Case J, Feng JY, Jordan R, Ray AS, Cihlar T, Siegel D, Mackman RL, Clarke MO, Baric RS, Denison MR, Agostini CM, Gallagher T. 2018. Coronavirus Susceptibility to the Antiviral Remdesivir (GS-5734) Is Mediated by the Viral Polymerase and the Proofreading Exoribonuclease Downloaded from. *MBio* 9:ee00221-18.
 82. Warren TK, Jordan R, Lo MK, Ray AS, Mackman RL, Soloveva V, Siegel D, Perron M, Bannister R, Hui HC, Larson N, Strickley R, Wells J, Stuthman KS, Van Tongeren SA, Garza NL, Donnelly G, Shurtleff AC, Retterer CJ, Gharaibeh D, Zamani R, Kenny T, Eaton BP, Grimes E, Welch LS, Gomba L, Wilhelmsen CL, Nichols DK, Nuss JE, Nagle ER, Kugelman JR, Palacios G, Doerffler E, Neville S, Carra E, Clarke MO, Zhang L, Lew

- W, Ross B, Wang Q, Chun K, Wolfe L, Babusis D, Park Y, Stray KM, Trancheva I, Feng JY, Barauskas O, Xu Y, Wong P, Braun MR, Flint M, McMullan LK, Chen S-S, Fearn R, Swaminathan S, Mayers DL, Spiropoulou CF, Lee WA, Nichol ST, Cihlar T, Bavari S. 2016. Therapeutic efficacy of the small molecule GS-5734 against Ebola virus in rhesus monkeys. *Nature* 531:381–385.
83. de Wit E, Feldmann F, Cronin J, Jordan R, Okumura A, Thomas T, Scott D, Cihlar T, Feldmann H. 2020. Prophylactic and therapeutic remdesivir (GS-5734) treatment in the rhesus macaque model of MERS-CoV infection. *Proc Natl Acad Sci* <https://doi.org/10.1073/pnas.1922083117>.
 84. Pruijssers AJ, George AS, Schä A, Baric RS, Denison MR, Sheahan TP. 2020. Remdesivir Inhibits SARS-CoV-2 in Human Lung Cells and Chimeric SARS-CoV Expressing the SARS-CoV-2 RNA Polymerase in Mice. *Cell Rep* 107940.
 85. Tempestilli M, Caputi P, Avataneo V, Notari S, Forini O, Scorzolini L, Marchioni L, Bartoli TA, Castilletti C, Lalle E, Capobianchi MR, Nicastri E, D'Avolio A, Ippolito G, Agrati C. 2020. Pharmacokinetics of remdesivir and GS-441524 in two critically ill patients who recovered from COVID-19. *J Antimicrob Chemother* dkaa239:1–4.
 86. Davis MR, Pham CU, Cies JJ. 2020. Remdesivir and GS-441524 plasma concentrations in patients with end-stage renal disease on haemodialysis. *J Antimicrob Chemother* 1–3.
 87. Cihlar T, Ray AS, Boojamra CG, Zhang L, Hui H, Laflamme G, Vela JE, Grant D, Chen J, Myrick F, White KL, Gao Y, Lin KY, Douglas JL, Parkin NT, Carey A, Pakdaman R, Mackman RL. 2008. Design and profiling of GS-9148, a novel nucleotide analog active against nucleoside-resistant variants of human immunodeficiency virus type 1, and its orally bioavailable phosphonoamidate prodrug, GS-9131. *Antimicrob Agents Chemother* 52:655–665.
 88. Babusis D, Curry MP, Denning JM, Wang T, Kirby B, Murakami E, Park Y, Lepist E-I, Mathias A, Symonds WT, Afdhal NH, McHutchinson JG, Ray AS. 2014. Translational Studies to Understand the Mechanism of Liver Delivery by Sofosbuvir 15th International Workshop on Clinical Pharmacology of HIV and Hepatitis Therapy. Washington, DC.
 89. Murphy BG, Perron M, Murakami E, Bauer K, Park Y, Eckstrand C, Liepnieks M, Pedersen NC. 2018. The nucleoside analog GS-441524 strongly inhibits feline infectious peritonitis (FIP) virus in tissue culture and experimental cat infection studies.

- Vet Microbiol 219:226–233.
90. Yan VC, Muller FL. 2020. Gilead should ditch remdesivir and focus on its simpler and safer ancestor. *Stat.*
 91. Yan V, Muller F. 2020. Comprehensive Summary Supporting Clinical Investigation of GS-441524 for Covid-19 Treatment. OSF Prepr <https://doi.org/10.31219/OSF.IO/MNHXU>.
 92. Li Y, Cao L, Li G, Cong F, Li Y, Sun J, Luo Y, Chen G, Li G, Wang P, Xing F, Ji Y, Zhao J, Zhang Y, Guo D, Zhang X. 2020. Remdesivir Metabolite GS-441524 Efficiently Inhibits SARS-CoV-2 Infection in Mouse Model. *bioRxiv* 2019:2020.10.26.353300.
 93. NCATS OpenData Portal. GS-441524 Pharmacokinetic (PK) Studies.
 94. Yin W, Mao C, Luan X, Shen DD, Shen Q, Su H, Wang X, Zhou F, Zhao W, Gao M, Chang S, Xie YC, Tian G, Jiang HW, Tao SC, Shen J, Jiang Y, Jiang H, Xu Y, Zhang S, Zhang Y, Xu HE. 2020. Structural basis for inhibition of the RNA-dependent RNA polymerase from SARS-CoV-2 by remdesivir. *Science* (80-) 368:1499–1504.
 95. Vernachio JH, Bleiman B, Bryant KD, Chamberlain S, Hunley D, Hutchins J, Ames B, Gorovits E, Ganguly B, Hall A, Kolykhalov A, Liu Y, Muhammad J, Raja N, Walters CR, Wang J, Williams K, Patti JM, Henson G, Madela K, Aljarah M, Gilles A, McGuigan C. 2011. INX-08189, a phosphoramidate prodrug of 6-O-methyl-2'-C-methyl guanosine, is a potent inhibitor of hepatitis C virus replication with excellent pharmacokinetic and pharmacodynamic properties. *Antimicrob Agents Chemother* 55:1843–1851.
 96. McGuigan C, Madela K, Aljarah M, Gilles A, Brancale A, Zonta N, Chamberlain S, Vernachio J, Hutchins J, Hall A, Ames B, Gorovits E, Ganguly B, Kolykhalov A, Wang J, Muhammad J, Patti JM, Henson G. 2010. Design, synthesis and evaluation of a novel double pro-drug: INX-08189. A new clinical candidate for hepatitis C virus. *Bioorganic Med Chem Lett* 20:4850–4854.
 97. Sizun G, Pierra C, Badaroux E, Rabeson C, Benzaria-Prad S, Surleraux D, Loi AG, Musiu C, Liuzzu M, Seifer M, Standring D, Sommadossi J-P, Gosselin G. 2015. Design, synthesis and antiviral evaluation of 2'-C-methyl branched guanosine pronucleotides: the discovery of IDX184, a potent liver-targeted HCV polymerase inhibitor. *Future Med Chem* 7.
 98. Yan VC, Pham CD, Arthur K, Yang KL, Muller FL. 2020. Aliphatic amines are viable

- pro-drug moieties in phosphonoamidate drugs. *Bioorganic Med Chem Lett* 30:127656.
99. Beaucage SL, Caruthers MH. 1981. Deoxynucleoside phosphoramidites-A new class of key intermediates for deoxypolynucleotide synthesis. *Tetrahedron Lett* 22:1859–1862.
 100. Sofia MJ, Bao D, Chang W, Du J, Nagarathnam D, Rachakonda S, Reddy PG, Ross BS, Wang P, Zhang H-R, Bansal S, Espiritu C, Keilman M, Lam AM, Steuer HMM, Niu C, Otto MJ, Furman PA. 2010. Discovery of a β -d -2'-Deoxy-2'- α -fluoro-2'- β - C - methyluridine Nucleotide Prodrug (PSI-7977) for the Treatment of Hepatitis C Virus. *J Med Chem* 53:7202–7218.
 101. Davey MS, Malde R, Mykura RC, Baker AT, Taher TE, Le Duff CS, Willcox BE, Mehellou Y. 2018. Synthesis and Biological Evaluation of (E)-4-Hydroxy-3-methylbut-2-enyl Phosphate (HMBP) Aryloxy Triester Phosphoramidate Prodrugs as Activators of V γ 9/V δ 2 T-Cell Immune Responses. *J Med Chem* 61:2111–2117.
 102. Elbaum D, Beconi MG, Monteagudo E, Marco A Di, Quinton MS, Lyons KA, Vaino A, Harper S. 2018. Fosmetpantotenate (RE-024), a phosphopantothenate replacement therapy for pantothenate kinase-associated neurodegeneration: Mechanism of action and efficacy in nonclinical models. *PLoS One* 13:1–27.
 103. Serpi M, Bibbo R, Rat S, Roberts H, Hughes C, Caterson B, Alcaraz MJ, Gibert AT, Verson CRA, McGuigan C. 2012. Novel phosphoramidate prodrugs of N-acetyl-(d)-glucosamine with antidegenerative activity on bovine and human cartilage explants. *J Med Chem* 55:4629–4639.
 104. Vellenki S, Nadella M, Mullamalla R, Siva V, Arumalla R, Pulyala R. 2012. US 2012/0238753 A1 Process for the Preparation of Adefovir Dipivoxil. US 2012/0238753. USPTO.
 105. Ripin DHB, Teager DS, Fortunak J, Basha SM, Bivins N, Boddy CN, Byrn S, Catlin KK, Houghton SR, Jagadeesh ST, Kumar KA, Melton J, Muneer S, Rao LN, Rao RV, Ray PC, Reddy NG, Reddy RM, Shekar KC, Silverton T, Smith DT, Stringham RW, Subbaraju G V., Talley F, Williams A. 2010. Process improvements for the manufacture of tenofovir disoproxil fumarate at commercial scale. *Org Process Res Dev* 14:1194–1201.
 106. Derstine BP, Tomlin JW, Peck CL, Dietz JP, Herrera BT, Cardoso FSP, Paymode DJ, Yue AC, Arduengo AJ, Opatz T, Snead DR, Stringham RW, McQuade DT, Gupton BF. 2020. An Efficient Synthesis of Tenofovir (PMPA): A Key Intermediate Leading to Tenofovir-

- based HIV Medicines. *Org Process Res Dev*
<https://doi.org/10.26434/chemrxiv.11900262.v1>.
107. Kadri H, Taher TE, Xu Q, Sharif M, Ashby E, Bryan RT, Willcox BE, Mehellou Y. 2020. Aryloxy Diester Phosphonamidate Prodrugs of Phosphoantigens (ProPAgens) as Potent Activators of V γ 9/V δ 2 T-Cell Immune Responses. *J Med Chem* 63:11258–11270.
 108. Meier C, Görbig U, Müller C, Balzarini J. 2005. CycloSal-PMEA and cycloAmb-PMEA: Potentially new phosphonate prodrugs based on the cyclosal-pronucleotide approach. *J Med Chem* 48:8079–8086.
 109. Lee WA, He G-X, Eisenberg E, Cihlar T, Swaminathan S, Mulato A, Cundy KC. 2005. Selective Intracellular Activation of a Novel Prodrug of the Human Immunodeficiency Virus Reverse Transcriptase Inhibitor Tenofovir Leads to Preferential Distribution and Accumulation in Lymphatic Tissue. *Antimicrob Agents Chemother* 49:1898–1906.
 110. Gunic E, Girardet JL, Ramasamy K, Stoisavljevic-Petkov V, Chow S, Yeh LT, Hamatake RK, Raney A, Hong Z. 2007. Cyclic monophosphate prodrugs of base-modified 2'-C-methyl ribonucleosides as potent inhibitors of hepatitis C virus RNA replication. *Bioorganic Med Chem Lett* 17:2452–2455.
 111. McKenna CE, Kashemirov BA, Eriksson U, Amidon GL, Kish PE, Mitchell S, Kim JS, Hilfinger JM. 2005. Cidofovir peptide conjugates as prodrugs. *J Organomet Chem* 690:2673–2678.
 112. DeFord J, Chu F, Anslyn E. 1996. Dimerization constants for phosphoric acid diesters. *Tetrahedron Lett* 37:1925–1928.
 113. Stefko M, Man S, Ke K. 2017. WO2017/157352A1 A Preparation Method of Diastereomerically Pure Tenofovir Alafenamide or Its Salts. WO2017/157352A1. World International Patent Organization, Czech Republic.
 114. DiRocco DA, Ji Y, Sherer EC, Klapars A, Reibarkh M, Dropinski J, Mathew R, Maligres P, Hyde AM, Limanto J, Brunskill A, Ruck RT, Campeau LC, Davies IW. 2017. A multifunctional catalyst that stereoselectively assembles prodrugs. *Science* (80-) 356:426–430.
 115. Chapman H, Kernan M, Prisbe E, Rohloff J, Sparacino M, Terhorst T, Yu R. 2001. Practical synthesis, separation, and stereochemical assignment of the PMPA pro-drug GS-7340. *Nucleosides, Nucleotides and Nucleic Acids* 20:621–628.

116. Becker MW, Chapman HH, Cihlar T, Eisenberg EJ, He G-X, Kernan MR, Lee WA, Prisbe EJ, Rohloff JC, Sparacino ML. 2008. US 7,390,791 B2 Prodrugs of Phosphonate Nucleotide Analogues. US 7,390,791 B2. USPTO.
117. Alanazi AS, James E, Mehellou Y. 2019. The ProTide Prodrug Technology: Where Next? *ACS Med Chem Lett* 10:2–5.
118. McGuigan C, Davies M, Pathirana R, Mahmood N, Hay AJ. 1994. Synthesis and anti-HIV activity of some novel diaryl phosphate derivatives of AZT. *Antiviral Res* 24:69–77.
119. Swamy KCK, Kumar NNB, Balaraman E, Kumar KVPP. 2009. Mitsunobu and Related Reactions: Advances and Applications. *Chem Rev* 109:2551–2651.
120. McGuigan C, Cahard D, Sheeka HM, De Clercq E, Balzarini J. 1996. Aryl Phosphoramidate Derivatives of d4T Have Improved Anti-HIV Efficacy in Tissue Culture and May Act by the Generation of a Novel Intracellular Metabolite. *J Med Chem* 39:1748–1753.
121. Bhatia HK, Singh H, Grewal N, Natt NK. 2014. Sofosbuvir: A novel treatment option for chronic hepatitis C infection. *J Pharmacol Pharmacother* 5:278.
122. Atherton FR, Openshaw HT, Todd AR. 1945. 174. Studies on phosphorylation. Part II. The reaction of dialkyl phosphites with polyhalogen compounds in presence of bases. A new method for the phosphorylation of amines. *J Chem Soc* 660.
123. Pungente MD, Weiler L. 2001. Synthesis and stereochemical elucidation of a 14-membered ring phosphonate. *Org Lett* 3:643–646.
124. Batesky DC, Goldfogel MJ, Weix DJ. 2017. Removal of Triphenylphosphine Oxide by Precipitation with Zinc Chloride in Polar Solvents. *J Org Chem* 82:9931–9936.
125. Volante RP. 1981. A new, highly efficient method for the conversion of alcohols to thioesters and thiols. *Tetrahedron Lett* 22:3119–3122.
126. McMinn DL, Greenberg MM. 1997. Synthesis of oligonucleotides containing 3'-alkyl amines using N-isobutyryl protected deoxyadenosine phosphoramidite. *Tetrahedron Lett* 38:3123–3126.
127. Hughes DL, Reamer RA, Bergan JJ, Grabowski EJJ. 1988. A mechanistic study of the Mitsunobu esterification reaction. *J Am Chem Soc* 110:6487–6491.
128. Melby ES, Soldat DJ, Barak P. 2011. Synthesis and detection of oxygen-18 labeled phosphate. *PLoS One* 6.

129. Yan VC, Pham C-D, Muller FL. 2020. Expedient Method for Direct Mono-amidation of Phosphonic and Phosphoric Acids. ChemRxiv
<https://doi.org/10.26434/chemrxiv.12073131.V1>.
130. Blagden SP, Rizzuto I, Suppiah P, O'Shea D, Patel M, Spiers L, Sukumaran A, Bharwani N, Rockall A, Gabra H, El-Bahrawy M, Wasan H, Leonard R, Habib N, Ghazaly E. 2018. Anti-tumour activity of a first-in-class agent NUC-1031 in patients with advanced cancer: results of a phase I study. *Br J Cancer* 119:815–822.
131. Chou T-F, Baraniak J, Kaczmarek R, Zhou X, Cheng J, Ghosh B, Wagner CR. 2007. Phosphoramidate Pronucleotides: A Comparison of the Phosphoramidase Substrate Specificity of Human and Escherichia coli Histidine Triad Nucleotide Binding Proteins. *Mol Pharm* 4:208–217.
132. Zhou X-J, Pietropaolo K, Chen J, Khan S, Sullivan-Bólyai J, Mayers D. 2011. Safety and pharmacokinetics of IDX184, a liver-targeted nucleotide polymerase inhibitor of hepatitis C virus, in healthy subjects. *Antimicrob Agents Chemother* 55:76–81.
133. Farquhar D, Khan S, Srivastva DN, Saunders PP. 1994. Synthesis and Antitumor Evaluation of Bis[(pivaloyloxy)methyl] 2,-Deoxy-5-fluorouridine 5-Monophosphate (FdUMP): A Strategy To Introduce Nucleotides into Cells. *J Med Chem* 37:3902–3909.
134. Pisaneschi F, Lin YH, Leonard PG, Satani N, Yan VC, Hammoudi N, Raghavan S, Link TM, Georgiou DK, Czako B, Muller FL. 2019. The 3S enantiomer drives enolase inhibitory activity in SF2312 and its analogues. *Molecules* 24.
135. Schwartzbaum JA, Fisher JL, Aldape KD, Wrensch M. 2006. Epidemiology and molecular pathology of glioma. *Nat Clin Pract Neurol* 2:494–503.
136. Brown JM. 2007. Tumor Hypoxia in Cancer Therapy. *Methods Enzymol* 435:295–321.
137. Vaupel P, Höckel M, Mayer A. 2007. Detection and characterization of tumor hypoxia using pO₂ histography. *Antioxid Redox Signal* 9:1221–35.
138. Beck R, Röper B, Carlsen JM, Huisman MC, Lebschi JA, Andratschke N, Picchio M, Souvatzoglou M, Machulla H-J, Piert M. 2007. Pretreatment ¹⁸F-FAZA PET predicts success of hypoxia-directed radiochemotherapy using tirapazamine. *J Nucl Med* 48:973–80.
139. Varia MA, Calkins-Adams DP, Rinker LH, Kennedy AS, Novotny DB, Fowler WC, Raleigh JA. 1998. Pimonidazole: A Novel Hypoxia Marker for Complementary Study of

- Tumor Hypoxia and Cell Proliferation in Cervical Carcinoma. *Gynecol Oncol* 71:270–277.
140. Wilson WR, Hay MP. 2011. Targeting hypoxia in cancer therapy. *Nat Rev Cancer* 11:393–410.
 141. Tercel M, Lee AE, Hogg A, Anderson RF, Lee HH, Siim BG, Denny WA, Wilson WR. 2001. Hypoxia-selective antitumor agents. 16. Nitroarylmethyl quaternary salts as bioreductive prodrugs of the alkylating agent mechlorethamine. *J Med Chem* 44:3511–22.
 142. Borch RF, Liu J, Schmidt JP, Marakovits JT, Joswig C, Gipp JJ, Mulcahy RT. 2000. Synthesis and Evaluation of Nitroheterocyclic Phosphoramidates as Hypoxia-Selective Alkylating Agents. *J Med Chem* 43:2258–2265.
 143. Li B, Sedlacek M, Manoharan I, Boopathy R, Duysen EG, Masson P, Lockridge O. 2005. Butyrylcholinesterase, paraoxonase, and albumin esterase, but not carboxylesterase, are present in human plasma. *Biochem Pharmacol* 70.
 144. Benito J, Ramierez M, Millward NZ, Velez J, Harutyunyan K, Lu H, Shi Y, Marte P, Jacamo R, Ma H, Konoplev S, McQueen T, Volgin A, Protopopova M, Mu H, Lee J, Battacharya P, Marszalek JR, Davis RE, Bankson J, Cortes J, Hart CP, Andreeff M, Konopleva M. 2016. Hypoxia-activated prodrug TH-302 targets hypoxic bone marrow niches in pre-clinical leukemia models. *Clin Cancer Res* 22:1687–1698.
 145. Wardman P, Clarke ED. 1976. Oxygen inhibition of nitroreductase: Electron transfer from nitro radical-anions to oxygen. *Biochem Biophys Res Commun* 69:942–949.
 146. McKeown SR. 2014. Defining normoxia, physoxia and hypoxia in tumours—implications for treatment response. *Br J Radiol* 87:20130676.
 147. Sanzey M, Rahim SAA, Oudin A, Dirkse A, Kaoma T, Vallar L, Herold-Mende C, Bjerkgvig R, Golebiewska A, Niclou SP. 2015. Comprehensive Analysis of Glycolytic Enzymes as Therapeutic Targets in the Treatment of Glioblastoma. *PLoS One* 10.
 148. Naylor MA, Stephens MA, Cole S, Threadgill MD, Stratford IJ, O'Neill P, Fielden EM, Adams GE. 1990. Synthesis and Evaluation of Novel Electrophilic Nitrofuran Carboxamides and Carboxylates as Radiosensitizers and Bioreductively Activated Cytotoxins *Journal of Medicinal Chemistry*.
 149. Adams GE, Clarke ED, Flockhart IR, Jacobs RS, Sehmi DS, Stratford IJ, Wardman P, Watts ME, Parrick J, Wallace RG, Smithen CE. 1979. Structure-activity Relationships in

- the Development of Hypoxic Cell Radiosensitizers. *Int J Radiat Biol Relat Stud Physics, Chem Med* 35:133–150.
150. Cretton-Scott E, Perigaud C, Peyrottes S, Licklider L, Camire M, Larsson M, La Colla M, Hildebrand E, Lалlos L, Bilello J, McCarville J, Seifer M, Liuzzi M, Pierra C, Badaroux E, Gosselin G, Surleraux D, Standring DN. 2008. In Vitro Antiviral Activity and Pharmacology of IDX184, A Novel and Potent Inhibitor of HCV Replication. *J Hepatol* 48:S220.
 151. Yan VC, Yang KL, Ballato ES, Arthur K, Georgiou DK, Muller FL. 2020. Bioreducible Pro-drug Inhibitors of Enolase. *ChemRxiv*
<https://doi.org/10.26434/chemrxiv.12033303.V1>.
 152. Satani N, Lin Y-H, Hammoudi N, Raghavan S, Georgiou DK, Muller FL. 2016. ENOblock Does Not Inhibit the Activity of the Glycolytic Enzyme Enolase. *PLoS One* 11:e0168739.
 153. Muller F, Yan V, Yang K, Ballato E, Pham C-D. 2020. WO2020154742A1 Inhibitors of the Enzyme Enolase for Precision Oncology. WO2020154742A1. World Intellectual Patent Organization.
 154. Lee WA, He G-X, Eisenberg E, Cihlar T, Swaminathan S, Mulato A, Cundy KC. 2005. Selective intracellular activation of a novel prodrug of the human immunodeficiency virus reverse transcriptase inhibitor tenofovir leads to preferential distribution and accumulation in lymphatic tissue. *Antimicrob Agents Chemother* 49:1898–906.
 155. Nathanson L, Hall TC, Schilling A, Miller S. 1969. Concurrent combination chemotherapy of human solid tumors: experience with a three-drug regimen and review of the literature. *Cancer Res* 29:419–25.
 156. Sullivan RD, Miller E, Sikes MP. 1959. Antimetabolite-metabolite combination cancer chemotherapy. Effects of intra-arterial methotrexate—intramuscular citrovorum factor therapy in human cancer. *Cancer* 12:1248–1262.
 157. Ross MB, Buzdar AU, Smith TL, Eckles N, Hortobagyi GN, Blumenschein GR, Freireich EJ, Gehan EA. 1985. Improved survival of patients with metastatic breast cancer receiving combination chemotherapy. Comparison of consecutive series of patients in 1950s, 1960s, and 1970s. *Cancer* 55:341–346.
 158. Frei III E, Cucchi CA, Rosowsky A, Tantravahi R, Bernal S, Ervin TJ, Ruprecht RM,

- Haseltine WA. 1985. Alkylating agent resistance: In vitro studies with human cell lines (resistant cells). *Proc Natl Acad Sci* 82:2158–2162.
159. Singh RK, Kumar S, Prasad DN, Bhardwaj TR. 2018. Therapeutic journey of nitrogen mustard as alkylating anticancer agents: Historic to future perspectives. *Eur J Med Chem* 151:401–433.
 160. Goodman LS, Wintrobe MM, Dameshek W, Goodman MJ, Gilman A, McLennan MT. 1984. Landmark article Sept. 21, 1946: Nitrogen mustard therapy. Use of methyl-bis(beta-chloroethyl)amine hydrochloride and tris(beta-chloroethyl)amine hydrochloride for Hodgkin's disease, lymphosarcoma, leukemia and certain allied and miscellaneous disorders. *JAMA* 251:2255–61.
 161. Wilkinson JF. 1963. Treatment of Leukæmias. *Proc R Soc Med* 56:644–648.
 162. Gardikas C, Wilkinson J. 1952. Alkylamines in the treatment of leukaemia. *Lancet* 2:161–6.
 163. Larionov L. 1956. Some biological and clinical results from the investigations of the chloroethylamines as anti-tumour drugs. *Br J Cancer* 10:26–32.
 164. McAlpine S. 1956. Nitrogen mustard in treatment of bronchial carcinoma. *Br Med J* 2:1412–3.
 165. Barberio R, Berry N, Bateman J, Cromer JK, Klopp CT. 1953. Combined administration of aureomycin and nitrogen mustard. II. Effects of the intra-arterial administration on human cancer. *Cancer* 6:280–287.
 166. Sullivan RD, Jones R, Schnabel TG, McShorey JC. 1953. The treatment of human cancer with intra-arterial nitrogen mustard (methylbis(2-chloroethyl)amine hydrochloride). Utilizing a simplified catheter technique. *Cancer* 6:121–134.
 167. Sullivan RD, Mescon H, Jones R. 1953. The effect of intra-arterial nitrogen-mustard. (Methylbis(2-chloroethyl)amine hydrochloride). Therapy on human skin. *Cancer* 6:288–293.
 168. Dameshek W, Weisfuse L, Stein T. 1949. Nitrogen Mustard Therapy in Hodgkin's Disease. *Blood* 4.
 169. Bateman J, Klopp C, Cromer J. 1951. Hematologic effects of regional nitrogen mustard therapy. *Blood* 6:26–38.
 170. Barberio J, Klopp C, Ayers W, Gross H. 1951. Effects of intra-arterial administration of

- nitrogen mustard. *Cancer* 4:1341–63.
171. Hilton J. 1984. Role of aldehyde dehydrogenase in cyclophosphamide-resistant L1210 leukemia. *Cancer Res* 44:5156–60.
 172. Tomita H, Tanaka K, Tanaka T, Hara A. 2016. Aldehyde dehydrogenase 1A1 in stem cells and cancer. *Oncotarget* 7.
 173. Emadi A, Jones RJ, Brodsky RA. 2009. Cyclophosphamide and cancer: golden anniversary. *Nat Rev Clin Oncol* 6:638–647.
 174. Sladek N. 1973. Bioassay and relative cytotoxic potency of cyclophosphamide metabolites generated in vitro and in vivo. *Cancer Res* 33:1150–8.
 175. Cox PJ, Phillips BJ, Thomas P. 1976. Studies on the selective action of cyclophosphamide (NSC-26271): Inactivation of the hydroxylated metabolite by tissue-soluble enzymes. *Cancer Treat Rep* 60:321–6.
 176. Pedersen NC, Perron M, Bannasch M, Montgomery E, Murakami E, Liepnieks M, Liu H. 2019. Efficacy and safety of the nucleoside analog GS-441524 for treatment of cats with naturally occurring feline infectious peritonitis. *J Feline Med Surg* 21:271–281.
 177. Dickinson PJ, Bannasch M, Thomasy SM, Murthy VD, Vernau KM, Liepnieks M, Montgomery E, Knickelbein KE, Murphy B, Pedersen NC. 2020. Antiviral treatment using the adenosine nucleoside analogue GS-441524 in cats with clinically diagnosed neurological feline infectious peritonitis. *J Vet Intern Med* jvim.15780.
 178. Beigel JH, Tomashek KM, Dodd LE, Mehta AK, Zingman BS, Kalil AC, Hohmann E, Chu HY, Luetkemeyer A, Kline S, Lopez de Castilla D, Finberg RW, Dierberg K, Tapson V, Hsieh L, Patterson TF, Paredes R, Sweeney DA, Short WR, Touloumi G, Lye DC, Ohmagari N, Oh M, Ruiz-Palacios GM, Benfield T, Fätkenheuer G, Kortepeter MG, Atmar RL, Creech CB, Lundgren J, Babiker AG, Pett S, Neaton JD, Burgess TH, Bonnett T, Green M, Makowski M, Osinusi A, Nayak S, Lane HC. 2020. Remdesivir for the Treatment of Covid-19 — Final Report. *N Engl J Med* <https://doi.org/10.1056/NEJMoa2007764>.
 179. WHO Solidarity Trial Consortium. 2020. Repurposed Antiviral Drugs for Covid-19 — Interim WHO Solidarity Trial Results. *N Engl J Med* NEJMoa2023184.
 180. 2020. WHO recommends against the use of remdesivir in COVID-19 patients.
 181. Food and Drug Administration. 2020. Fact Sheet for Health Care Providers Emergency

Use Authorization (EUA) of VEKLURY ® (remdesivir).

182. Yan VC, Muller FL. 2020. Captisol and GS-704277, but not GS-441524, are credible mediators of remdesivir's nephrotoxicity. *Antimicrob Agents Chemother* 64:01920–1920.
183. Vieira T, Stevens AC, Chtchemeline A, Gao D, Badalov P, Heumann L. 2020. Development of a Large-Scale Cyanation Process Using Continuous Flow Chemistry En Route to the Synthesis of Remdesivir. *Org Process Res Dev* 24:2113–2121.
184. Xu Y, Barauskas O, Kim C, Babusis D, Murakami E, Kornyejev D, Lee G, Stepan G, Perron M, Bannister R, Schultz BE, Sakowicz R, Porter D, Cihlar T, Feng JY. 2020. Off-target In Vitro Profiling Demonstrates that Remdesivir Is a Highly Selective Antiviral Agent. *Antimicrob Agents Chemother* <https://doi.org/10.1128/aac.02237-20>.
185. Bieganski P, Garrison PN, Hodawadekar SC, Faye G, Barnes LD, Brenner C. 2002. Adenosine Monophosphoramidase Activity of Hint and Hnt1 Supports Function of Kin28, Ccl1, and Tfb3. *J Biol Chem* 277:10852–10860.
186. Wichmann D, Sperhake J-P, Lütgehetmann M, Steurer S, Edler C, Heinemann A, Heinrich F, Mushumba H, Kniep I, Schröder AS, Burdelski C, de Heer G, Nierhaus A, Frings D, Pfefferle S, Becker H, Brederke-Wiedling H, de Weerth A, Paschen H-R, Sheikzadeh-Eggers S, Stang A, Schmiedel S, Bokemeyer C, Addo MM, Aepfelbacher M, Püschel K, Kluge S. 2020. Autopsy Findings and Venous Thromboembolism in Patients With COVID-19. *Ann Intern Med* pp: M20-2003.
187. Beigel JH, Tomashek KM, Dodd LE, Mehta AK, Zingman BS, Kalil AC, Hohmann E, Chu HY, Luetkemeyer A, Kline S, Lopez de Castilla D, Finberg RW, Dierberg K, Tapson V, Hsieh L, Patterson TF, Paredes R, Sweeney DA, Short WR, Touloumi G, Lye DC, Ohmagari N, Oh M, Ruiz-Palacios GM, Benfield T, Fätkenheuer G, Kortepeter MG, Atmar RL, Creech CB, Lundgren J, Babiker AG, Pett S, Neaton JD, Burgess TH, Bonnett T, Green M, Makowski M, Osinusi A, Nayak S, Lane HC. 2020. Remdesivir for the Treatment of Covid-19 — Preliminary Report. *N Engl J Med* NEJMoa2007764.
188. Cooke D. 1963. Section of Medicine with Section of Pathology-Serum Enzymes in Clinical Practice. *Sect Med with Sect Pathol* 56.
189. Testa B, Mayer JM. 2006. Hydrolysis in Drug and Prodrug Metabolism: Chemistry, Biochemistry, and Enzymology. Wiley.
190. Yong JM. 1967. Origins of serum alkaline phosphatase. *J Clin Pathol* 20:647–53.

191. Choy K-T, Wong AY-L, Kaewpreedee P, Sia SF, Chen D, Hui KPY, Chu DKW, Chan MCW, Cheung PP-H, Huang X, Peiris M, Yen H-L. 2020. Remdesivir, lopinavir, emetine, and homoharringtonine inhibit SARS-CoV-2 replication in vitro. *Antiviral Res* 178:104786.
192. Hu W juan, Chang L, Yang Y, Wang X, Xie Y chao, Shen J shan, Tan B, Liu J. 2020. Pharmacokinetics and tissue distribution of remdesivir and its metabolites nucleotide monophosphate, nucleotide triphosphate, and nucleoside in mice. *Acta Pharmacol Sin* 1–6.
193. WHO, Sheahan TP, Sims AC, Leist SR, Schäfer A, Won J, Brown AJ, Montgomery SA, Hogg A, Babusis D, Clarke MO, Spahn JE, Bauer L, Sellers S, Porter D, Feng JY, Cihlar T, Jordan R, Denison MR, Baric RS, Graham RL, Menachery VD, Lisa E, Case JB, Leist SR, Pyrc K, Feng JY, Trantcheva I, Bannister R, Park Y, Babusis D, Clarke MO, Mackman RL, Spahn JE, Palmiotti CA, Siegel D, Ray AS, Cihlar T, Jordan R, Denison MR, Baric RS. 2018. Summaries of evidence from selected experimental therapeutics. WHO R&D Bluepr.
194. Wang M, Cao R, Zhang L, Yang X, Liu J, Xu M, Shi Z, Hu Z, Zhong W, Xiao G. 2020. Remdesivir and chloroquine effectively inhibit the recently emerged novel coronavirus (2019-nCoV) in vitro. *Cell Res. Springer Nature*.
195. Murphy BG, Perron M, Murakami E, Bauer K, Park Y, Eckstrand C, Liepnieks M, Pedersen NC. 2018. The nucleoside analog GS-441524 strongly inhibits feline infectious peritonitis (FIP) virus in tissue culture and experimental cat infection studies. *Vet Microbiol* 219:226–233.
196. Addie D, Belák S, Boucraut-Baralon C, Egberink H, Frymus T, Gruffydd-Jones T, Hartmann K, Hosie MJ, Lloret A, Lutz H, Marsilio F, Pennisi MG, Radford AD, Thiry E, Truyen U, Horzinek MC. 2009. Feline infectious peritonitis. ABCD guidelines on prevention and management. *J Feline Med Surg* 11:594–604.
197. Wang Y, Zhang D, Du G, Du R, Zhao J, Jin Y, Fu S, Gao L, Cheng Z, Lu Q, Hu Y, Luo G, Wang K, Lu Y, Li H, Wang S, Ruan S, Yang C, Mei C, Wang Y, Ding D, Wu F, Tang X, Ye X, Ye Y, Liu B, Yang J, Yin W, Wang A, Fan G, Zhou F, Liu Z, Gu X, Xu J, Shang L, Zhang Y, Cao L, Guo T, Wan Y, Qin H, Jiang Y, Jaki T, Hayden FG, Horby PW, Cao B, Wang C. 2020. Remdesivir in adults with severe COVID-19: a randomised,

- double-blind, placebo-controlled, multicentre trial. *Lancet* 395:1569–1578.
198. COVID-19 Provisional Counts - Weekly Updates by Select Demographic and Geographic Characteristics.
 199. Silverman E. 2020. NIH will study Gilead's remdesivir-like compound against Covid-19. *Stat.*
 200. Andrews CW, Bennett L, Yu LX. 2000. Predicting human oral bioavailability of a compound: Development of a novel quantitative structure-bioavailability relationship. *Pharm Res* 17:639–644.
 201. Hammond JR, Stolk M, Archer RGE, McConnell K. 2004. Pharmacological analysis and molecular cloning of the canine equilibrative nucleoside transporter 1. *Eur J Pharmacol* 491:9–19.
 202. Kondo H, Shinoda T, Nakashima H, Watanabe T, Yokohama S. 2003. Characteristics of the gastric pH profiles of unfed and fed cynomolgus monkeys as pharmaceutical product development subjects. *Biopharm Drug Dispos* 24:45–51.
 203. Chen EP, Mahar Doan KM, Portelli S, Coatney R, Vaden V, Shi W. 2008. Gastric pH and gastric residence time in fasted and fed conscious cynomolgus monkeys using the Bravo® pH system. *Pharm Res* 25:123–134.
 204. Hatton GB, Yadav V, Basit AW, Merchant HA. 2015. Animal Farm: Considerations in Animal Gastrointestinal Physiology and Relevance to Drug Delivery in Humans. *J Pharm Sci* 104:2747–2776.
 205. Food and Drug Administration. 2002. ZOVIRAX® (acyclovir).
 206. Laskin OL. 1983. Clinical Pharmacokinetics of Acyclovir. *Clin Pharmacokinet* 8:187–201.
 207. Krasny HC, De Miranda P, Blum MR, Elion GB. 1981. Pharmacokinetics and bioavailability of acyclovir in the dog. *J Pharmacol Exp Ther* 216:281–288.
 208. Jarvis LM. 2020. Scaling up remdesivir amid the coronavirus crisis. *C&EN*.
 209. Cohen E, Azad A. 2020. The US government's supply of Covid-19 drug remdesivir runs out at the end of the month. *CNN*.
 210. Barekatain Y, Yan V, Ackroyd J, Poral A, Tran T, Georgiou D, Arthur K, Lin Y-H, Satani N, Ballato E, deCarvalho A, Verhaak R, de Groot J, Huse J, Asara J, Muller F. 2019. Methylthioadenosine is Not Dramatically Elevated in MTAP -Homozygous Deleted

Primary Glioblastomas. bioRxiv 769885.

211. Cantor JR, Abu-Remaileh M, Kanarek N, Freinkman E, Gao X, Louissaint A, Lewis CA, Sabatini DM. 2017. Physiologic Medium Rewires Cellular Metabolism and Reveals Uric Acid as an Endogenous Inhibitor of UMP Synthase. *Cell* 169:258-272.e17.

VITA

Victoria C. Yan was born in the San Francisco Bay Area, the daughter of Drs. Pearl G. Wu and James K. Yan. After completing her secondary education at Aragon High School in 2015, she entered Mount Holyoke College in South Hadley, Massachusetts, where she conducted physical organic chemistry research with Dr. Gary J. Snyder. She also conducted research at MD Anderson Cancer Center with Profs. Steven W. Millward and Florian L. Muller from June 2017 to December 2017 as undergraduate research assistant. Victoria received the degree of American Bachelor's in biochemistry from Mount Holyoke College in May 2018. In July 2018, she entered the University of Texas MD Anderson Cancer Center UTHHealth Graduate School of Biomedical Sciences.

Permanent Address:

570 Pullman Road
Hillsborough, CA, 94010